Concrete Breakout Strength of Embedded Pipe When Subjected to Lateral Loads

by

Paul Wichmann

A Report Submitted to the Faculty of the

Milwaukee School of Engineering

in Partial Fulfillment of the

Requirements of the Degree of

Master of Science in Civil Engineering

Milwaukee, WI

May 2019

Abstract

Hand railings are a part of everyday life. These railings need to be designed such that they do not fail. How can the live loads from people be approximated? The International Building Code (IBC) attempts to answer this question by requiring the railing to resist either a 200 lb. lateral point load or a 50 plf lateral load, whichever is the worst case based on post spacing, be resisted by the railing by placing the load at the top rail at a minimum of 42 in. from the ground. If the posts are spaced at four ft. the load from the point load will be the same as the 50 plf load.

Railings are connected a variety of ways into the base material whether that is cast-in-place, post-installed or welded. The specific connection that was chosen to test was a 1 ¼ in. nominal diameter schedule 80 pipe, cast-in-place into concrete. The embedment depth, edge distance and slab thickness were varied. The parameters chosen mimic standard dimensions used in practice.

Based on ACI 318-14 provisions, a theoretical capacity is determined to be compared to the actual tested capacity. Due to the applied lateral load at an eccentricity of 42 in., a moment is inherently applied into the concrete. The code is not clear how to account for the moment in the concrete when the ACI code provision assumes the connection to only see shear. The paper explores whether simply uncoupling the moment is a sufficient assumption to make and how the results compare to what previous research found. The testing described in this paper was also intended to verify whether the parameters for each connection satisfy the strength requirement laid out in IBC for railings and whether ACI 318-14 can accurately predict the concrete breakout strength of embedded pipe when subjected to lateral loads.

The testing methods included casting vertical pipe pieces with varying parameters into concrete pieces. The concrete pieces are turned such that the pipes are horizontal and placed into a wooden frame to prevent rotation. Weights are hung in a wooden basket at 42 in. until either concrete breakout failure occurs, or the pipe yielded until the basket weights touched the ground. The test data include 36 total tests with varying parameters to mimic standard dimension used in practice.

From the test data, the three lowest tests failed at 260 lb., 295 lb. and 295 lb. All three of these tests had the same parameters, corner test, Ca_1 of three in. (distance to edge parallel to shear load), Ca_2 of three in. (distance to edge perpendicular to shear load), and h_{ef} of three in. (embedment depth of post). The results as a whole, matched ACI 318-14 within a percent difference of 2.13%. Due to the close match of results, the design assumption of uncoupling the moment to get the shear force in the concrete is valid and that designs used in practice are valid to resist the minimum load specified by IBC.

Acknowledgments

First off, I would like to acknowledge my advisor, Dr. Zachar, and my committee, Dr. Davis and Dr. Raebel, for assisting this research through continued guidance and support.

Next, I would like to acknowledge Richard DeSimone for coming forward with this potential project and for continued guidance.

Next, I would like to acknowledge Jeff MacDonald for accommodating me in SG 100 so I could run my testing and for also helping me get the necessary equipment required for my testing.

Next, I would like to acknowledge Badger Rail for donating the pipes that were embedded in the concrete, without the pipes, the testing would have not taken place.

Next, I would like to acknowledge my parents, Tony and Kathy Wichmann for their continued support throughout my years in college.

Next, I would like to acknowledge Frank Sena, Alex Rathke, Alex Darville and Seth LiaBraaten for their assistance during concrete pour days and for the use for their equipment.

Last, I would like to acknowledge Hollis Tharp for the support throughout the duration of the project.

Table of Contents

List of Figures

List of Tables

Nomenclature

Symbols

A_{v_o}	projected area of one fastener unlimited by edge influences, cone overlapping or member thickness
A_v	projected area, shear
c_1	distance from center of fastener to edge of concrete in one direction. Where shear is present, c_1 is the direction of the shear force
c_2	distance from center of a fastener to edge of concrete in direction orthogonal to c_1. Where shear is present, c_2 is in the direction perpendicular to shear force
d_o	outside diameter of fastener
$d_{o,test}$	outside diameter of fastener for the specific test
f_c'	concrete compressive strength, measured on 6 by 12 in. cylinders
$f_{c,test}'$	concrete compressive strength, measured on 6 by 12 in. cylinders, for the test
f_{cc}'	concrete compressive strength, measured on 200 mm cubes
$f_{cc,test}'$	concrete compressive strength, measured on 200 mm cubes, for the test
h	thickness of concrete member in which a fastener is anchored
h_{ef}	effective embedment depth
V	shear load
V_n	nominal shear strength
$V_{n,\perp}$	nominal shear strength with load applied perpendicular to the edge
$V_{n,\parallel}$	nominal shear strength with load applied parallel to the edge
$V_{u,test}$	actual shear strength of the test

$V_{u,prediction}$	the predicted actual shear strength
Ψ_4	effect of eccentricity of shear load
Ψ_5	tuning factor considering disturbance of symmetric stress distribution caused by a corner
α	slope of concrete breakout
θ	angle

Abbreviations

ACI	American Concrete Institute
ASCE	American Society of Civil Engineers
CCD	Concrete Capacity Design
Ft^2	feet squared
in	inch
lb	pound
MSOE	Milwaukee School of Engineering
OBS	oriented strand board
plf	pounds per linear foot
psi	pounds per square inch
WT	wide flange beam tee

Chapter 1 - Project Introduction

1.1 - Background

Hand railings are a part of everyday life. These railings need to be designed such that they do not fail. Railings can fail a number of ways depending on the material they are made out of, the method of attachment into base material and what the base material is. How can the live loads on the railing from people be approximated? The International Building Code (IBC) attempts to answer this question by requiring the following from IBC 2015, section 1607.8 Loads on Handrails, Guards, Grab Bars, Seats and Vehicle Barriers:

1) 1607.8.1 Handrails and guards. Handrail assemblies and guards shall be designed to resist a linear load of 50 pounds per linear foot (plf) (0.73 kN/m) in accordance with Section 4.5.1 of ASCE (American Society of Civil Engineers) 7 …

2) 1607.8.1.1 Concentrated Load. Handrails and guards shall be designed to resist a concentrated load of 200 pounds (0.89kN), in accordance with Section 4.5.1 of ASCE 7.

Per ASCE 7, the load specified must be placed at the "top" of the handrail or guard which is a minimum of 42 in. (American Society of Engineers [ASCE], 2016). For the provisions listed in IBC 2015, for the lateral load on the post to be equivalent the posts need to be spaced at 4 feet on center. If the posts are spaced closer than 4 feet, the 200 lb. concentrated load will control. If the posts are spaced further than 4 feet, the 50 plf will control. Railings are connected a variety of ways into the base material, whether that be cast-in-place, post-installed or welded. With the lateral load acting at an eccentricity of 42 in., this puts a moment into the connection of the post and the base material of the connection has to resist the moment. One of the base materials commonly used is concrete. If the moment becomes sufficiently large, the concrete can fail a

number of ways depending on the parameter of the concrete and location of the post in the concrete.

1.2 - Objective

The testing carried out for this project specifically looked at pipes cast into concrete. This is to mimic a railing post, cast into concrete with dimension commonly used in practice. The variable parameters were

1. Embedment depth of the pipe in the concrete,
2. Concrete slab thickness,
3. Distance from edge of concrete to the center of the pipe.

The main objectives of this project were to compare the results from testing with what ACI (American Concrete Institute) 318-14 predicts will result in the failure of concrete breakout when subjected to shear. The project also sought to determine which tests will satisfy the lateral live load strength requirements set forth in IBC. The parameters for the project were to mimic standard dimensions commonly used in practice for a handrail post embedded in concrete.

This capstone project report seeks to answer how the lateral loads on an embedded railing post affect the behavior of the concrete breakout failure method. By varying the parameters, it is possible to observe and measure how the actual results compare to theoretical results predicted by the ACI 318-14 code. With the test results, the design assumption that uncoupling the moment to get the shear force can also be explored to see if this is a valid design assumption. A literature review was conducted on the pertinent research behind the equations ACI uses to predict the breakout capacity that the concrete has when subjected to shear loads.

Chapter 2 - Literature Review

2.1 - Introduction

This chapter mainly focuses on the literature that led to the design methods that are currently in ACI 318 – 14 to determine the breakout capacity of concrete when subjected to shear force perpendicular to the edge.

2.2 – The Work of Fuchs, Eligehausen and Breen

The Concrete Capacity Design (CCD), discussed in greater detail in the study by Werner Fuchs, Rolf Eligehausen and John E. Breen (1995), attempts to provide a "user friendly" and "highly transparent model and for the design of post-installed steel anchors or cast-in-place headed studs or bolts" (Fuchs, Eligenhausen and Breen, 1995). This approach to predicting the concrete capacity is compared to the well-known provisions, of its time, from ACI 349-85, *Code Requirements for Nuclear Safety Related Concrete Structures*. Both methods "predict the concrete failure load in uncracked concrete under monotonic loading" (Fuchs, Eligenhausen and Breen, 1995). The test bank of data used in the comparison included approximately 1200 European and American tests. The paper goes on to explain why the CCD method can accurately predict the concrete failure load for all applications of the fasteners tested. The paper also discusses the applications that are sometimes unconservative and sometimes conservative in ACI 349. The CCD method, on the other hand, is "more user-friendly for design". The authors recommend the CCD method as a basis for design. The CCD method can more accurately predict the concrete failure load on fasteners in uncracked concrete under a monotonic load and is currently used in today's most modern edition of code, ACI 318-14 Building Code Requirements for Structural Concrete (Fuchs, Eligenhausen and Breen, 1995).

2.2.1 - Behavior Under Shear Loading According to ACI 349-85

Failure modes for shear are given in Figure 1.

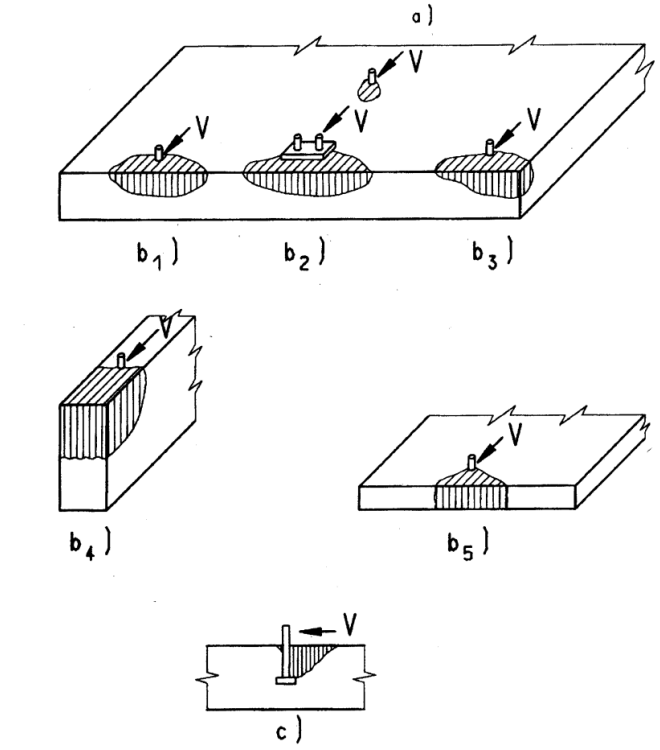

Figure 1 - Failure Modes for Fasteners Under Shear Loading: (a) Steel Failure Preceded by Concrete Spall; (b) Concrete Breakout; (c) Concrete Pryout Failure for Fasteners far From Edge.

From Fuchs, Eligehausen and Breen (1995), p. 76.

In shear, a brittle concrete failure will occur when the anchor is placed close enough to the edge as seen in Figure 1(b). For anchors embedded sufficiently far enough from the edge, two failure methods can occur. The first failure method for anchors located sufficiently far from the edge, is steel failure as seen in Figure 1(a), which is proceeded with the spalling of concrete in front of the anchor. The second failure method for anchors located sufficiently far from the edge is concrete pryout, as seen in Figure 1(c). Concrete pryout may occur when the anchor has a small ratio of embedment depth to anchor diameter and also has a high tensile capacity.

Figures 2 and 3 show the concrete breakout cone for a single anchor, as idealized by ACI 349 (Fuchs, Eligenhausen and Breen, 1995). It is evident that the concrete cone failure load depends on the tensile capacity of the concrete.

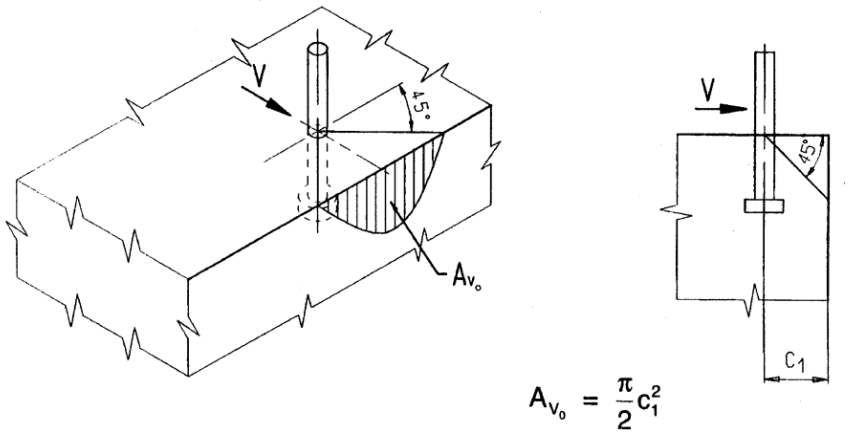

Figure 2 - Concrete Breakout Idealized According to ACI 349: Single Fastening Installed in Thick Concrete Member.

From Fuchs, Eligehausen and Breen (1995), p. 78.

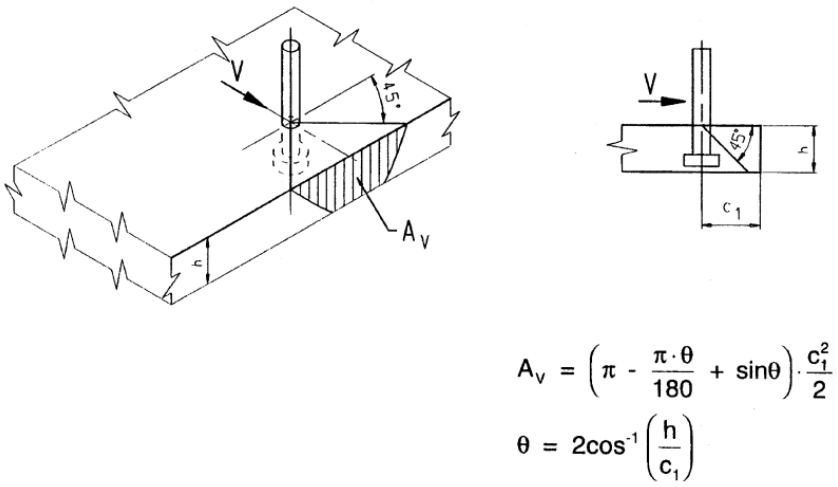

Figure 3 - Concrete Breakout Idealized According to ACI 349: Single Fastening Installed in Thin Concrete Member ($h < 2c_1$).

From Fuchs, Eligehausen and Breen (1995), p. 78.

The equations for Figures 2 and 3 are listed, respectively:

$$A_{v_o=\frac{\pi}{2}\cdot c_1^2},\ in^2 \quad , \tag{1}$$

$$A_v = \left(\pi - \frac{\pi\cdot\theta}{180} + sin\theta\right)\cdot\frac{c_1^2}{2},\ in^2 \quad , \tag{2}$$

$$\theta = 2cos^{-1}\left(\frac{h}{c_1}\right). \tag{3}$$

The shear capacity of an individual anchor failing the concrete, Figure 2, assuming that the concrete half-cone is fully developed, is

$$V_{no} = \phi\cdot 4\sqrt{f_c'}\cdot\frac{\pi}{2}c_1^2,\ lb. \tag{4}$$

In applications when the overall depth of the concrete member is small $(h < c_1)$ and/or the spacing is close $(s < 2\cdot c_1)$ and/or the edge distance perpendicular to the load direction is small $(c_2 < c_1)$, then the load has to be reduced with the aid of the projected area on the side of the concrete member,

$$V_n = A_V\cdot 4\cdot\sqrt{f_c'},\ \ lb \tag{5}$$

$$= \frac{A_V}{A_{Vo}}\cdot 4\cdot\sqrt{f_c'}\cdot\frac{\pi}{2}\cdot c_1^2\ , \tag{6}$$

where,

$A_V =$ actual projected area,

$A_{Vo} =$ projected area of one fastener unlimited by edge influences, cone overlapping or member thickness, Figure 2,

$= \pi/2\cdot c_1^2$.

It should be noted that the cone concept seen in Figure 3, per ACI 349, is the projected area seen, and gets complex to solve for when the projected area is influenced by slab thickness and/or the overlap of failure cones (Fuchs, Eligenhausen and Breen, 1995).

2.2.2 - Behavior Under Shear Loading According to CCD Methodology

The CCD methodology for determining the concrete failure cone for an individual fastener assumes an idealized rectangular pyramid projected area instead of the cone projected area that ACI 349 assumes, as seen in Figure 4 (Fuchs, Eligenhausen and Breen, 1995).

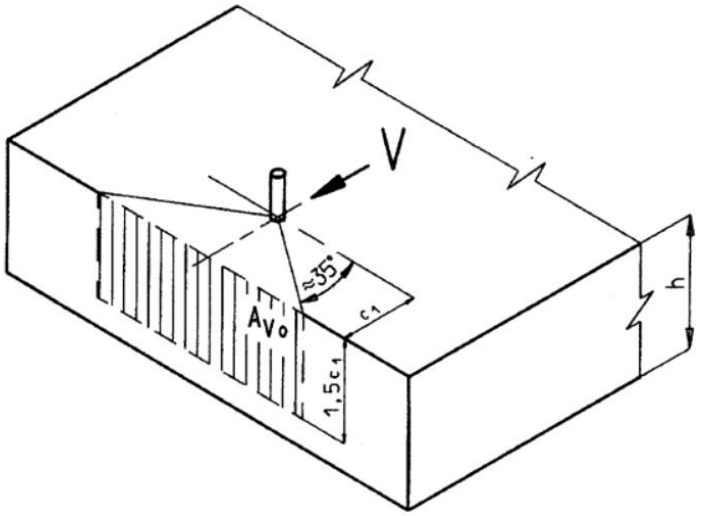

Figure 4 – Concrete Failure Zone Simplified Design Model According to CCD Method.

From Fuchs, Eligehausen and Breen (1995), p. 83.

Figure 5 shows the concrete failure zone of a single fastening installed in thick concrete member not influenced by member thickness or edge distance parallel to shear load (Fuchs, Eligenhausen and Breen, 1995).

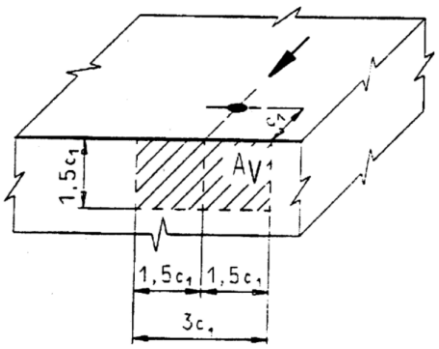

$$A_V = A_{V_o} \quad \text{(single fastening)}$$
$$= 1.5c_1(2 \cdot 1.5c_1)$$
$$= 4.5 \cdot c_1^2$$

Figure 5 – CCD Failure Zone Simplified Design Model: Single Fastening Installed in Thick Concrete Member Not Influenced by Member Thickness or Edge Distance Parallel to Shear Load.

From Fuchs, Eligehausen and Breen (1995), p. 84.

Figure 6 shows the failure zone of a single fastening installed in thick concrete with its capacity limited by edge distance parallel to the direction of the shear load (Fuchs, Eligenhausen and Breen, 1995).

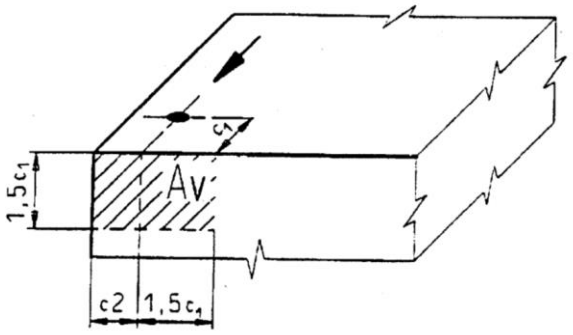

$$A_V = 1.5c_1(1.5c_1 + c_2)$$
$$\text{if: } c_2 \leq 1.5c_1$$

Figure 6 – CCD Failure Zone Simplified Design Model: Single Fastening Installed in Thick Concrete Member, Capacity Limited by Edge Distance Parallel to Direction of Load.

From Fuchs, Eligehausen and Breen (1995), p. 84.

Figure 7 shows the failure zone of a single fastening only influenced by member thickness (Fuchs, Eligenhausen and Breen, 1995).

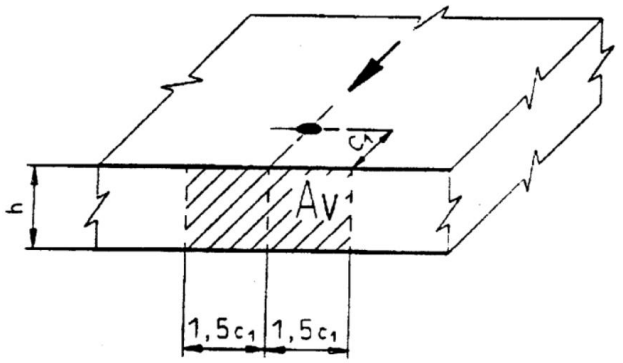

Figure 7 - CCD Failure Zone Simplified Design Model: Single Fastening Only Influenced by Member Thickness.

From Fuchs, Eligehausen and Breen (1995), p. 84.

The equations for Figures 5, 6 and 7 are given, respectively:

$$A_V = A_{V_o},\ in^2 \quad \text{(single fastener)} \tag{4}$$

$$= 1.5c_1(2 \cdot 1.5c_1),\ in^2$$

$$= 4.5 \cdot c_1^2,\ in^2$$

$$A_v = 1.5c_1(1.5c_1 + c_2), in^2 \tag{5}$$

if: $c_2 \leq 1.5c_1, in^2$

$$A_V = 2 \cdot 1.5c_1 \cdot h, in^2 \tag{6}$$

If: $h \leq 1.5c_1$.

The authors point out the relative ease for calculating the projected area for the CCD method as seen in Equations (4), (5) and (6), when compared to the calculation of the projected areas for the ACI 349 method, as seen in Equations (1), (2) and (3) (Fuchs, Eligenhausen and Breen, 1995).

For an individual anchor in a thick uncracked structural member under shear load toward the free edge, the concrete capacity is

$$V_{no} = 13(1/d_o)^{0.2}\sqrt{d_o}\cdot\sqrt{f_c'}\cdot c_1^{1.5},\ lb \tag{7}$$

where,

$d_o =$ outside diameter of fastener, in.,

$l \ =$ activated load-bearing length of fastener, in., $\leq 8d_o$,

$= h_{ef}$ for fasteners with a constant overall stiffness, such as headed studs, undercut anchors and torque controlled expansive anchors, where there is no distance sleeve, or the expansion sleeve also has the function of the distance sleeve

$= 2d_o$ for torque-controlled expansive anchors with distance sleeves separated from the expansion sleeve,

$c_1 =$ edge distance in loading direction, in.

According to Equation (7), the shear failure load does not increase with the failure surface area, which is proportional to c_1^2. It is actually proportional to $c_1^{1.5}$. This is due to size effect. Furthermore, the failure load is influenced by the anchor stiffness and diameter (Fuchs, Eligenhausen and Breen, 1995).

The shear load capacity of a single anchor loaded toward the edge can be evaluated in Equation (8):

$$V_n = \frac{A_v}{A_{vo}} \cdot \psi_4 \cdot \psi_5 \cdot V_{no},\ lb \tag{8}$$

where,

A_v = actual projected area at side of concrete member, idealizing the shape of the fracture area of individual anchors as a half-pyramid with side length $1.5c_1$ and $3c_1$, as seen in Figure 6 and 7,

A_{vo} = projected area of one fastener unlimited by corner influences, spacing or member thickness, idealizing the shape of the fracture area as a half-pyramid with side lengths $1.5c_1$ and $3c_1$, as seen in Figure 4 and 5,

ψ_4 = effect of eccentricity of shear,

$$= \frac{1}{1+2e'_v/(3c_1)}, \tag{9}$$

e'_v = distance between resultant shear force of fasteners of group resisting shear and centroid of sheared fasteners,

ψ_5 = tuning factor considering disturbance of symmetric stress distribution caused by a corner,

$$= 1 \ \ if \ \ c_2 \geq 1.5c_1,$$

$$= 0.7 + 0.3 \cdot \frac{c_2}{1.5c_1} \ \ if \ \ c_2 \leq 1.5c_1, \tag{10}$$

c_1 = edge distance in direction of loading, in. as seen in Figure 5; for anchors in a narrow, thin member with $c_{2,max} < 1.5c_1$ ($c_{2,max}$ = maximum value of edge distances perpendicular to the loading direction) and $h < 1.5c_1$, the edge distance inserted into in Equations (8), (9) and (10) →

V_n, ψ_4 and ψ_5 is limited to c_1= max $\left(c_{2,max}/1.5\,;\ h/1.5\right)$. This gives a constant failure load independent of the edge distance c_1,

c_2 = edge distance perpendicular to load direction, as seen in Figure 6 (Fuchs, Eligenhausen and Breen, 1995).

2.2.3 - Comparison of Main Influence Parameters Between ACI 349 and CCD Methods

The main differences between the ACI 349 and CCD methods are as follows; they are also summarized in Table 1:

1. The way the edge distance c_1 influences the capacity of shear loading.

2. The assumed failure slope of the failure cone surface. ACI 349 assumes 45°, whereas CCD assumes ~35°. Examples of this can be observed in Figure 2 and 4, respectively.

3. The assumed projected area of failure. ACI 349 assumes a cone, while CCD approximates ACI 349's cone as a rectangular pyramid. Examples of the assumed failure cones can be observed in Figure 2 and 4, respectively. Both methods consider the influence of overlapping projected failure surfaces and influences from edges. Due to this, calculations are made easier by the use of CCD's rectangles and not ACI's 349 circles.

4. The CCD method takes into account disturbances of the stresses in the concrete caused by the influence of load eccentricities and edges. ACI 349 does not account for these influences (Fuchs, Eligenhausen and Breen, 1995).

Table 1 – Comparison of the Influence of Main Parameters on Maximum Load Predicted by ACI 349 and CCD Methods.

		ACI 349-85	CCD method
Anchorage depth, tension		h_{ef}^2	$h_{ef}^{1.5}$
Edge distance, shear		c_1^2	$c_1^{1.5}$
Slope of failure cone		$\alpha = 45$ deg	$\alpha \approx 35$ deg
Required spacing to develop full anchor capacity		$2\,h_{ef}$, tension $2\,c_1$, shear	$3\,h_{ef}$, tension $3\,c_1$, shear
Required edge distance to develop full anchor capacity		$1\,h_{ef}$, tension $1\ c_1$, shear	$1.5\,h_{ef}$, tension $1.5\ c_1$, shear
Small spacing or close to edge	1 direction	Nonlinear (area-proportional) reduction	Linear reduction
	2 directions		Nonlinear reduction
Eccentricity of load		—	Taken into account

Note. **From Fuchs, Eligehausen and Breen (1995), p. 85.**

2.2.3 - Comparison of Test Data Between ACI 349 and CCD Methods

This section includes the reproduced data extracted from the original data base from Fuchs (1991) in "Development of a Proposal for the Design of Fastenings to Concrete," to show the reader the number of tests that support the research. The original summary can be found in Fuchs' paper. Fuchs *et al.* (1995) only considered tests that resulted in concrete breakout.

Table 2, 3 and 4 provide the reader a general overview of the number of shear tests performed and the different parameters tested. The European tests with an anchor under shear loading varied slightly from the tests performed in the United States (U.S.). The European tests utilized a sheet of fluoropolymer between the concrete and the steel plate. The purpose of this sheet is to minimize the friction between the concrete and the steel surface caused by reduction of prestressing force with time and also by the use of a plate with a relatively smooth surface (e.g., greased, cold formed, or painted plate). The U.S. tests did not utilize the fluoropolymer sheet in their testing. The steel plate was attached directly to the concrete surface with no fluoropolymer

sheet in between. Due to the increases in friction between the steel and concrete, the U.S. test's yielded higher values (Fuchs, Eligenhausen and Breen, 1995).

Table 2 – Single Fastenings with Post-Installed Fasteners and Fully Developed Concrete Breakout, Test Series – Shear Loading.

Country of test	n	f'_{cc200}, N/mm^2			h_{ef}, mm			d, mm			c_1, mm		
		Minimum	Average	Maximum	Minimum	Average	Maximum	Minimum	Average	Maximum	Minimum	Average	Maximum
USA	60	21.3	31.7	53.9	25.0	94.5	220.0	8.0	20.9	32.0	40.0	128.3	300.0
D	84	16.1	25.7	48.4	27.4	70.3	167.6	6.4	14.6	25.4	38.1	98.0	203.2
Σ	144	16.1	28.2	53.9	25.0	80.4	220.0	6.4	17.2	32.0	38.1	110.6	300.0

Note. **From Fuchs, Eligehausen and Breen (1995), p. 87.**

Table 3 – Single Fastenings with Post-Installed Fasteners in Concrete Members with Limited Thickness, Single Tests – Shear Loading.

Country of test	n	f'_{cc200}, N/mm^2			h_{ef}, mm			d, mm			c_1, mm			c_2, mm		
		Minimum	Average	Maximum	Minimum	Average	Maximum	Minimum	Average	Maximum	Minimum	Average	Maximum	Minimum	Average	Maximum
D	38	35.2	42.8	46.4	155.0	250.8	306.0	20.0	27.5	40.0	63.0	140.2	220.0	62.5	184.1	300.0

Note. **From Fuchs, Eligehausen and Breen (1995), p. 87.**

Table 4 – Double Fastenings in Thick Concrete Members, Single Tests.

Anchorage device	Country of test	n	f'_{cc200}, N/mm^2			h_{ef}, mm			d, mm			c_1, mm			c_2, mm		
			Minimum	Average	Maximum	Minimum	Average	Maximum	Minimum	Average	Maximum	Minimum	Average	Maximum	Minimum	Average	Maximum
Expansion anchor	D	36	20.5	24.8	27.2	80.0	81.7	100.0	18.0	20.7	24.0	80.0	172.1	200.0	80.0	190.0	400.0

Note. **From Fuchs, Eligehausen and Breen (1995), p. 87.**

Figure 8, shows the comparison between the European and U.S. results of a single post-installed anchor fastener in thick concrete members with the design procedures for ACI 349 and CCD, as depicted on the graphs. The tests performed had the following varying parameters,

1. Concrete strengths,
2. Anchor diameters,
3. Ratios of embedment depth to anchor diameter.

Due to the varying parameters between the tests, the failure load was transformed to a concrete strength of $f'_{cc} = 25$ N/mm^2 ($f'_c = 3070$ psi), anchor diameter $d_o = 18$mm (0.71 in.) and a ratio $l/d_o = 8$, by multiplying the failure load with the following factors $(25/f'_{cc,test})^{0.5} \cdot (18/d_{o,test})^{0.5} \cdot [8/\ (l/d)]^{0.2}_{test}$. The concrete breakout failure loads in the U.S. tested higher when compared to the European results, especially at a smaller edge distance. As mentioned before, this variation of test results at the smaller edge distances can be attributed to the use of the fluoropolymer sheet in the U.S. tests that was not used in the European tests. The absence of the fluoropolymer sheet results in increased friction between the steel and concrete resulting in higher shear capacity (Fuchs, Eligenhausen and Breen, 1995).

Fuchs *et al.* (1995) found that the failure loads predicted by CCD agreed well with the average failure loads measured in the European tests. However, the failure loads predicted by ACI 349, are conservative for small edge distances and unconservative for large edge distances. Fuchs *et al.* (1995) attribute this variance in the failure loads predicted by ACI 349 due to the neglect of size effect on the test. The U.S. results yielded conservative results on both CCD and ACI 349; this is due to the increased friction from differing testing procedures (Fuchs, Eligenhausen and Breen, 1995).

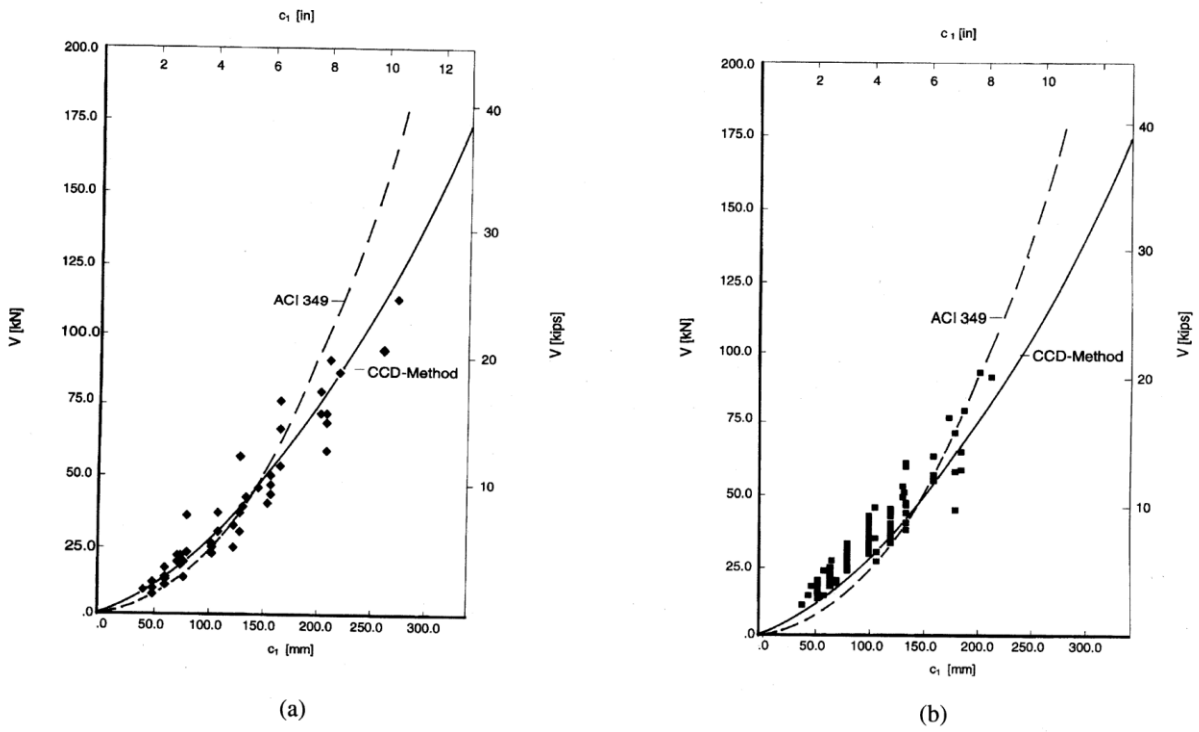

Figure 8 – Comparison of Shear Test Results with ACI 349 and CCD Method for Single Post-Installed Fasteners in Thick Concrete Member: (a) European Tests; (b) U.S. Tests.

From Fuchs, Eligehausen and Breen (1995), p. 92.

Figures 9 and 10 show the average values of the ratio $V_{u,test}/V_{n,predicted}$ and the corresponding coefficients of variation for the post-installed fasteners for both the European and U.S. test results, respectively.

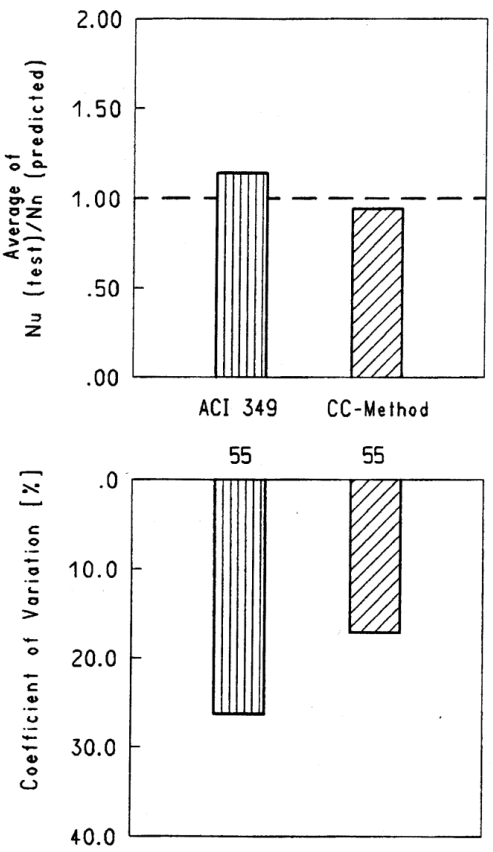

Figure 9 – Comparison of Design Procedures for European Tests with Single Post-Installed Fasteners on Thick Concrete Members – Shear Loading Toward Edge

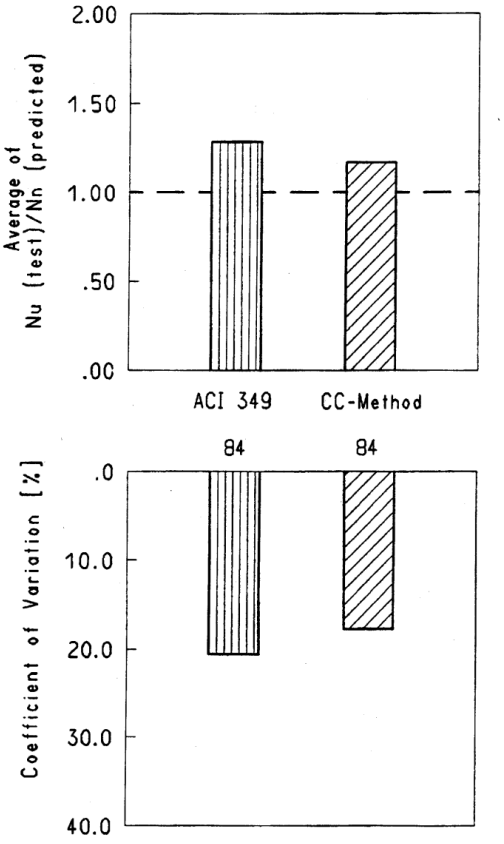

Figure 10 – Comparison of Design Procedures for U.S. Tests with Single Post-Installed Fasteners in Thick Concrete Members – Shear Loading Toward Edge

From Fuchs, Eligehausen and Breen (1995), p. 92.

Figures 9 and 10 show that the ACI 349 values, on average, are more conservative but, as Fuchs *et al.* (1995) state, this is due to the fact that most of the tests are done with small edge distances. Please note that the Y axis of Figures 9 and 10, read "Average of $N_{u,\,test}/N_{n,\,predicted}$ ". The authors may have made a mistake and the Y axis for Figures should actually read " Average of $V_{u,\,test}/V_{n,\,predicted}$." N_u denotes a tensile load. Fuchs *et al.* (1995) also cover tensile loading in the study but

it is not covered in this paper. The authors go on to point out that the coefficients of variation for ACI 349 are larger (Fuchs, Eligenhausen and Breen, 1995).

2.2.4 - Conclusions of Study

In this study, Fuchs *et al.* (1995) found the concrete capacity of fastenings with cast-in-place headed studs and post installed anchors in uncracked concrete as predicted by ACI 349 and the CCD method. The predicted results, as found by the two methods, were compared to the test results in Table 2, 3 and 4. Based on the results and comparisons, the following conclusions were drawn by Fuchs *et al.* (1995):

1. ACI 349 assumes that the predicted failure load increases with the square of the embedment depth. On the other hand, the CCD method takes into account size effect and assumes the failure load to be proportional to the embedment depth to the 1.5 power.
2. In certain applications, such as a single anchor in thin concrete members loaded in shear, the capacity is more accurately depicted by the CCD method, when compared to ACI 349. ACI 349 found the capacities in the certain cases are significantly unconservative. The authors attribute this to the fact that ACI 349 assumes a 45-degree failure cone. The CCD method, on the other hand, assumes an inclination of 35 degrees for the failure surface, which produces better agreement with test results.
3. Both methods produce results accurately predicting the mean capacity. In certain situations, the coefficient of variation of the ratio of the measured failure load per ACI 349 is significantly larger, ~45%. Whereas, the CCD method, for all cases, produced a coefficient of variation that was consistent and smaller across all applications, 15-20%.

4. The calculation to find the projected failure area is easier in the CCD method due to the use of rectangles. This makes calculations more user friendly when compared to the ACI 349's use of circular area (Fuchs, Eligenhausen and Breen, 1995).

Chapter 3 - Methods

3.1 - Specimen

This chapter mainly covers material, configuration of test specimens and the procedure of testing of the specimens.

3.1.1 - Configuration

A total of 36 pipes were cast-in place into four different concrete blocks. Each concrete block has two corner tests and a varying amount of non-corner tests in between the two corner tests.

Figure 11 shows a side view of a typical concrete member.

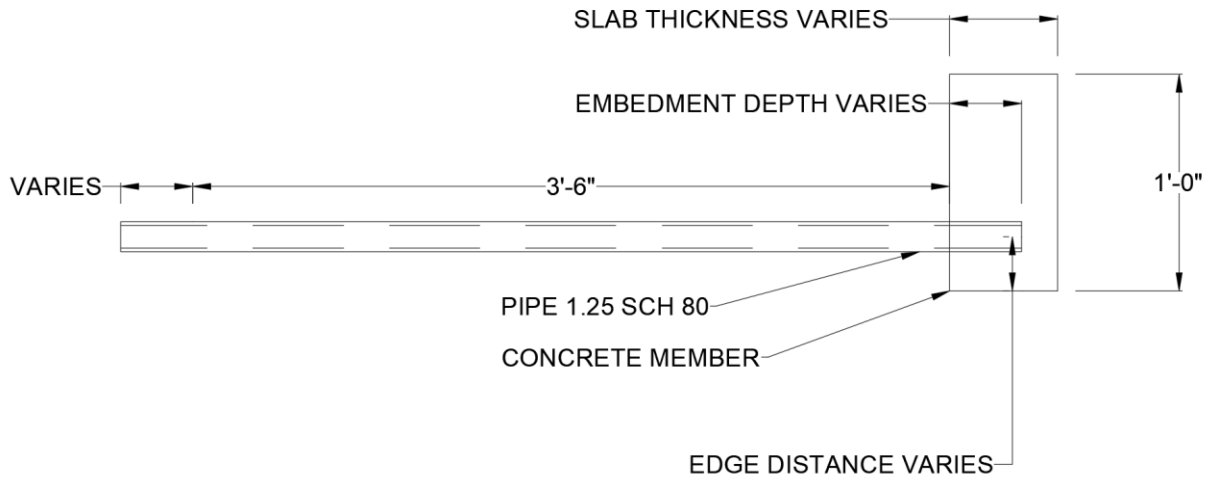

Figure 11 – Experimental Specimen.

Figure 12 shows a view looking directly down the embedded pipes.

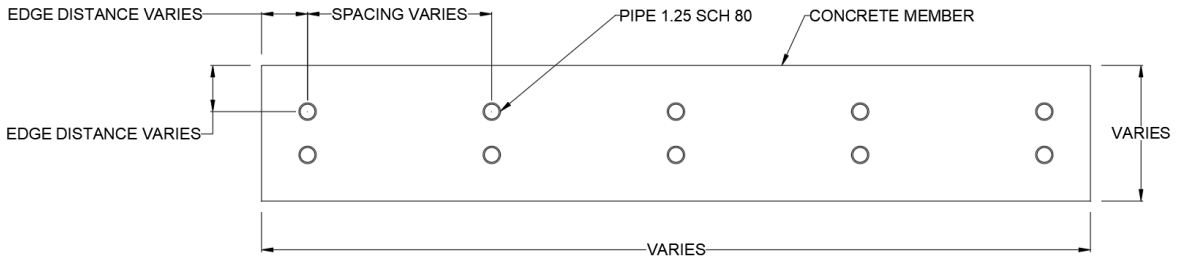

Figure 12 – Experimental Specimen.

Figure 13 shows the layout of the inside of the concrete form that includes all four concrete members and all 36 tests. The pipe type, setback and embed depth is given on the left side of the figure and corresponds with each row. The test number is noted in the figure.

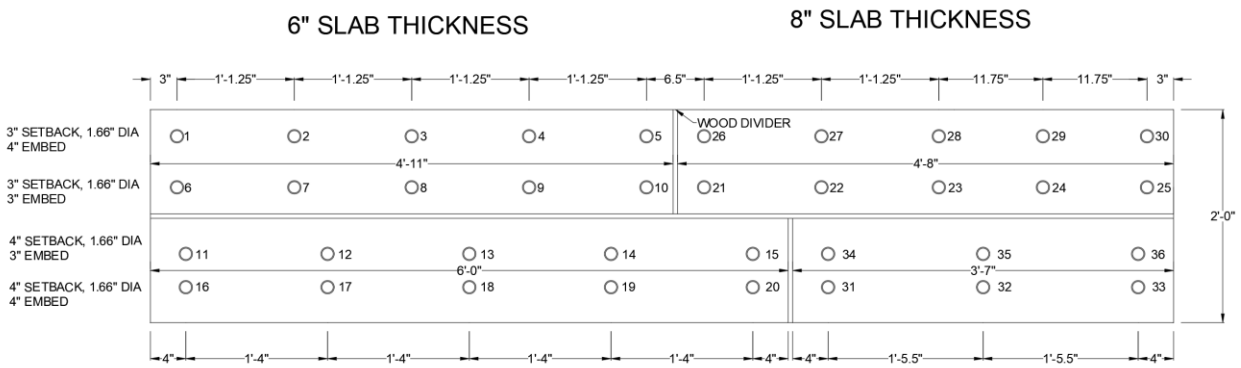

Figure 13 – Experimental Specimen.

Table 5 gives the test number and the corresponding dimensions of the parameters for that test.

Table 5 – Test Number and Planned Dimensions of Parameters of Each Test.

Post	Slab Depth [in]	Edge Distance, C_{a1} [in]	Edge Distance, C_{a2} [in]	Embed Depth [in]
1	6	3	3	4
2	6	3	N/A	4
3	6	3	N/A	4
4	6	3	N/A	4
5	6	3	3	4
6	6	3	3	3
7	6	3	N/A	3
8	6	3	N/A	3
9	6	3	N/A	3
10	6	3	3	3
11	6	4	4	3
12	6	4	N/A	3
13	6	4	N/A	3
14	6	4	N/A	3
15	6	4	4	3
16	6	4	4	4
17	6	4	N/A	4
18	6	4	N/A	4
19	6	4	N/A	4
20	6	4	4	4
21	8	3	3	3
22	8	3	N/A	3
23	8	3	N/A	3
24	8	3	N/A	3
25	8	3	3	3
26	8	3	3	4
27	8	3	N/A	4
28	8	3	N/A	4
29	8	3	N/A	4
30	8	3	3	4
31	8	4	4	4
32	8	4	N/A	4
33	8	4	4	4
34	8	3	4	3
35	8	3	N/A	3
36	8	3	4	3

3.1.2 - Formwork

The concrete forms were made out of dimensional lumber, plywood and screws. Figure 14 shows the form that was used for the project. The lumber laying inside the form, with holes drilled into them, are the pipe holders while the concrete cures.

Figure 14 – Empty Concrete Form.

Figure 15 is a picture taken during the second pour day. There were no pictures taken during the first pour day. The first and second concrete pour day happened one week apart.

Figure 15 – 2nd Concrete Pour Day.

Figure 16 shows the concrete directly after the second pour day with the pipes embedded.

Figure 16 – Post 2nd Pour Day.

Figure 17 shows the laboratory where the concrete for the project was poured. As seen in the figure, multiple other projects took place at the same time in the laboratory. Figure 18 shows the concrete form after the pipe holders had just been removed.

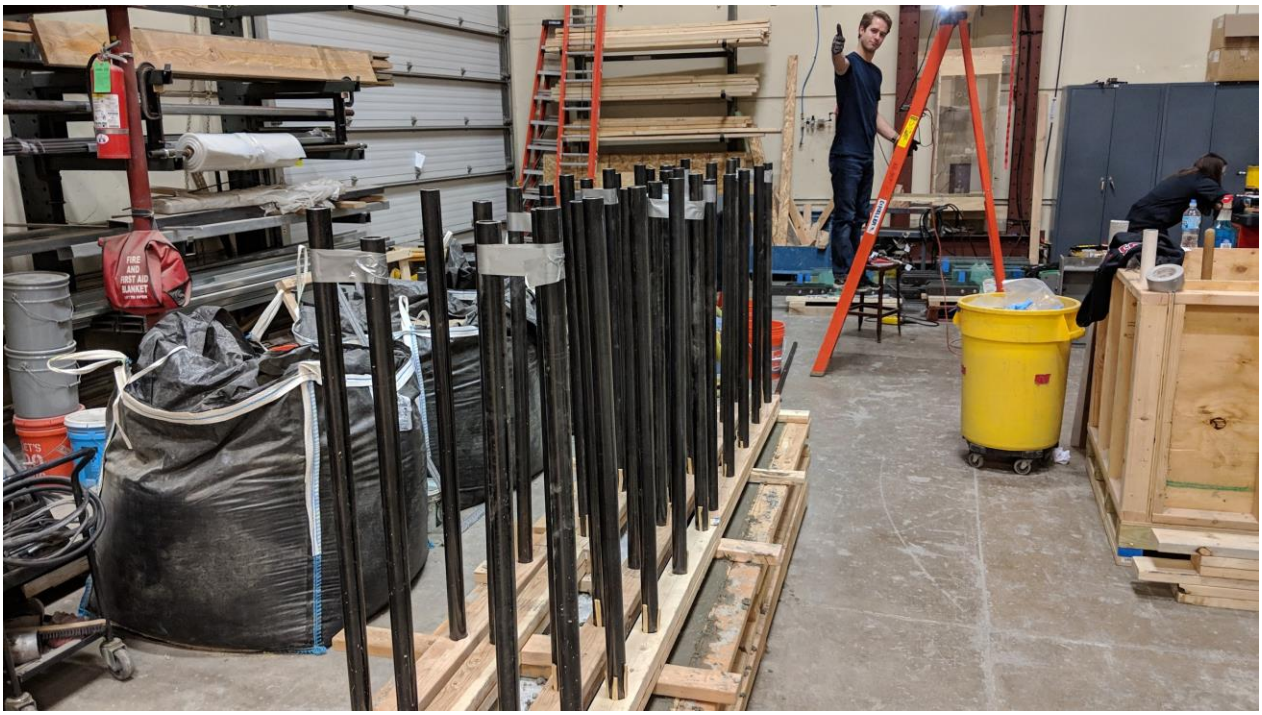

Figure 17 – Laboratory Area.

Figure 18 – Concrete Members Fully Cured.

Figure 19 shows the concrete members without the form sides. Two, one inch thick foam pads were used to achieve a slab thickness of six in.

Figure 19 – Concrete Members with Form Walls Stripped.

3.1.3 - Concrete

The ratio that was used to make the concrete for the concrete members was 1-part cement to 2.4-parts sand to 2.6-parts aggregate. Table 6 shows the amount used for each batch. The concrete mixer used in Figure 15, had a capacity of 2.5 ft^2. The concrete mix was designed to yield a 28-day strength of 4000 psi.

Table 6 – Concrete Ratio.

Cement	0.33	ft^3
Sand	0.79	ft^3
Aggregate	0.86	ft^3
Total	1.98	ft^3

(a)

Cement	31.02	lb
Sand	79.20	lb
Aggregate	85.80	lb
Total	196.02	lb

(b)

Table 7 lays out the results of the concrete cylinder compressive tests. The concrete cylinders could not be tested exactly at 28 days. The cylinders were tested as soon as possible after the 28-day mark.

Table 7 – Concrete Cylinder Results.

Tests Embedded in Concrete	Date Poured	Test	Test Date	Force [lb]	Diameter [in]	Strength [psi]	Average Strength [psi]
11-20, 31-36	2/2/2019	7 Day	2/9/2019	33300	3	4711	
11-20, 31-36	2/2/2019	37 Day	3/11/2019	43000	3	6083	
11-20, 31-36	2/2/2019	37 Day	3/11/2019	40400	3	5715	
11-20, 31-36	2/2/2019	37 Day	3/11/2019	47500	3	6720	6173
1-10, 21-30	2/9/2019	7 Day	2/16/2019	37800	3	5348	
1-10, 21-30	2/9/2019	30 Day	3/11/2019	51300	3	7257	
1-10, 21-30	2/9/2019	30 Day	3/11/2019	48000	3	6791	
1-10, 21-30	2/9/2019	30 Day	3/11/2019	50200	3	7102	7050

Figure 20 shows the compressive strength for the first concrete pour.

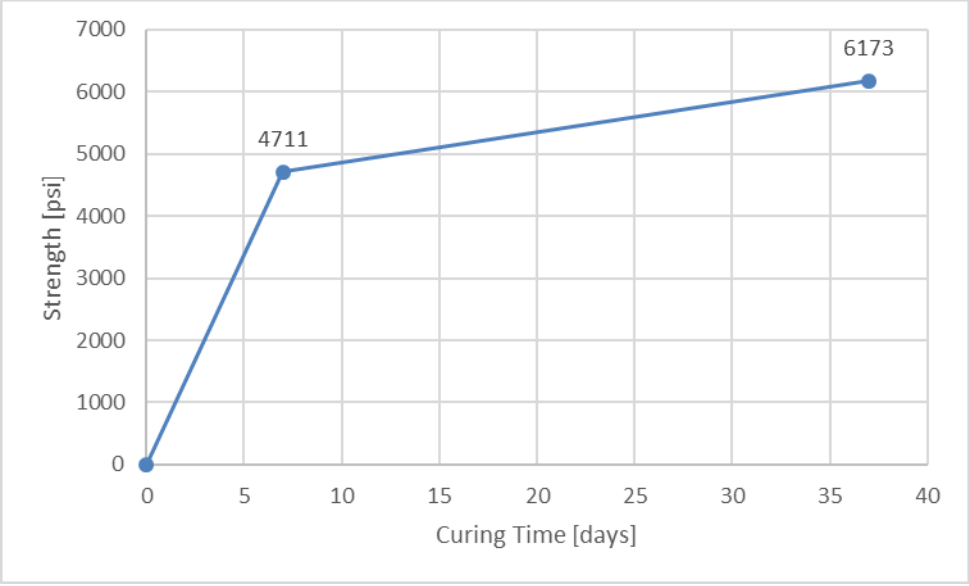

Figure 20 – Compressive Strength for Tests 11-20 and 31-36.

Figure 21 shows the compressive strength for the second concrete pour. The concrete yielded a higher than expected compressive strength for both pours. This could be due to a couple of reasons.

1. The water was added by hand until a workable mix was reached.
2. The mix design could be incorrect and favor higher strength.

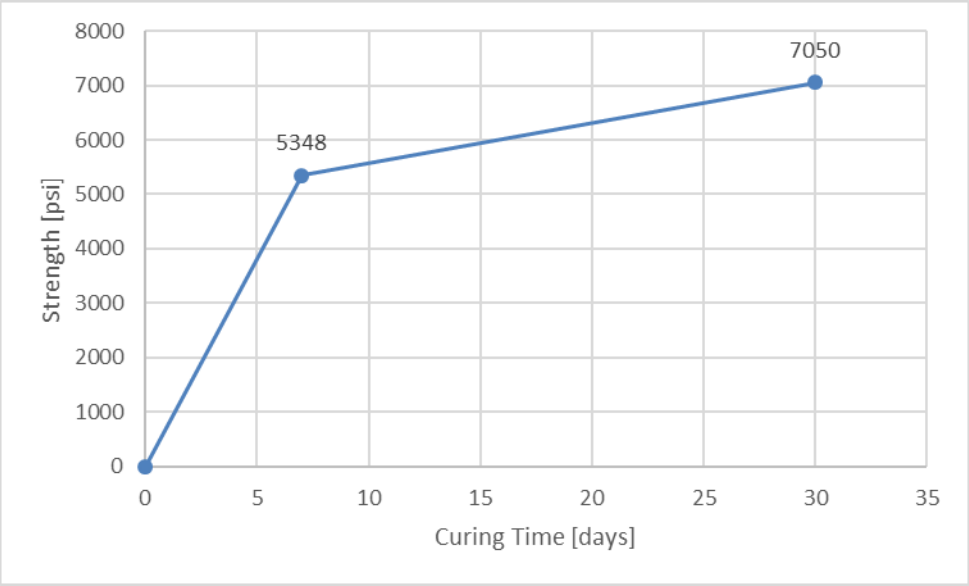

Figure 21 – Compressive Strength for Tests 1-10 and 21-30.

Both concrete pours yielded higher than expected final compressive strengths. All pictures of the compressive tests can be found in the appendix.

3.1.4 - Steel

Badger Railing, located in Milwaukee, WI, donated the pipe that was utilized in testing. The pipe utilized was 36 pieces of ASTM A500 1-1/4 in. schedule 80 at 50 in. long. The yield strength of the pipe was 68,000 psi. The certification for the pipe, that was provided by Badger Railing, can be found in the appendix.

3.2 - Setup

3.2.1 - Testing Configuration

As is seen in Figure 22, the testing frame consisted of dimensional lumber, screws and oriented strand board (OSB). Each A-frame was situated to be in between the projected concrete breakout failure area. The A-frames were made such that both the 6 -in. and 8-in. slab depth concrete members both fit. The concrete members, after being lifted by the overhead crane into the testing frame, were tightly shimmed into place. The concrete members were tightly shimmed to help prevent the rotation of the concrete as the load was applied.

Figure 22 – Initial Testing Frame Configuration.

As seen in Figure 23, a plywood gusset was retro-fitted to the existing frame to prevent the wood from splitting where the plywood gusset plates were added.

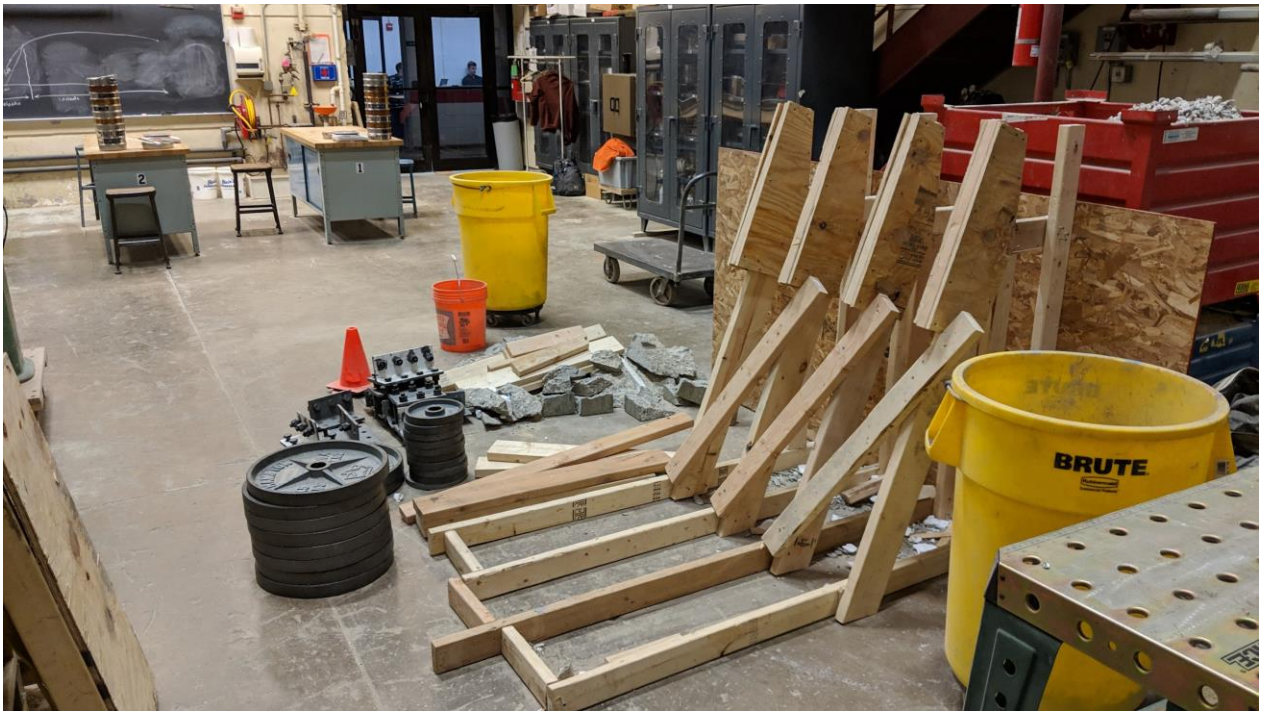

Figure 23 – Final Testing Frame Configuration.

3.2.2 - Testing Procedure for Concrete Breakout

Each block was positioned into the testing frame as best as possible so that the reactions from the supports did not interact with the projected concrete breakout failure area. The corner pipes were tested first, followed by the pipes located closer toward the center of the concrete member. A hose clamp was added so the carabiner hanging on the pipe did not slide off as the pipe deflected as the load was increased. The hose clamp was situated such that the carabiner would inflict a point load at an eccentricity of 42 in. The failure load was determined for the specific test. The wooden basket, which was made to hang the weights, as seen in Figure 22, was placed on the pipe at the correct location. The wooden basket with the yellow straps and metal hardware, altogether, weighed 25 lb. Next, the 45 lb. weights were added until approximately 75% of the predicted failure load was reached. At this point, the 10 lb. weights were added until a concrete

breakout failure was achieved, or four 10 lb. plates were added with no concrete breakout failure. If no concrete breakout failure was achieved, the four 10 lb. weights were removed, and a 45 lb. weight was then added, and the process was repeated until either concrete breakout failure resulted or until all ten 45 lb. plates had been added. After all of the 45 lb. weights were added, the 10 lb. plates were added to achieve breakout failure. If still no breakout failure had been reached, scrap angles and WT's were used. These weighed approximately 20 lb. apiece.

3.2.3 - Testing Procedure for Deflection

Either a laser pointer or a metal rod was attached to the end pipe prior to testing. The distance between the end of the pipe and the surface where the deflection measurements would be recorded was measured. An initial mark was made with no load on the pipe. The deflection was marked at each load step for each test. Through the bending of the pipe, the actual deflection was then calculated.

3.2.4 - Testing Procedure for Rotation

The rotation of the concrete specimen in the wooden testing frame was measured by using either measuring the rotation of the end of an untested pipe or the end of a 2X4 piece of wood that was clamped to the concrete piece. A vertical 2X4 piece of wood was fixed in front of point of measure on either the pipe or the 2X4. A mark was made on the vertical 2X4 before any weights was added. A mark was added at each load step so the total distance could be recorded at failure of the concrete. The measurement from the vertical 2X4 to mid depth of the slab was recorded. Using trigonometry, the amount of rotation in the concrete specimen and the amount of deflection at the load during testing can be found.

Chapter 4 – Results

This section covers the results of the testing performed.

4.1 – As-Built Dimensions per Test

The parameters for each test were measured so that a more accurate prediction of failure for each test could be made. Table 8 lists the specific as-built dimensions for each test performed.

Table 8 - As-Built Dimensions per Test.

Test	Slab Depth, D [in]	C_{a1} [in]	C_{a2} [in]	Embed Depth, h_{ef} [in]	Diameter of Anchor, d_a [in]	f'c [ksi]
1	6.25	2.875	3.13	3.94	1.66	7.05
2	6.25	3	N/A	4	1.66	7.05
3	6	3	N/A	3.94	1.66	7.05
4	6.13	3	N/A	3.94	1.66	7.05
5	6.13	3	3.38	3.88	1.66	7.05
6	6.25	3.25	3.38	2.94	1.66	7.05
7	6.25	3	N/A	2.88	1.66	7.05
8	6	3.13	N/A	2.88	1.66	7.05
9	6.13	3.25	N/A	3	1.66	7.05
10	6.13	3.13	3.38	2.69	1.66	7.05
11	6.13	4	4.13	2.88	1.66	6.17
12	6.25	4.13	N/A	3.5	1.66	6.17
13	6.38	4	N/A	2.88	1.66	6.17
14	6.25	4	N/A	2.88	1.66	6.17
15	6.13	4	4.13	2.88	1.66	6.17
16	6.13	4	4.13	4	1.66	6.17
17	6.25	4	N/A	4	1.66	6.17
18	6.38	4.13	N/A	3.88	1.66	6.17
19	6.25	4	N/A	4.19	1.66	6.17
20	6.13	4	4.38	4	1.66	6.17
21	8	3	2.75	3	1.66	7.05
22	8.25	3	N/A	2.81	1.66	7.05
23	8.25	3	N/A	2.81	1.66	7.05
24	8.25	3	N/A	2.75	1.66	7.05
25	8.25	3	3.13	2.81	1.66	7.05
26	8	3.13	2.75	3.75	1.66	7.05
27	8.13	3.31	N/A	3.81	1.66	7.05
28	8.13	3.38	N/A	4	1.66	7.05
29	8.25	3.5	N/A	3.75	1.66	7.05
30	8.5	3.63	3.25	3.75	1.66	7.05
31	8	4.38	4.13	4.5	1.66	6.17
32	8	4.25	N/A	3.88	1.66	6.17
33	8	4.25	4	5.06	1.66	6.17
34	8	2.75	3.88	3.75	1.66	6.17
35	8	2.88	N/A	2.94	1.66	6.17
36	8.25	2.81	4.13	3	1.66	6.17

4.2 - Failure Modes

This project focused on tests that either had the projected failure cone influenced by edge distance at a corner or not influenced at a corner (non-corner). The slab depth varied, but according to Equation (5), the maximum embedded post of 4 in. would not have its projected failure cone influenced by the minimum slab depth of 6 in.

4.2.2 - Concrete Breakout in Corner Tests

Table 9 lists the failure loads for all corner tests, along with the type of failure. For the tests listed as "yield", the pipe never reached full yield for any test, the pipe yielded enough that the bottom of the weight holding basket would touch the ground beneath it, rendering the test complete. For the test listed as "no test", the particular test was not testable due to major cracking from previous adjacent tests.

Table 9 – Failure Loads and Type of Failure for Corner Tests.

Test	Predicted Failure Load Per As-Builts [lb]	Failure Load [lb]	Breakout, Pipe Yield or No Test?	$V_{u,tested}/V_{n,predicted}$
1	313	340	Breakout	1.09
5	345	0	No test	N/A
6	322	345	Breakout	1.07
10	289	295	Breakout	1.02
11	449	445	Breakout	0.99
15	449	365	Breakout	0.81*
16	551	555	Breakout	1.01
20	572	565	Breakout	0.99
21	257	260	Breakout	1.01
25	267	295	Breakout	1.10
26	314	388	Breakout	1.24
30	427	505	Breakout	1.18
31	671	680	Yield	1.01
33	677	671	Yield	0.99
34	312	427	Breakout	1.37*
36	292	340	Breakout	1.16

The asterisk in the $V_{u,tested}/V_{n,predicted}$ column of Table 9 denotes a possible outlier to the test group. Test 15 had honey combing in the concrete due to lack of compaction in this area of the concrete, this likely negatively influenced the capacity of the test. Test 34 likely had a larger than expected breakout area and had a reaction from the test frame supports that positively influenced the capacity of the test.

4.2.3 - Concrete Breakout in Non-Corner Tests

Table 10 lists the failure loads for all non-corner tests, along with the type of failure. For the tests listed as “yield”, the pipe never reached full yield for any test, but the pipe yielded enough that the bottom of the weight holding basket touched the ground beneath it, rendering the test complete. For the test listed as “no test”, the particular test was not testable due to major cracking from previous adjacent tests.

Table 10 – Failure Loads and Type of Failure for Non-Corner Tests.

Test	Predicted Failure Load Per As-Builts [lb]	Failure Load [lb]	Breakout, Pipe Yield or No Test?	$V_{u,tested}/V_{n,predicted}$
2	429	0	No test	N/A
3	429	505	Breakout	1.18
4	429	0	No test	N/A
7	352	425	Breakout	1.21
8	384	435	Breakout	1.13
9	424	485	Breakout	1.14
12	707	634	Breakout	0.90
13	586	505	Breakout	0.86*
14	586	525	Breakout	0.90
17	720	695	Yield	0.97
18	753	735	Yield	0.98
19	741	685	Yield	0.92
22	347	385	Breakout	1.11
23	347	416	Breakout	1.20
24	342	365	Breakout	1.07
27	511	615	Breakout	1.20
28	549	705	Yield	1.28
29	566	615	Yield	1.09
32	798	650	Yield	0.81*
35	308	340	Breakout	1.10

The asterisk in the $V_{u,tested}/V_{n,predicted}$ column of Table 10 denotes a possible outlier to the test group. The breakout cone for Test 13 likely had influence from another breakout cone that negatively influenced the capacity of the test. Test 32 had a low $V_{u,tested}/V_{n,predicted}$ value due to the pipe yield resulting in the basket of weights touching the ground rendering the test complete and not allowing for the concrete to breakout.

4.3 - Comparison of Non-Corner and Corner Tests

Table 11 displays the average of $V_{u,tested}/V_{n,predicted}$.

Table 11 – Average of $V_{u,tested}/V_{n,predicted}$.

Average of $V_{u,tested}/V_{n,predicted}$	
Non-Corner and Corner	1.082
Edge	1.083
Corner	1.080

Figure 24 represents the data of Table 10.

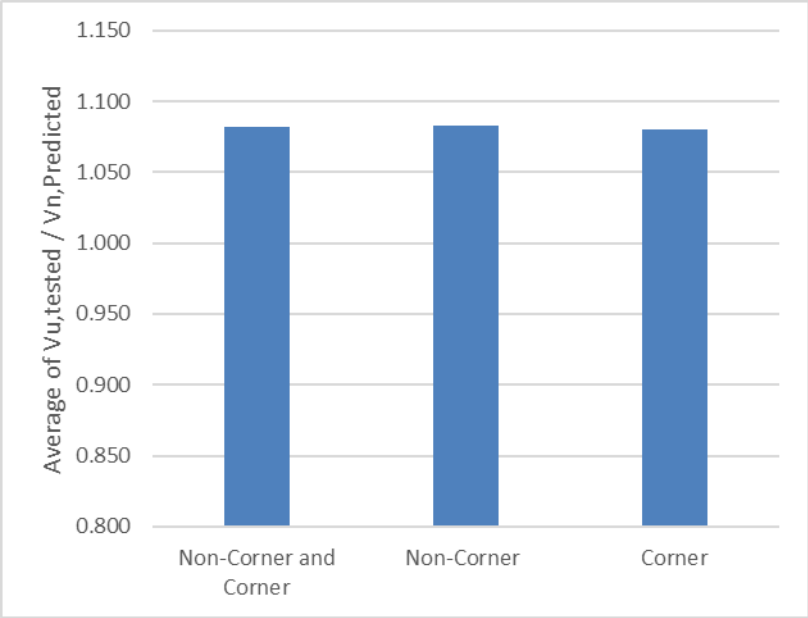

Figure 24 - Average of $V_{u,tested}/V_{n,predicted}$.

Table 12 displays the coefficient of variation for the respective tests.

Table 12 – Coefficient of Variation.

Coefficient of Variation		
Non-Corner and Corner	12.02	%
Edge	11.76	%
Corner	12.73	%

Figure 25 represents the data from Table 12.

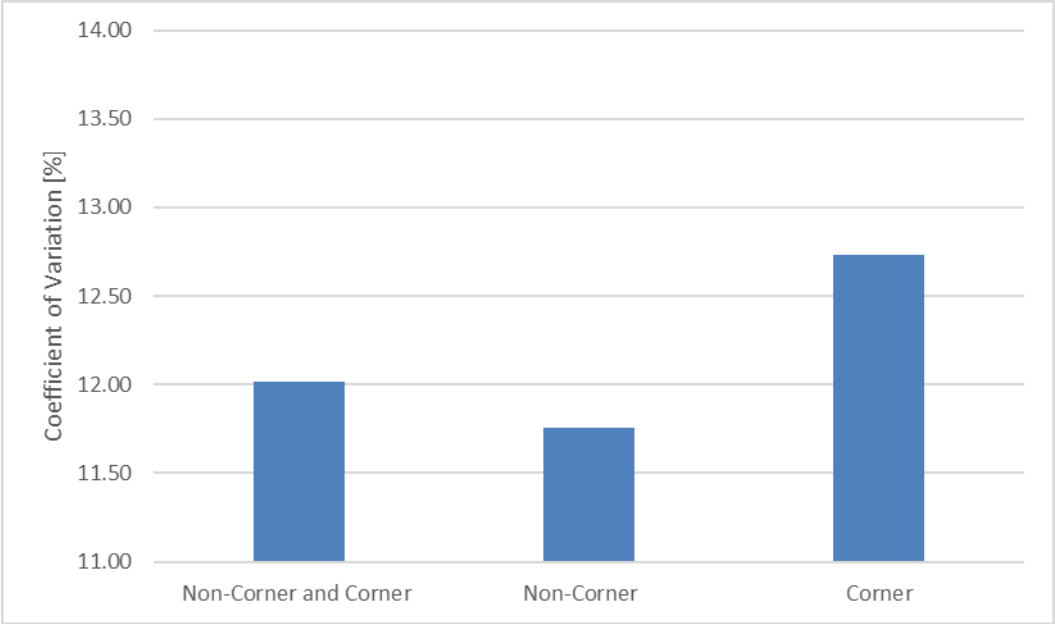

Figure 25 – Coefficient of Variation.

The $V_{u,tested}/V_{n,predicted}$ and the coefficient of variation were two of the main comparisons that Fuchs *et al.* (1995) used in their research.

Due to the large amount of test data that Fuchs *et al.* (1995) were comparing, Fuchs *et al.* (1995) normalized the results of the tests so the results could be better compared due to the varying parameters. The actual graphs that Fuchs *et al.* (1995) used in their paper are given in Figures 8, 9 and 10. Tables 13 and 14 and Figures 26 and 27 represent the normalized results from this capstone project testing, so the results can be compared to the results of Fuchs *et al.* (1995). The results were normalized using the same equation as Fuchs *et al.* (1995).

Table 13 – Normalized Average of $V_{u,tested}/V_{n,predicted}$.

Average of $V_{u,tested}/V_{n,predicted}$	
Non-Corner and Corner	0.938
Non-Corner	0.959
Corner	0.940

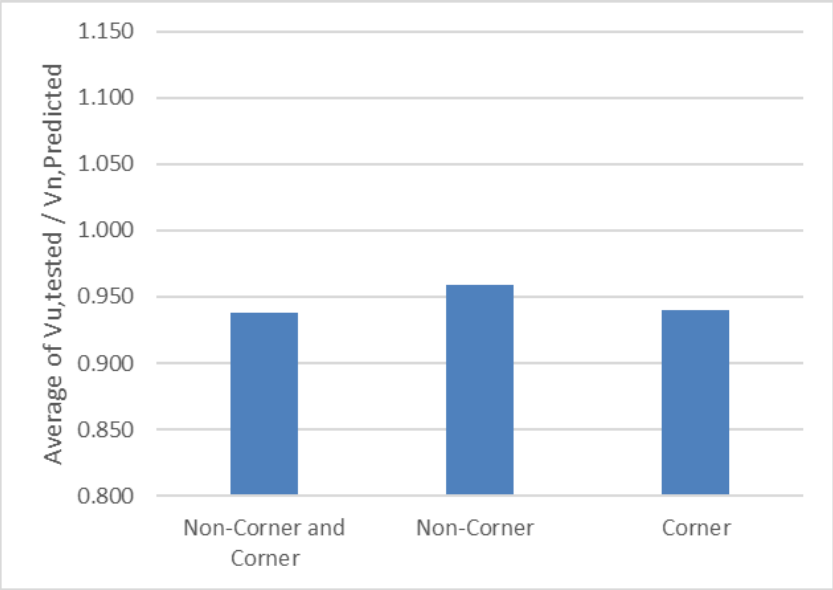

Figure 26 – Normalized Average of $V_{u,tested}/V_{n,predicted}$.

Table 14 and Figure 27 represent the coefficient of variation for the normalized results.

Table 14 – Coefficient of Variation for Normalized Results.

Coefficient of Variation		
Non-Corner and Corner	12.75	%
Non-Corner	13.05	%
Corner	13.00	%

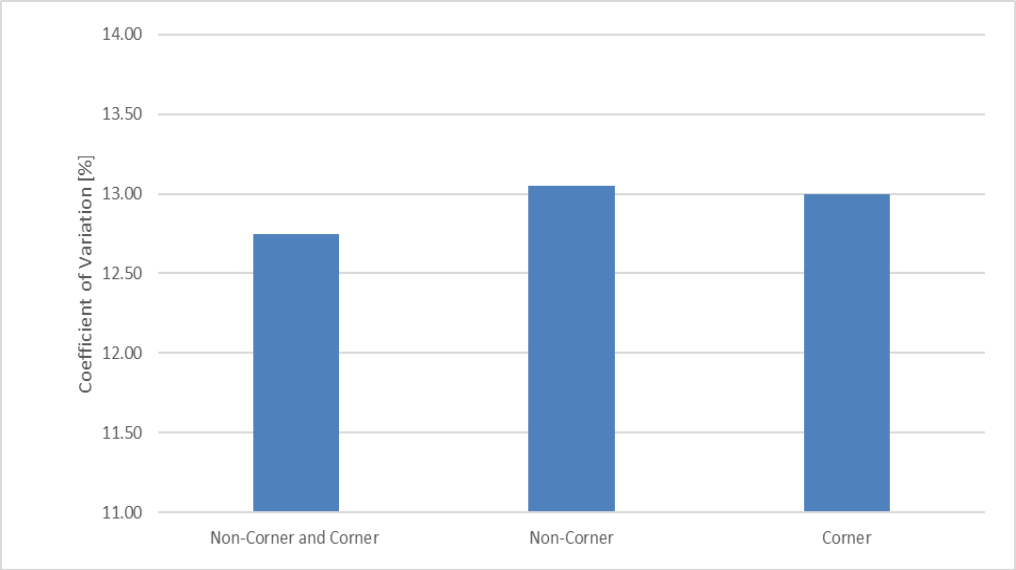

Figure 27 - Coefficient of Variation for Normalized Results.

4.4 - Deflection

The deflection at the point of the load for each test was recorded. Figures 28 through 60 display the deflection at each load step. The difference between the two plots on each graph represents the plastic deformation in the pipe from testing and the deflection from the rotation of the concrete test specimen inside the wooden test frame.

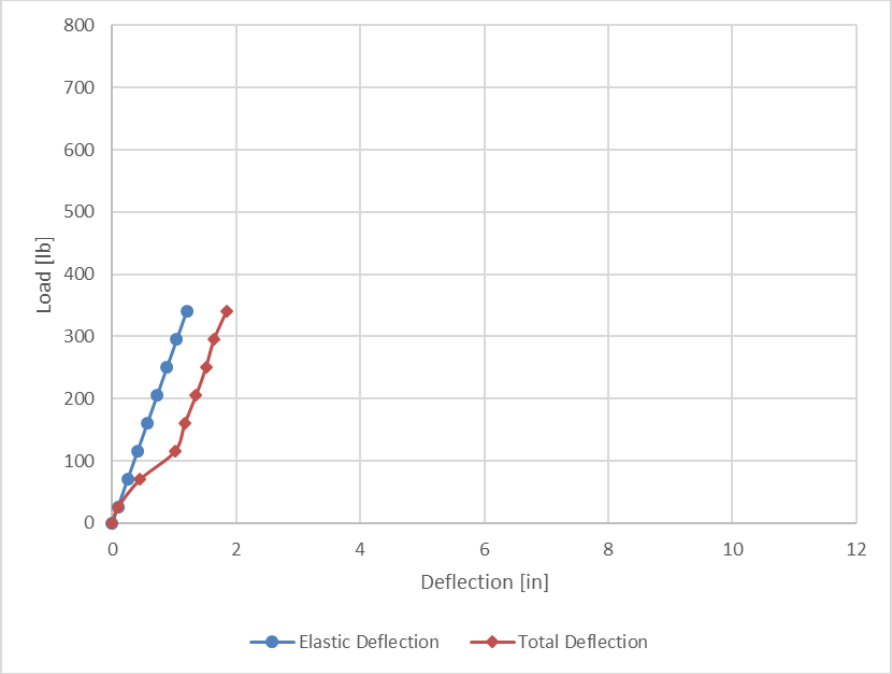

Figure 28 – Deflection of Test 1, 6-in. Slab Thickness, Corner, 3-in. Setback, 4-in. Embed.

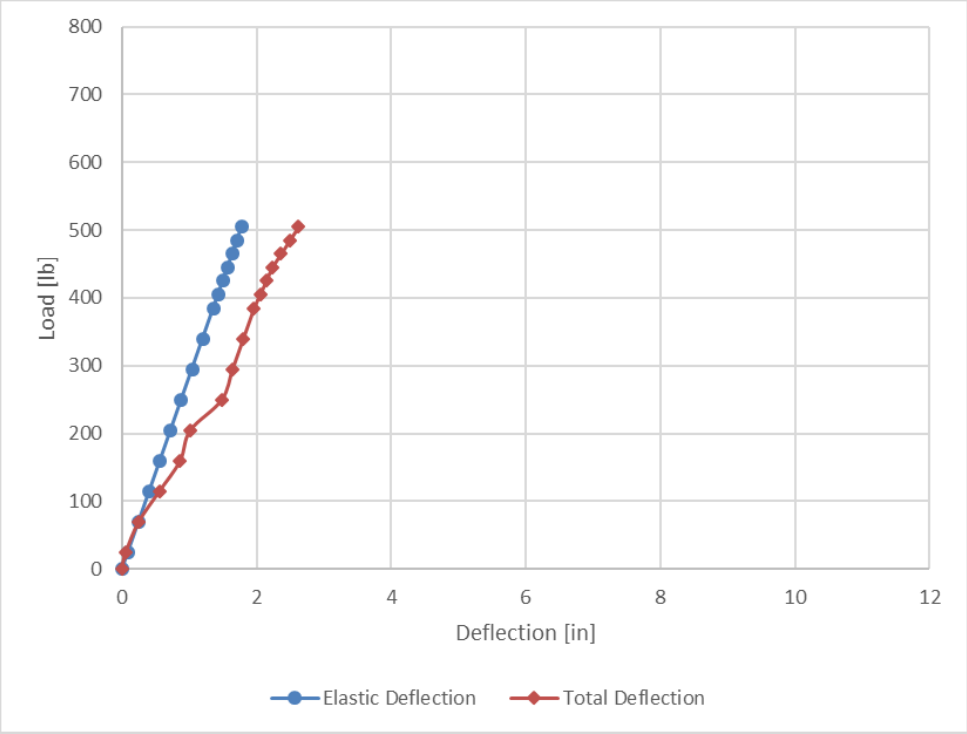

Figure 29 – Deflection of Test 3, 6-in. Slab Thickness, Non-Corner, 3-in. Setback, 4-in. Embed.

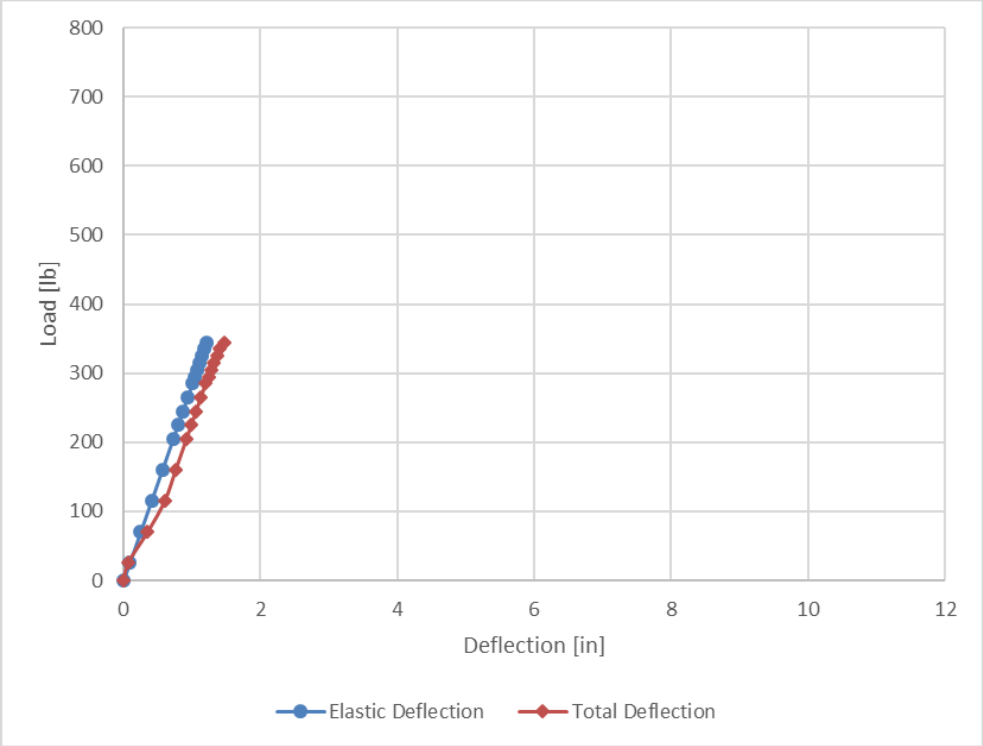

Figure 30 – Deflection of Test 6, 6-in. Slab Thickness, Corner, 3-in. Setback, 3-in. Embed.

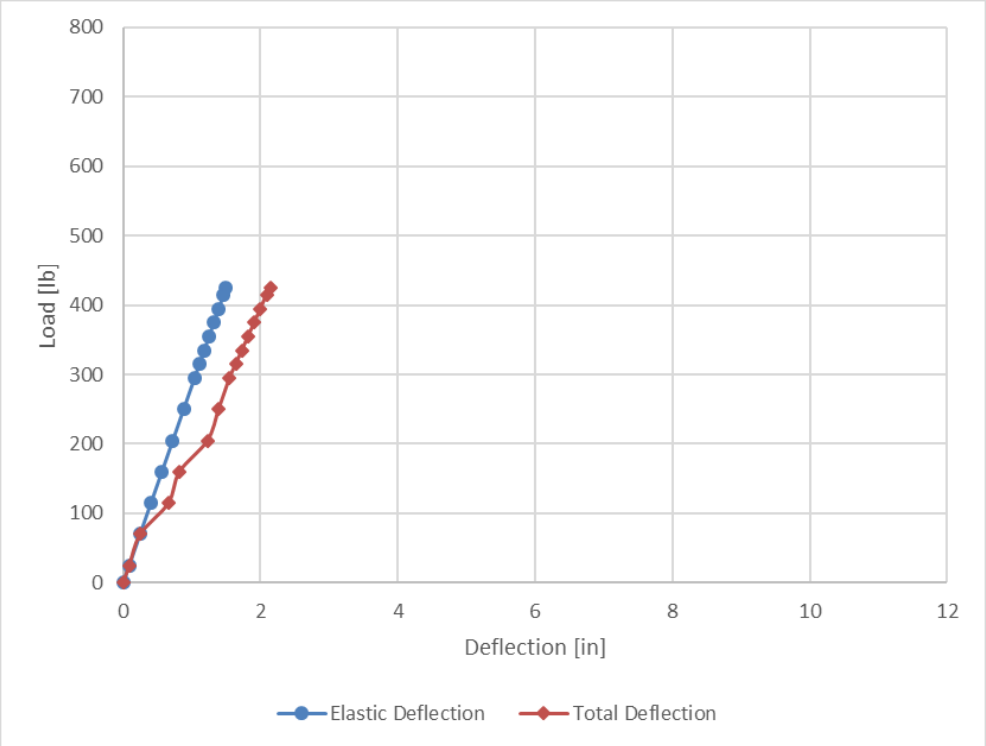

Figure 31 – Deflection of Test 7, 6-in. Slab Thickness, Non-Corner, 3-in. Setback, 3-in. Embed.

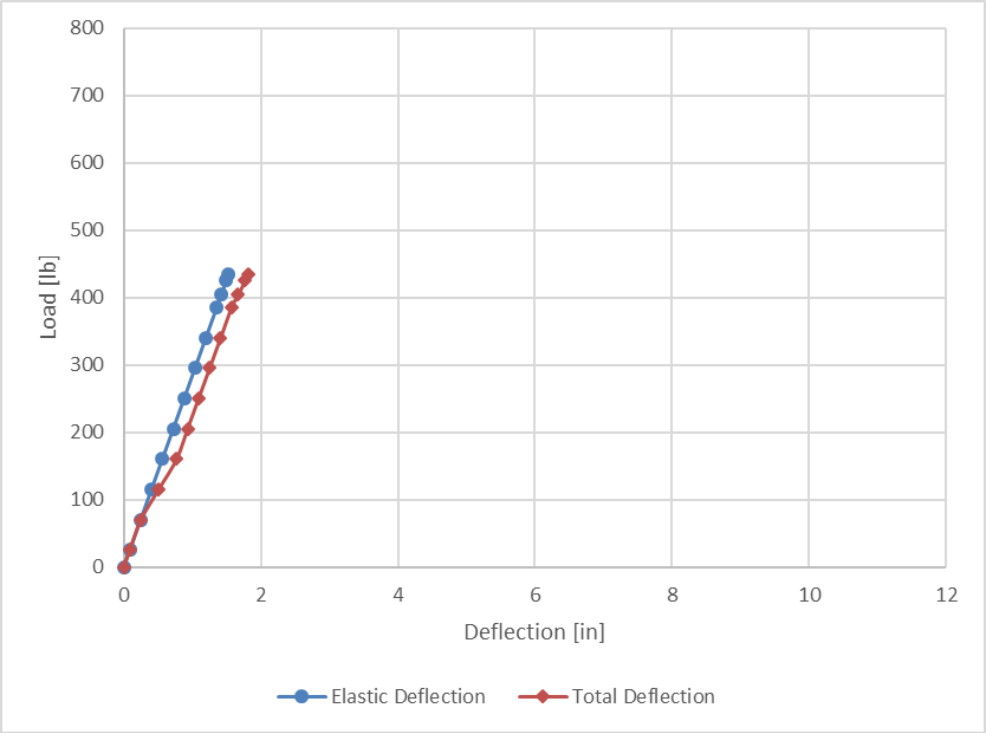

Figure 32 – Deflection of Test 8, 6-in. Slab Thickness, Non-Corner, 3-in. Setback, 3-in. Embed.

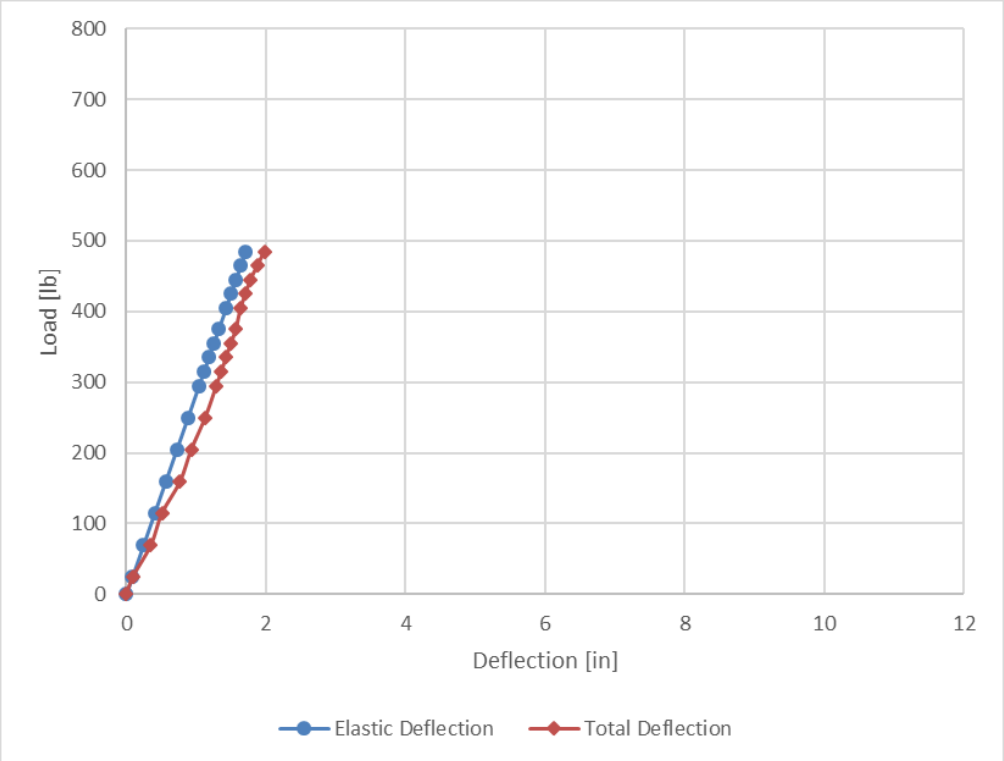

Figure 33 – Deflection of Test 9, 6-in. Slab Thickness, Non-Corner, 3-in. Setback, 3-in. Embed.

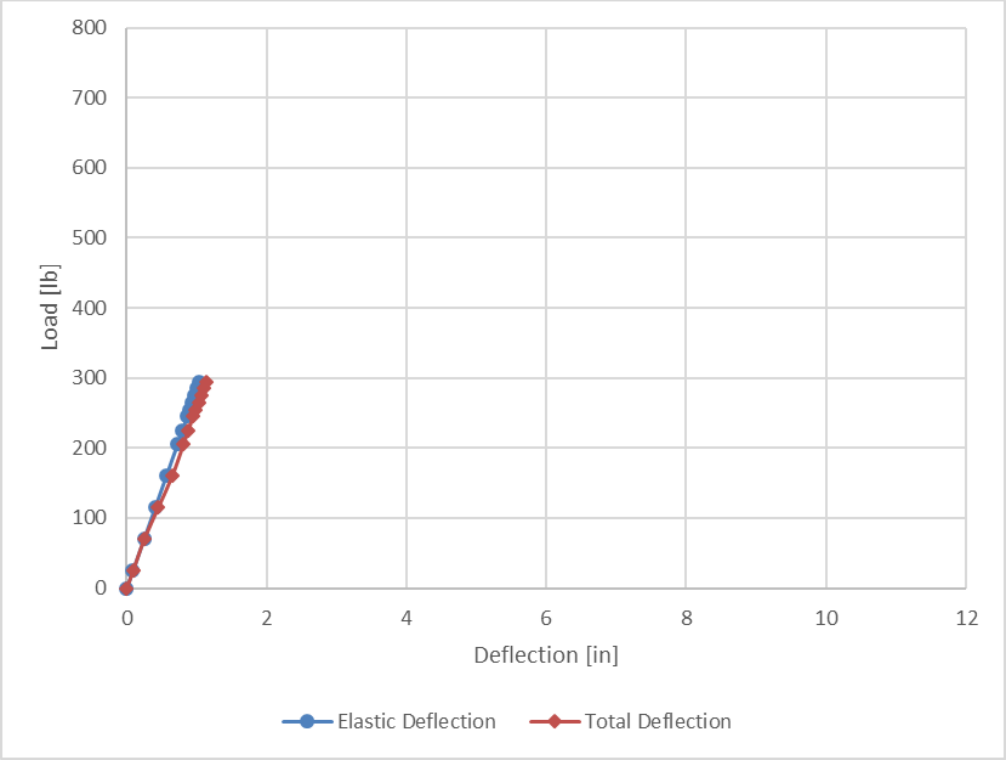

Figure 34 – Deflection of Test 10, 6-in. Slab Thickness, Corner, 3-in. Setback, 3-in. Embed.

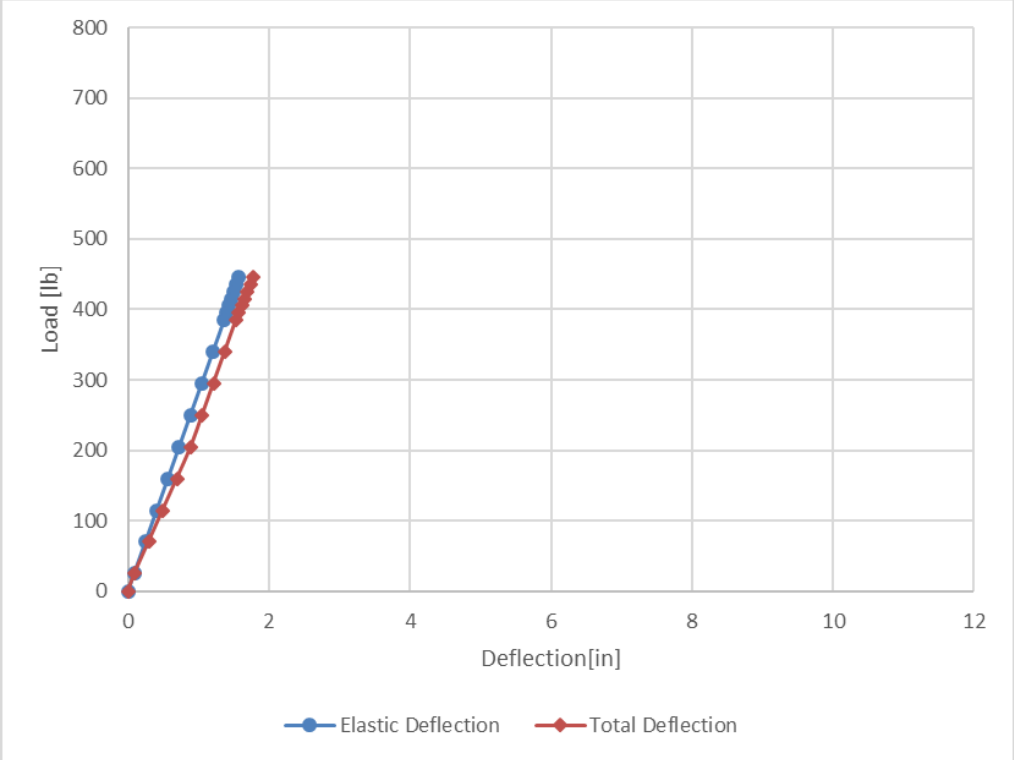

Figure 35 – Deflection of Test 11, 6-in. Slab Thickness, Corner, 4-in. Setback, 3-in. Embed.

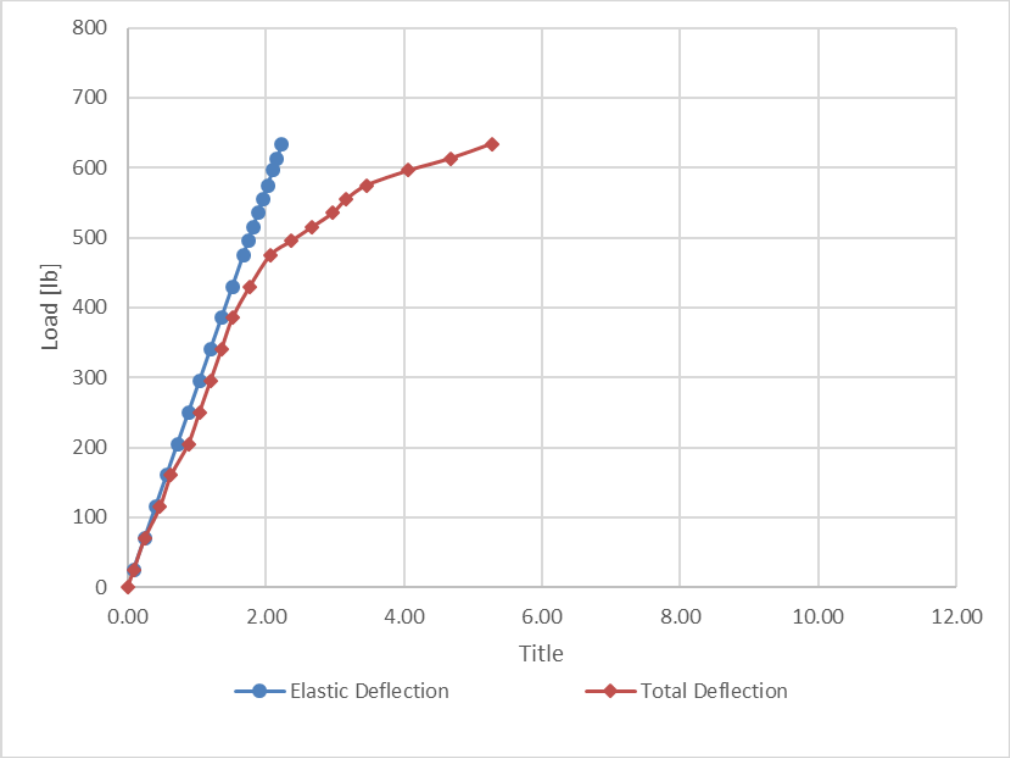

Figure 36 – Deflection of Test 12, 6-in. Slab Thickness, Non-Corner, 4-in. Setback, 3-in. Embed.

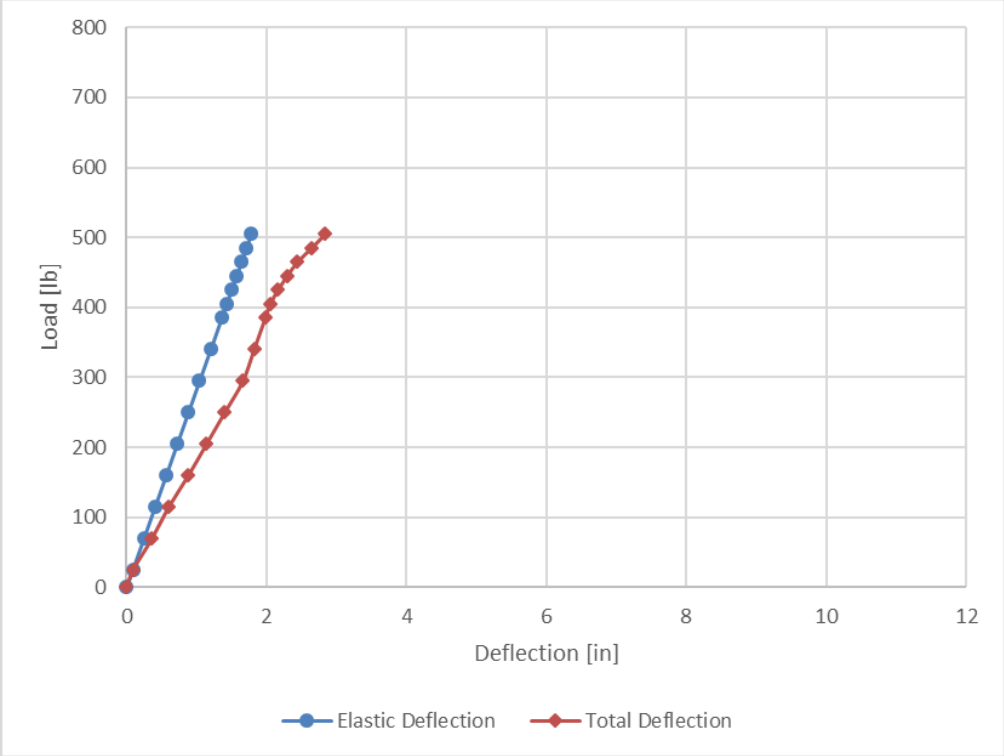

Figure 37 – Deflection of Test 13, 6-in. Slab Thickness, Non-Corner, 4-in. Setback, 3-in. Embed.

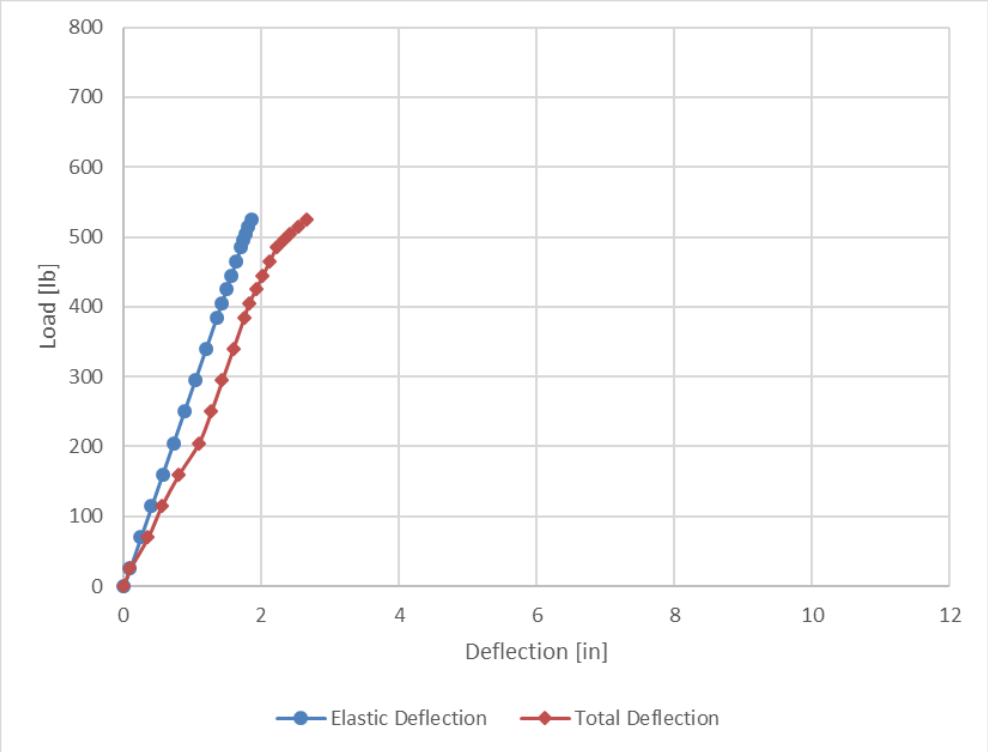

Figure 38 – Deflection of Test 14, 6-in. Slab Thickness, Non-Corner, 4-in. Setback, 3-in. Embed.

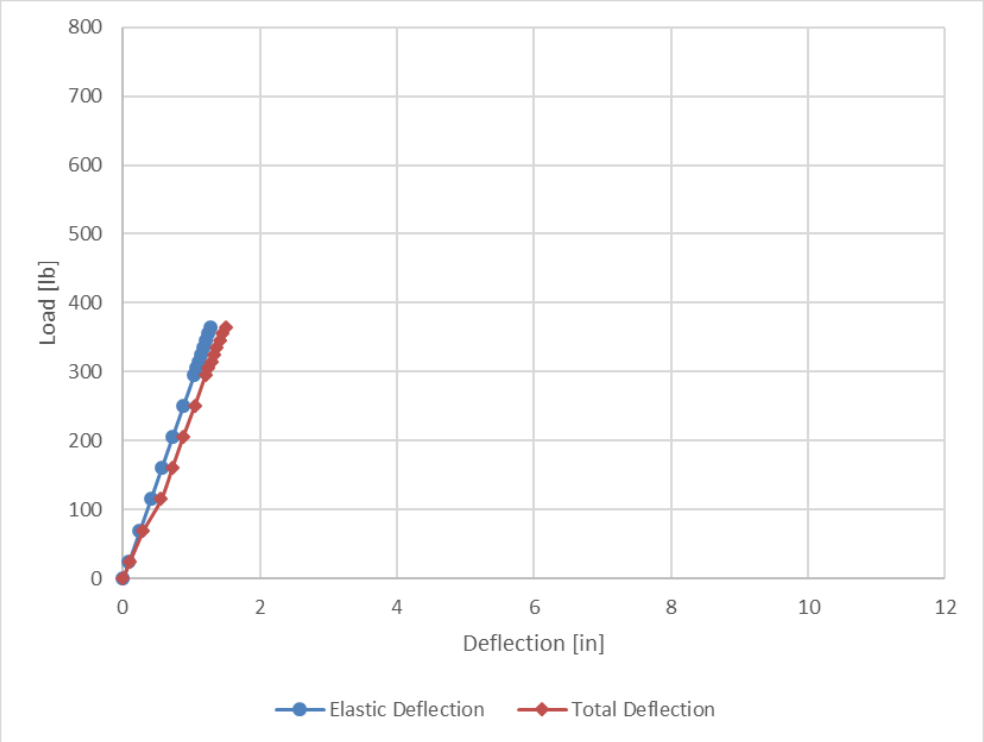

Figure 39 – Deflection of Test 15, 6-in. Slab Thickness, Corner, 4-in. Setback, 3-in. Embed.

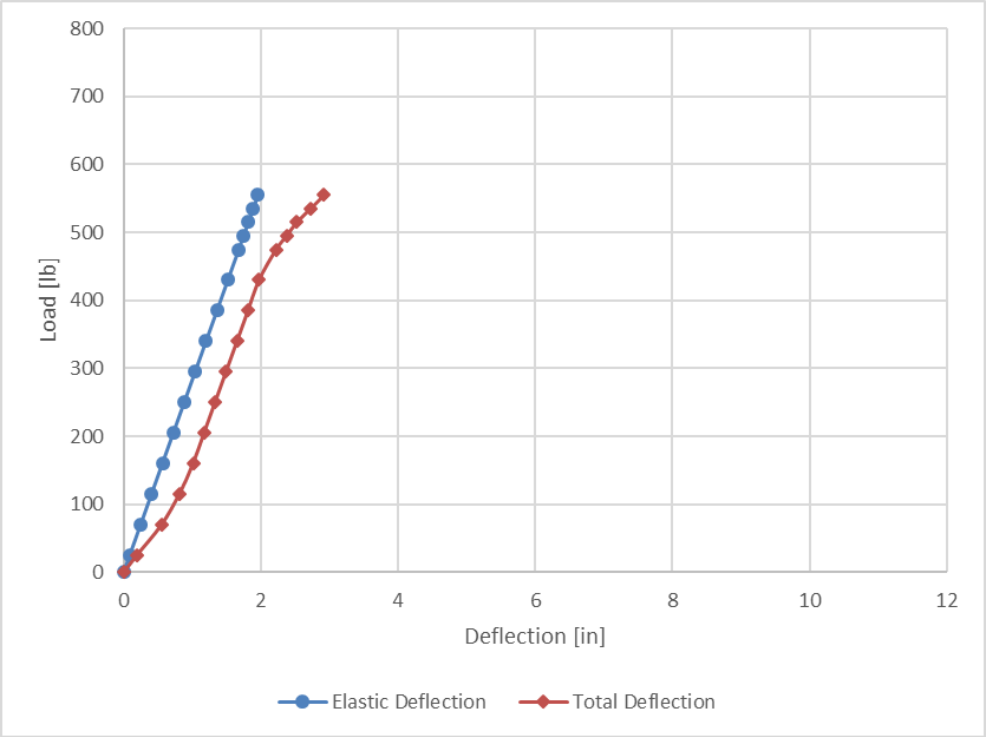

Figure 40 – Deflection of Test 16, 6-in. Slab Thickness, Corner, 4-in. Setback, 4-in. Embed.

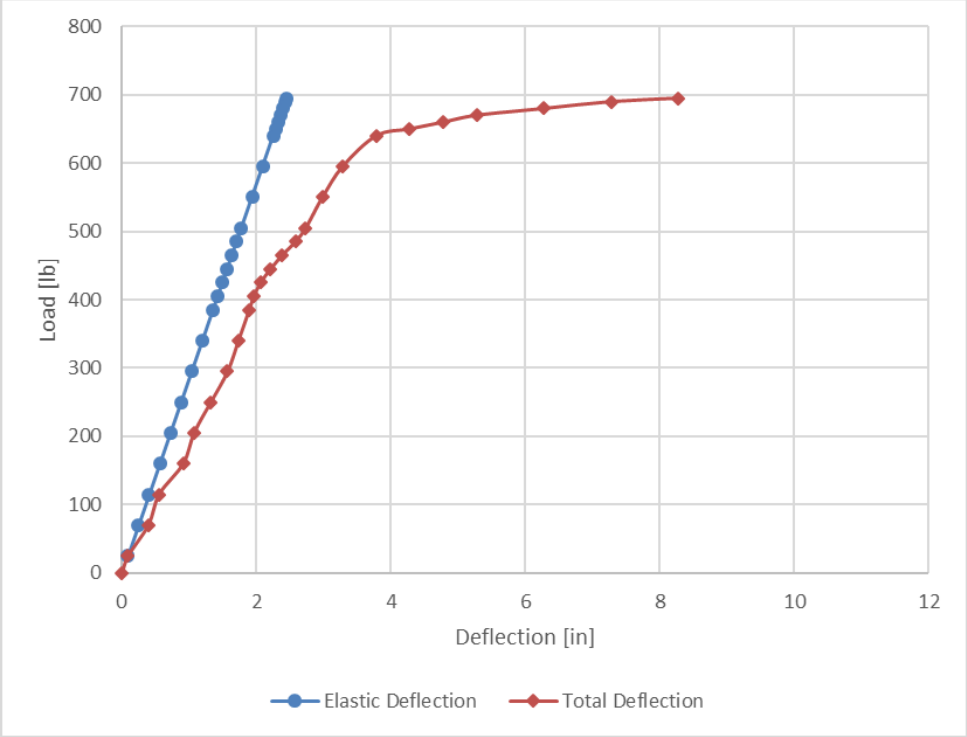

Figure 41 – Deflection of Test 17, 6-in. Slab Thickness, Non-Corner, 4-in. Setback, 4-in. Embed.

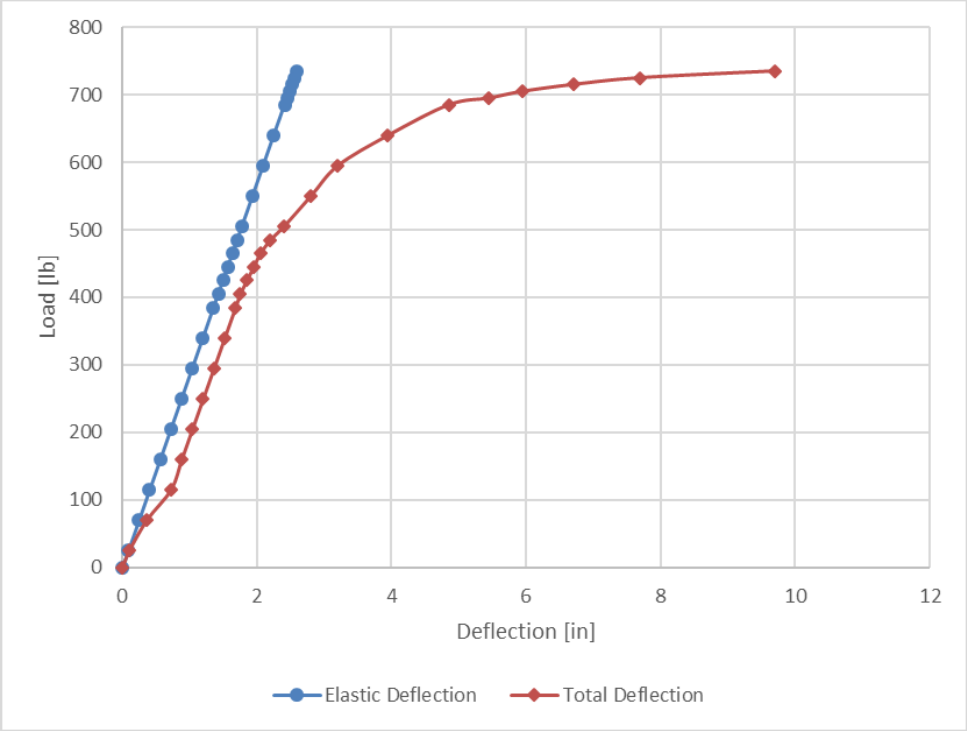

Figure 42 – Deflection of Test 18, 6-in. Slab Thickness, Non-Corner, 4-in. Setback, 4-in. Embed.

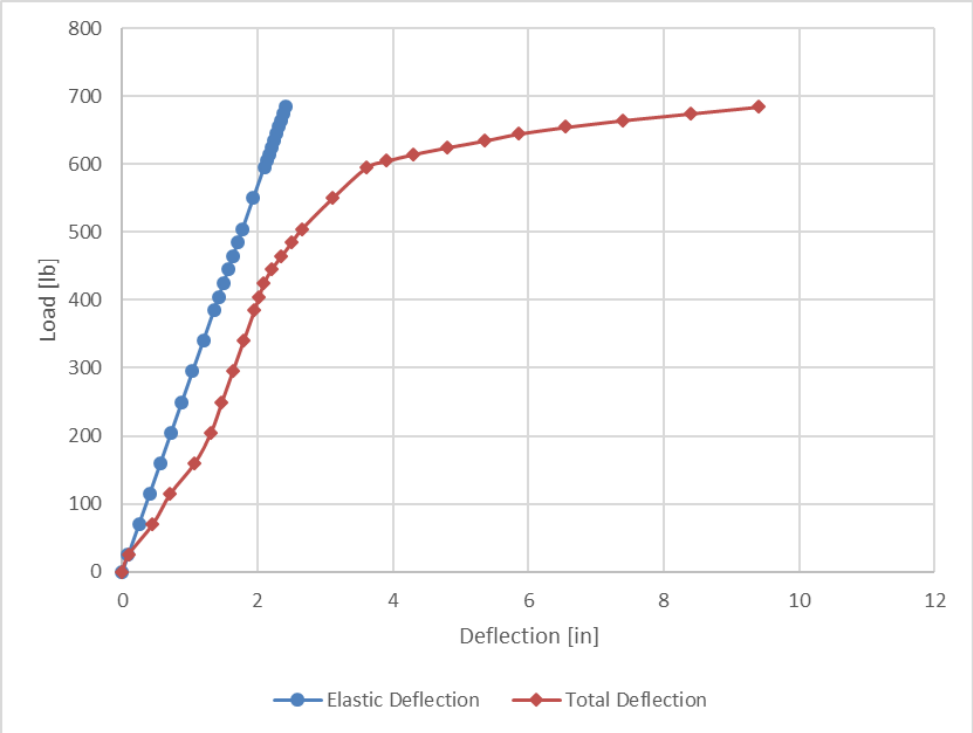

Figure 43 – Deflection of Test 19, 6-in. Slab Thickness, Non-Corner, 4-in. Setback, 4-in. Embed.

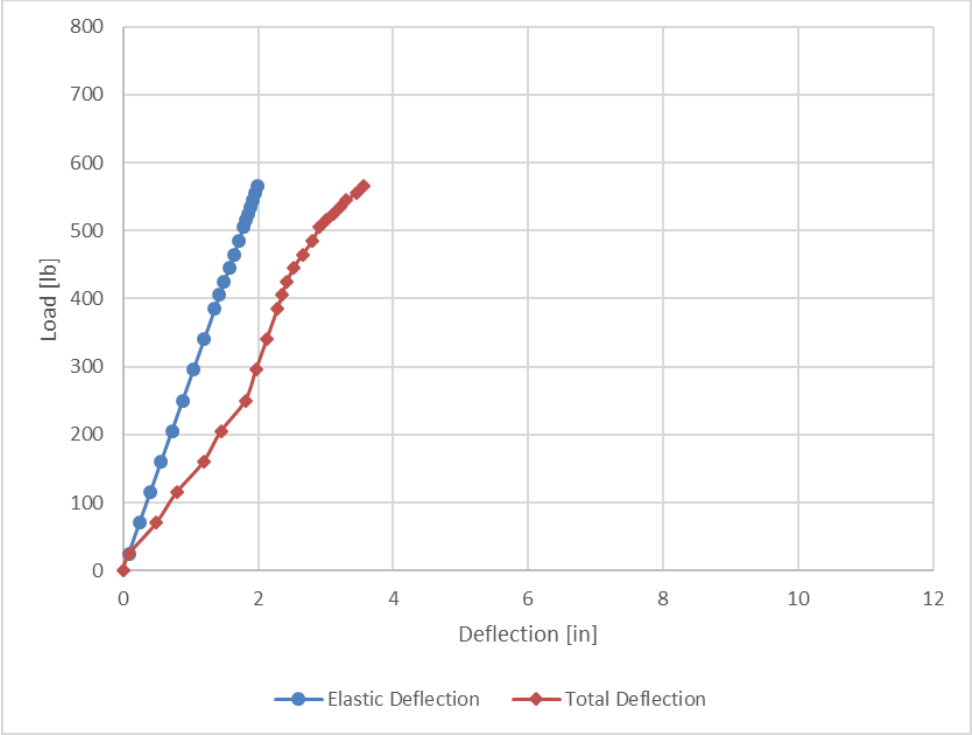

Figure 44 – Deflection of Test 20, 6-in. Slab Thickness, Corner, 4-in. Setback, 4-in. Embed.

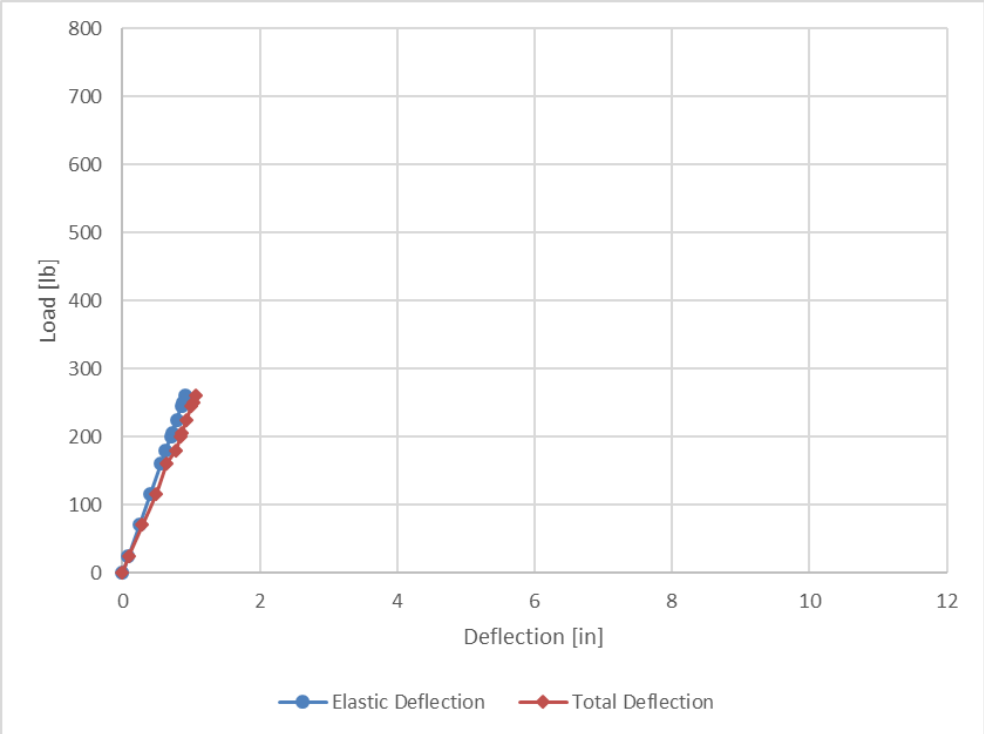

Figure 45 – Deflection of Test 21, 8-in. Slab Thickness, Corner, 3-in. Setback, 4-in. Embed.

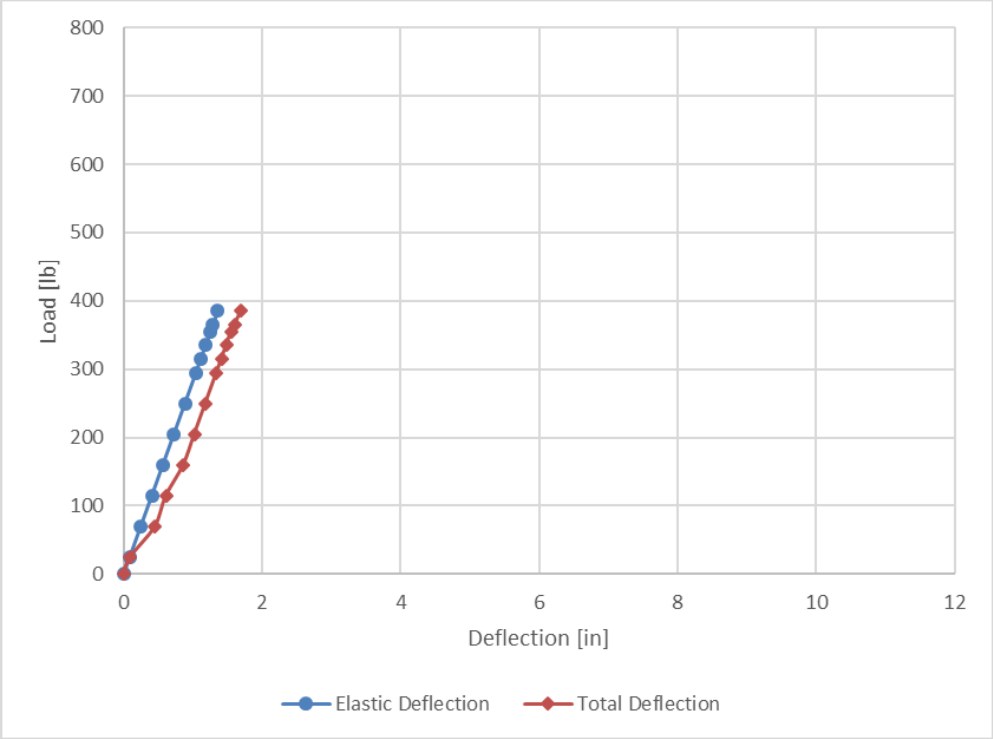

Figure 46 – Deflection of Test 22, 8-in. Slab Thickness, Non-Corner, 3-in. Setback, 4-in. Embed.

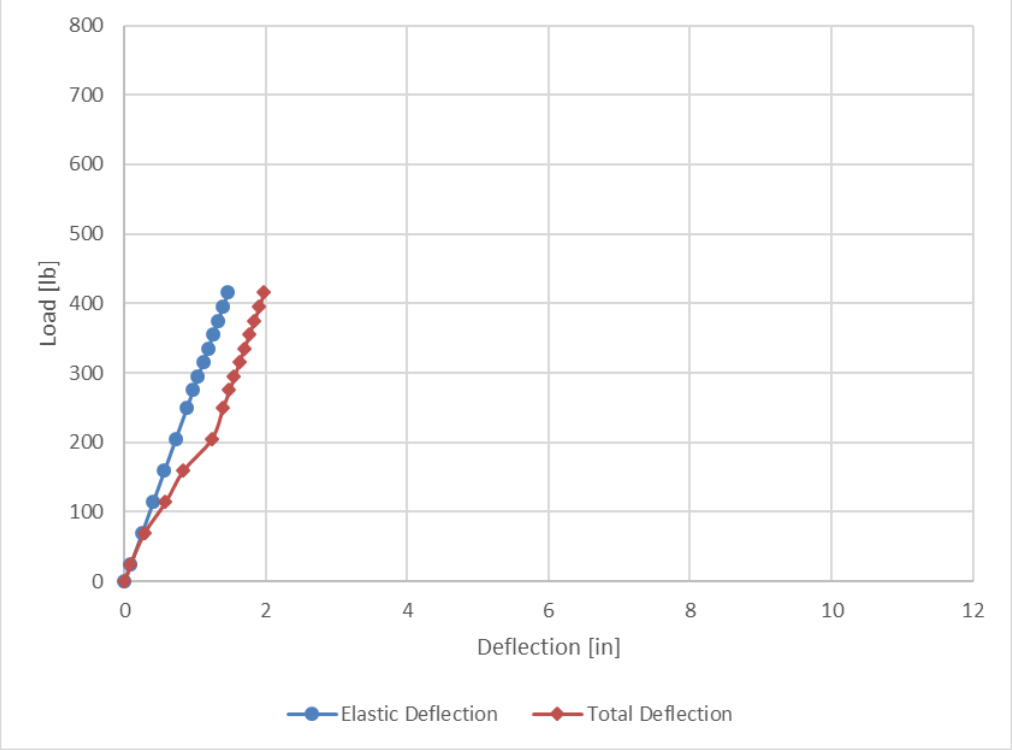

Figure 47 – Deflection of Test 23, 8-in. Slab Thickness, Non-Corner, 3-in. Setback, 4-in. Embed.

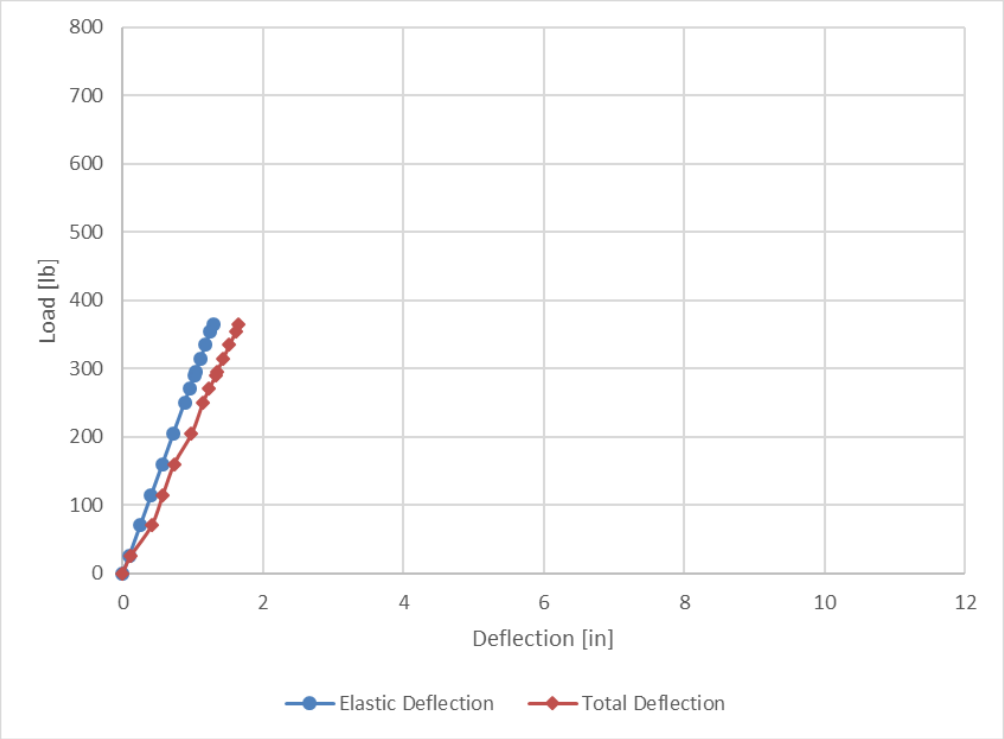

Figure 48 – Deflection of Test 24, 8-in. Slab Thickness, Non-Corner, 3-in. Setback, 4-in. Embed.

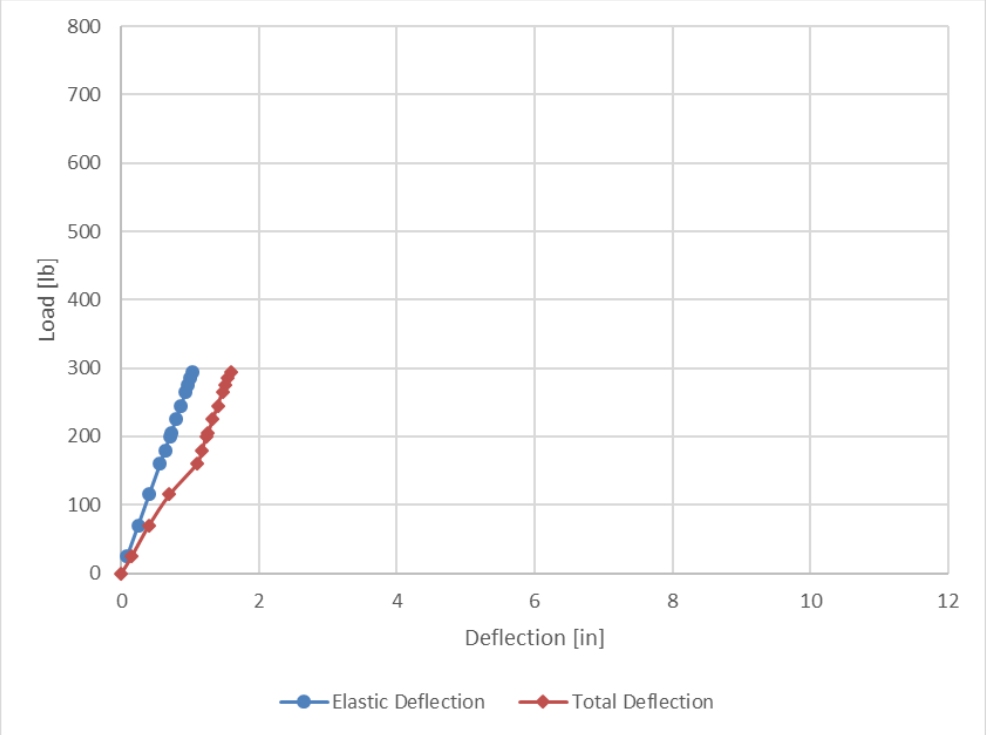

Figure 49 – Deflection of Test 25, 8-in. Slab Thickness, Corner, 3-in. Setback, 4-in. Embed.

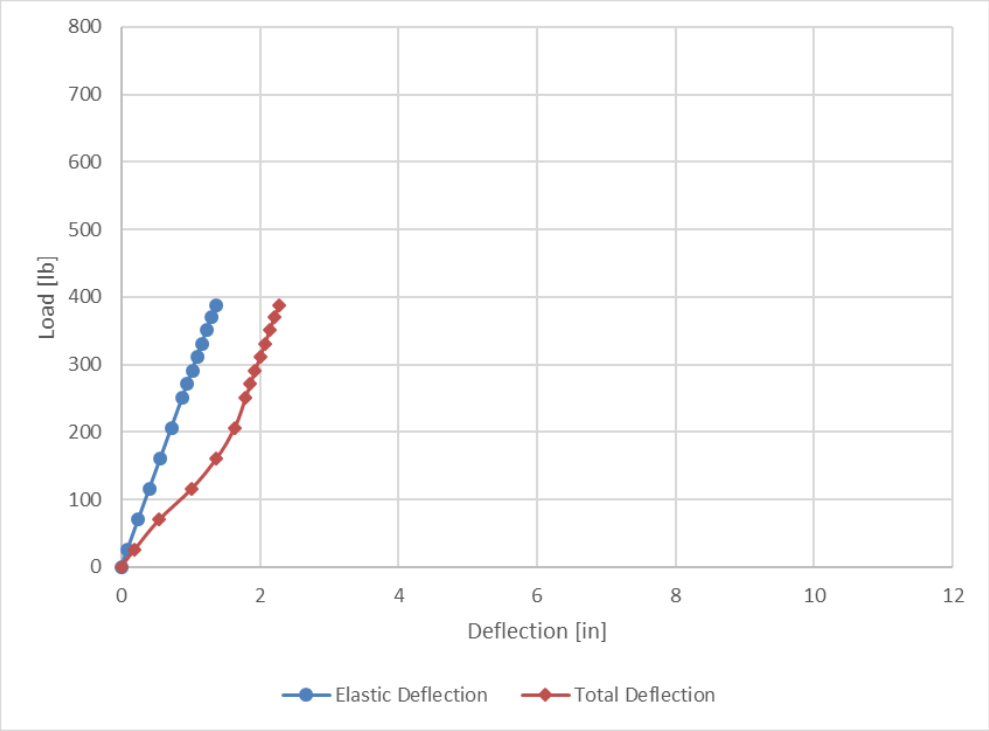

Figure 50 – Deflection of Test 26, 8-in. Slab Thickness, Corner, 3-in. Setback, 3-in. Embed.

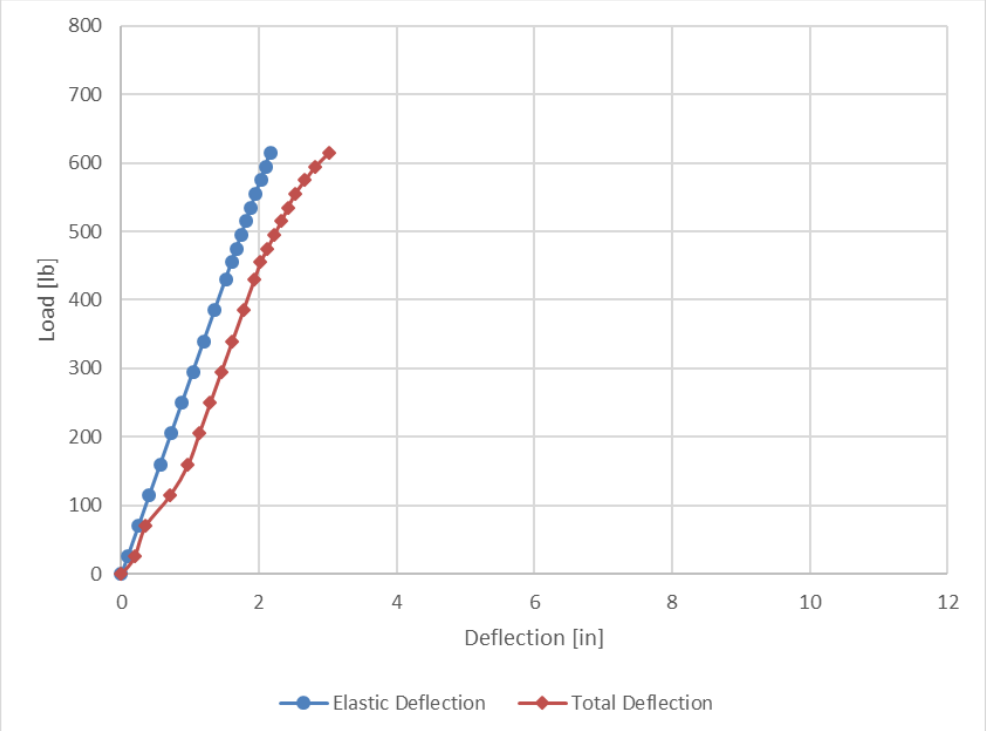

Figure 51 – Deflection of Test 27, 8-in. Slab Thickness, Non-Corner, 3-in. Setback, 3-in. Embed.

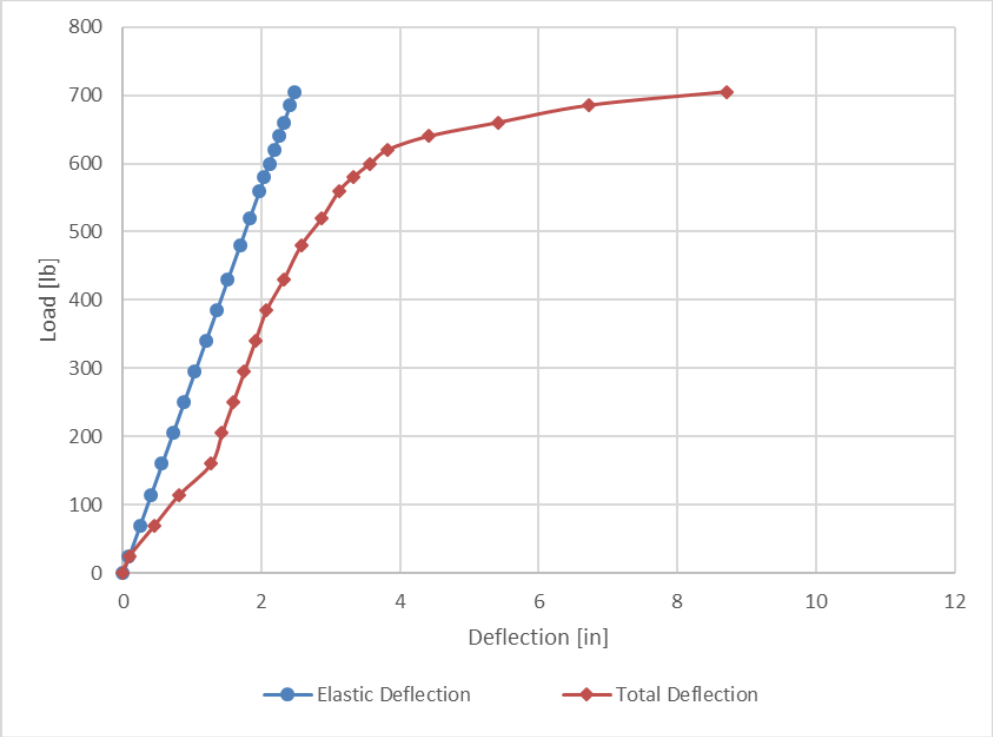

Figure 52 – Deflection of Test 28, 8-in. Slab Thickness, Non-Corner, 3-in. Setback, 3-in. Embed.

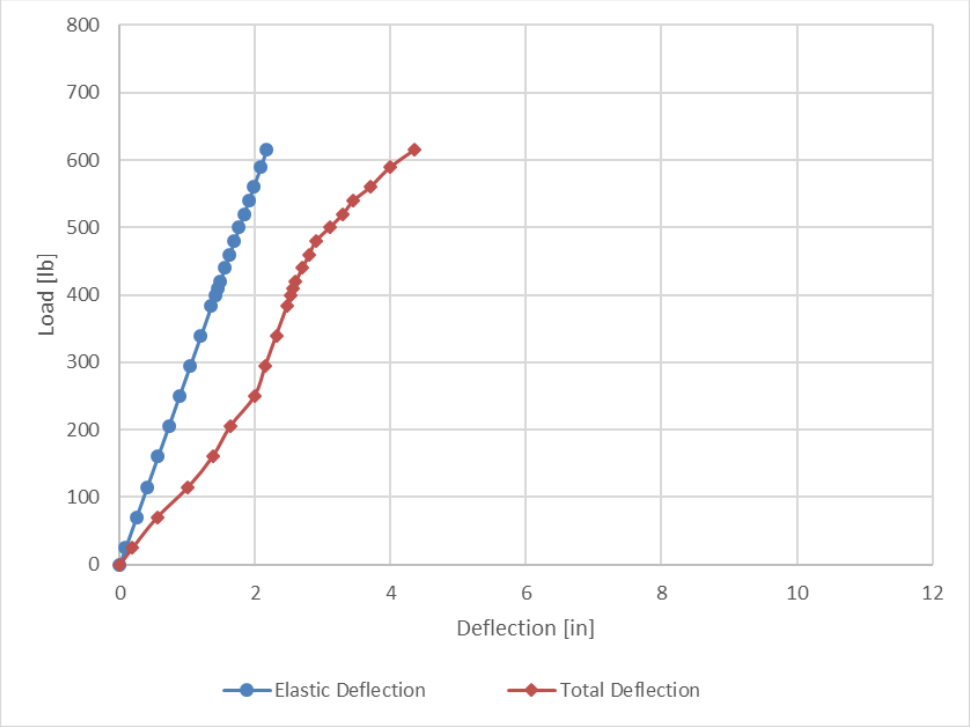

Figure 53 – Deflection of Test 29, 8-in. Slab Thickness, Non-Corner, 3-in. Setback, 3-in. Embed.

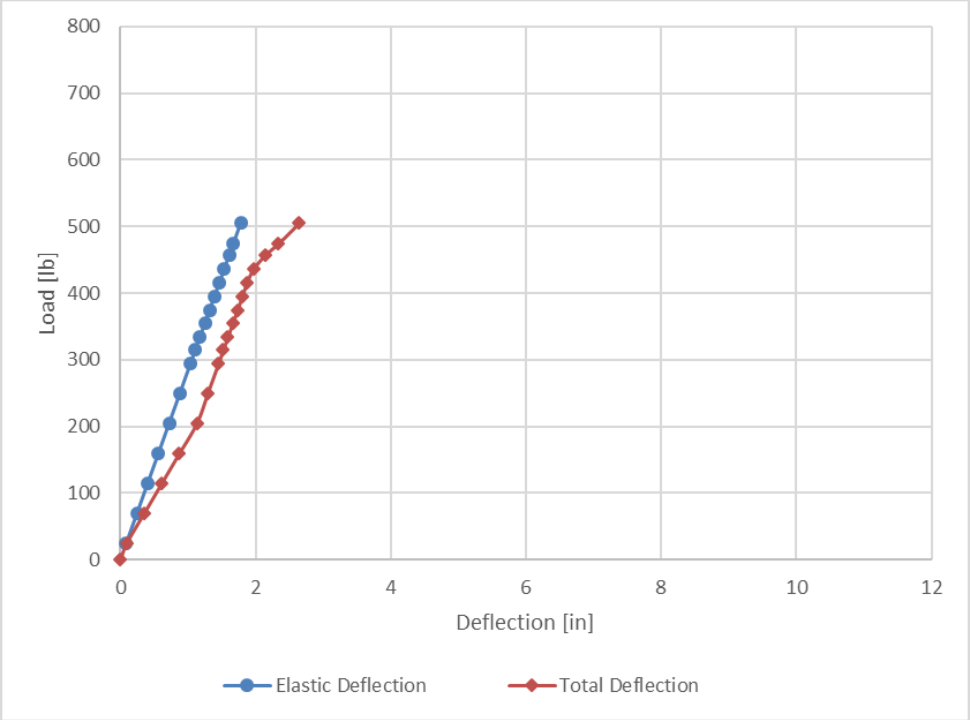

Figure 54 – Deflection of Test 30, 8-in. Slab Thickness, Corner, 3-in. Setback, 3-in. Embed.

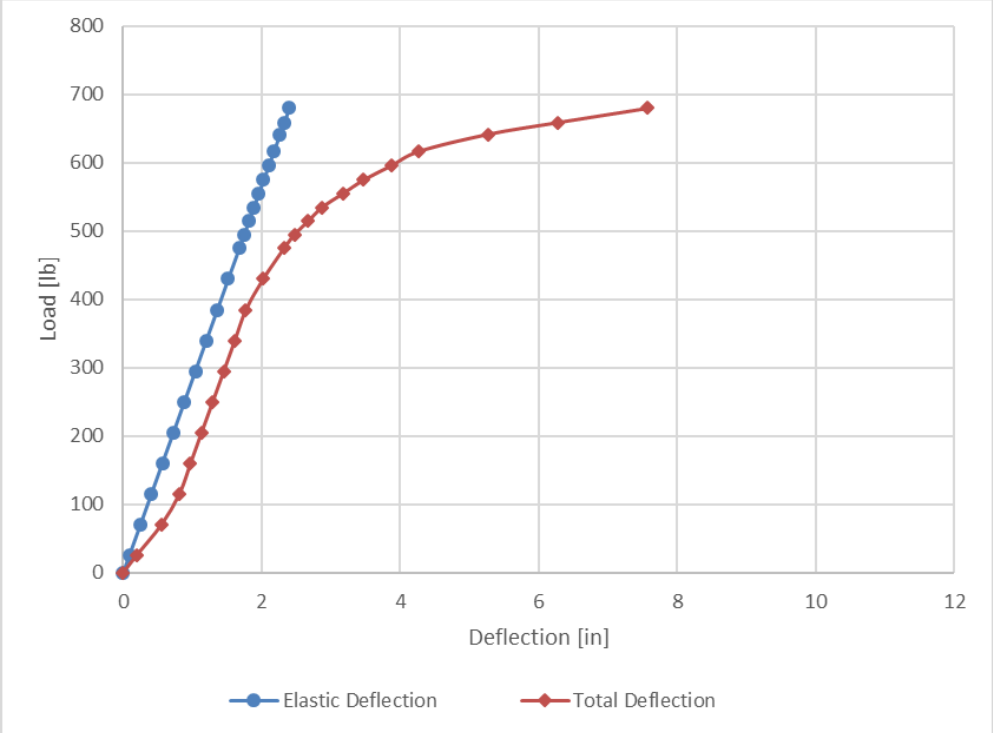

Figure 55 – Deflection of Test 31, 8-in. Slab Thickness, Corner, 4-in. Setback, 3-in. Embed.

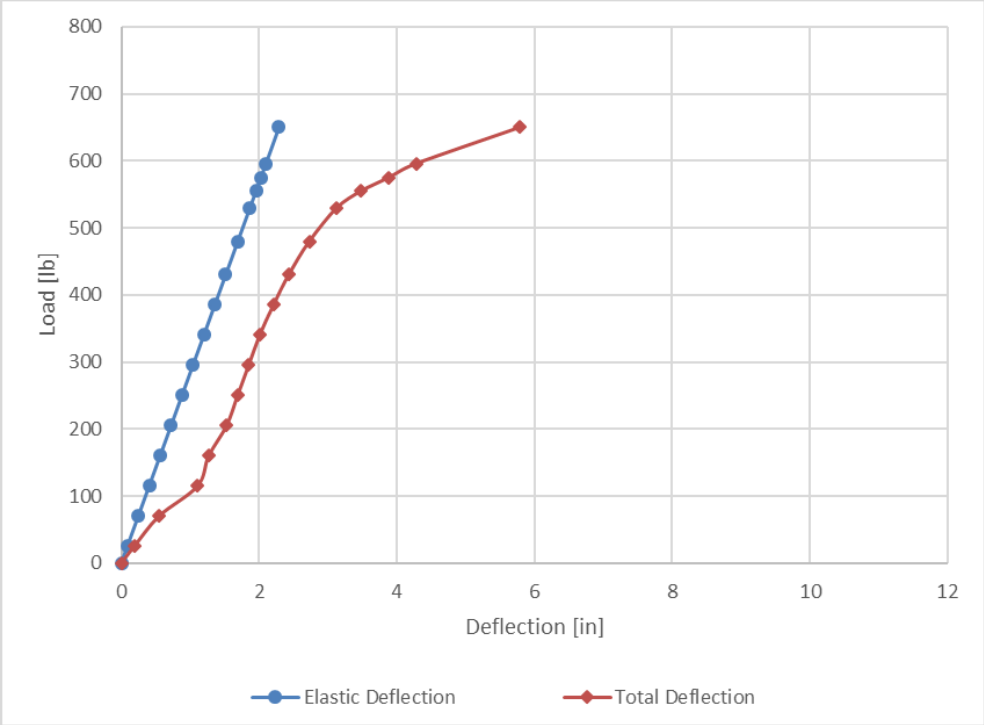

Figure 56 – Deflection of Test 32, 8-in. Slab Thickness, Non-Corner, 4-in. Setback, 3-in. Embed.

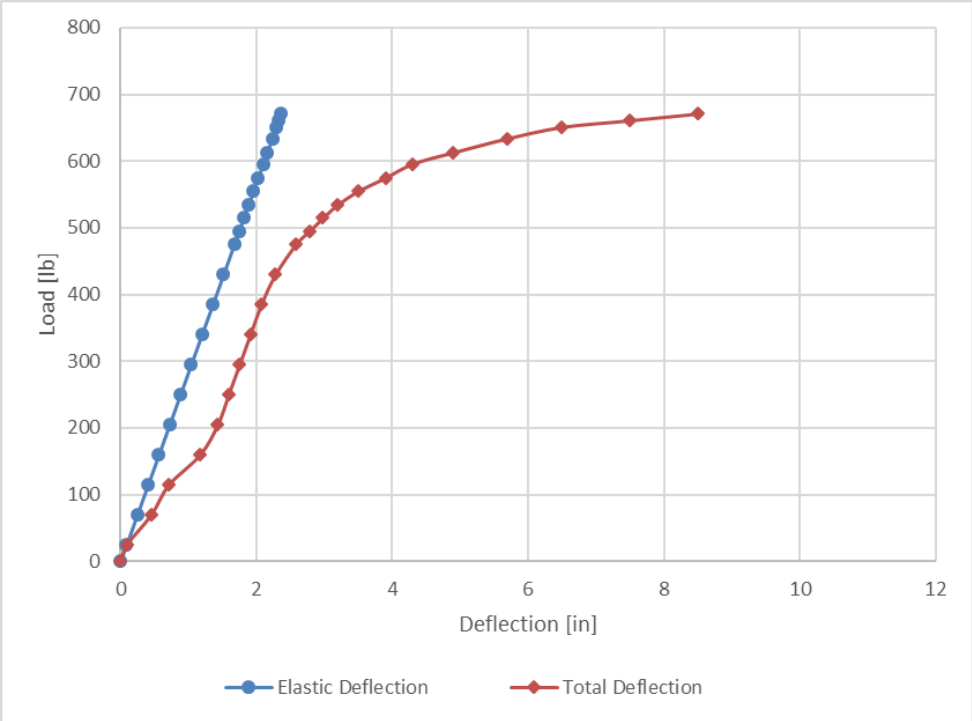

Figure 57 – Deflection of Test 33, 8-in. Slab Thickness, Corner, 4-in. Setback, 3-in. Embed.

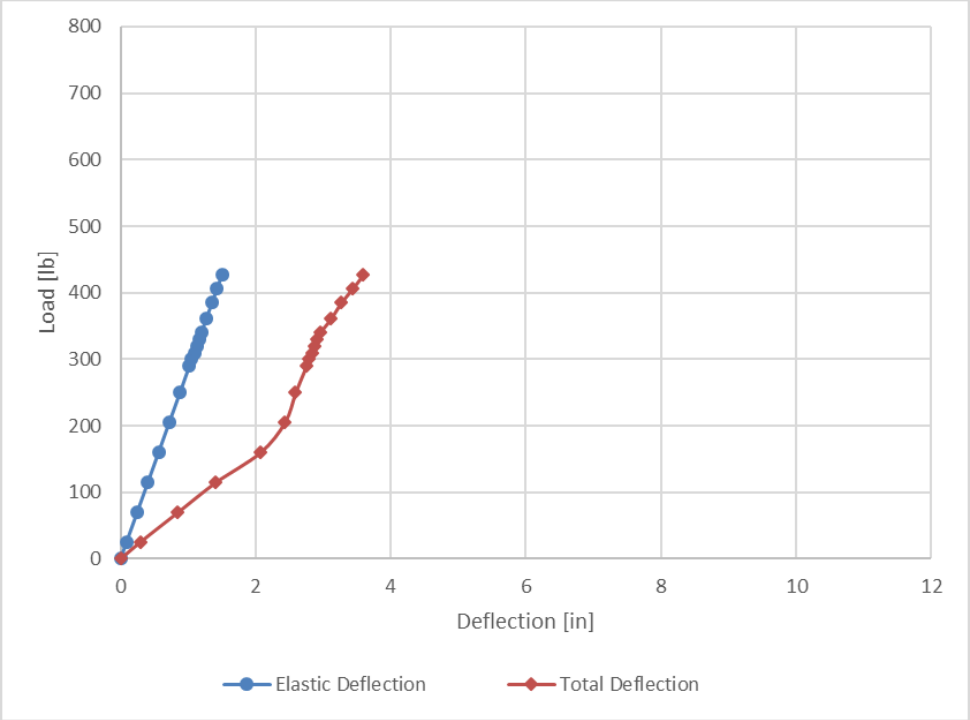

Figure 58 – Deflection of Test 34, 8-in. Slab Thickness, Corner, 4-in. Setback, 4-in. Embed.

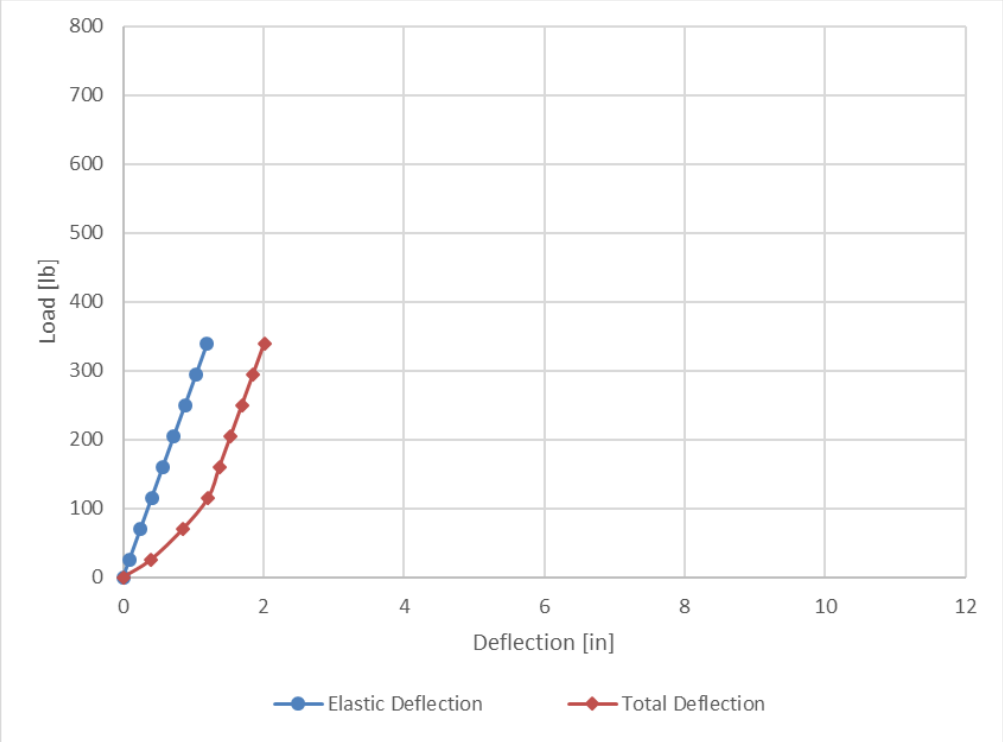

Figure 59 – Deflection of Test 35, 8-in. Slab Thickness, Non-Corner, 4-in. Setback, 4-in. Embed.

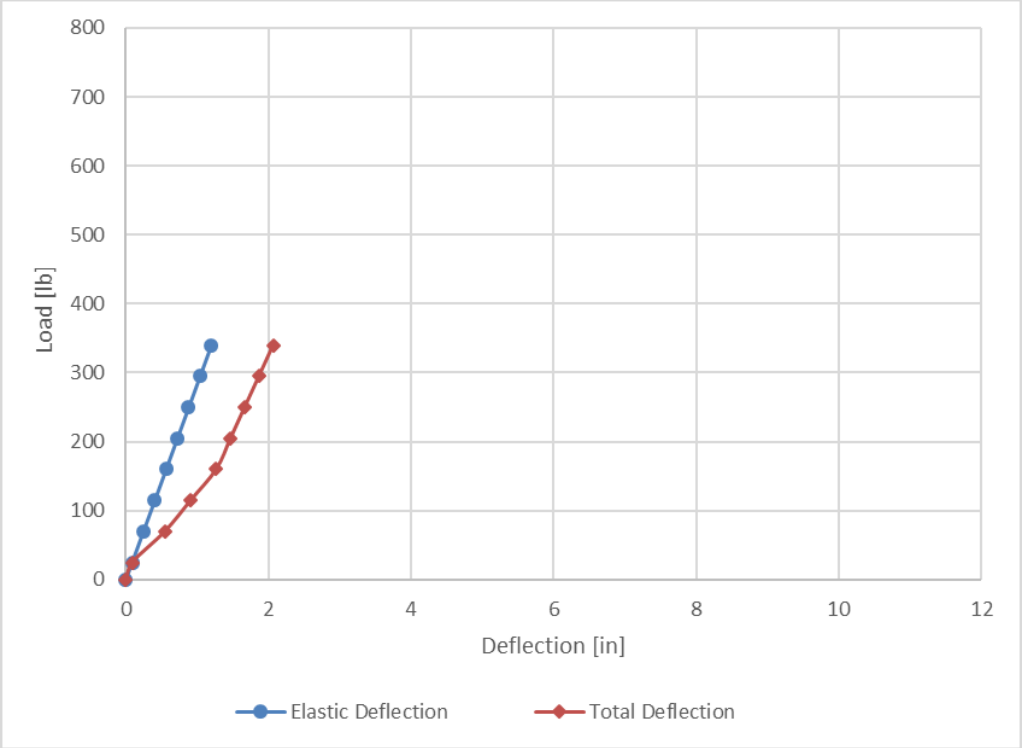

Figure 60 – Deflection of Test 36, 8-in. Slab Thickness, Corner, 4-in. Setback, 4-in. Embed.

4.5 - Rotation

Due to the nature of wood not being completely rigid, the rotation of the concrete test specimen inside the wooden test frame was measured for most tests. The reason that the rotation was not measured for all tests was that rotation was not originally planned on as a data point to be measured. After consultation with the members of the capstone project committee, it was decided to take this measurement. Table 15 lists the rotation of the concrete test specimen in the wooden test frame for the listed test. The table also lists the amount of deflection at the point load from the rotation of the concrete specimen in the wooden test frame.

Table 15 - Rotation of Concrete member During Testing.

Test	Length from Center of Slab to Measuement Surface [in]	Deflection [in]	Rotation [Radians]	Rotation [Degrees]	Length from Center of Slab to Load [in]	Deflection from Rotation [in]
1	49	0.750	0.0153	0.8769	45	0.69
2	No Test of Specimen	N/A	N/A	N/A	45	N/A
3	14.5	0.188	0.0129	0.7409	45	0.58
4	No Test of Specimen	N/A	N/A	N/A	45	N/A
5	No Test of Specimen	N/A	N/A	N/A	45	N/A
6	49	0.250	0.0051	0.2923	45	0.23
7	49	0.500	0.0102	0.5846	45	0.46
8	Rotation Not Tested	N/A	N/A	N/A	45	N/A
9	Rotation Not Tested	N/A	N/A	N/A	45	N/A
10	50	0.125	0.0025	0.1432	45	0.11
11	25	0.125	0.0050	0.2865	45	0.23
12	24	0.125	0.0052	0.2984	45	0.23
13	25.5	0.500	0.0196	1.1233	45	0.88
14	25	0.500	0.0200	1.1458	45	0.90
15	25	0.100	0.0040	0.2292	45	0.18
16	19	0.250	0.0132	0.7538	45	0.59
17	19	0.250	0.0132	0.7538	45	0.59
18	19	0.125	0.0066	0.3769	45	0.30
19	18.5	0.375	0.0203	1.1612	45	0.91
20	18	0.375	0.0208	1.1935	45	0.94
21	Rotation Not Tested	N/A	N/A	N/A	46	N/A
22	Rotation Not Tested	N/A	N/A	N/A	46	N/A
23	Rotation Not Tested	N/A	N/A	N/A	46	N/A
24	Rotation Not Tested	N/A	N/A	N/A	46	N/A
25	Rotation Not Tested	N/A	N/A	N/A	46	N/A
26	50	1.125	0.0225	1.2889	46	1.04
27	14.5	0.125	0.0086	0.4939	46	0.40
28	14.5	0.375	0.0259	1.4815	46	1.19
29	50	1.500	0.0300	1.7184	46	1.38
30	50	0.875	0.0175	1.0026	46	0.81
31	7	0.125	0.0179	1.0230	46	0.82
32	7	0.125	0.0179	1.0230	46	0.82
33	7	0.125	0.0179	1.0230	46	0.82
34	6.5	0.250	0.0384	2.2026	46	1.77
35	6.5	0.125	0.0192	1.1017	46	0.88
36	6.5	0.125	0.0192	1.1017	46	0.88

Table 16 gives the minimum, maximum and average rotation of the concrete specimens as they underwent loading during testing.

Table 16 - Range of Rotation.

Max Rotation [Degrees]	2.203
Average Rotation [Degrees]	0.901
Minimum Rotation [Degrees]	0.143
Standard Deviation of Rotation	0.480

Table 17 gives the minimum, maximum and average deflection from the rotation of the concrete specimen in the wooden test frame during testing.

Table 17 – Range of Deflection at Load from Rotation.

Max Deflection from Rotation [in]	1.769
Average Deflection from Rotation [in]	0.717
Minimum Deflection from Rotation [in]	0.113
Standard Deviation of Deflection from Rotation	0.386

Chapter 5 – Discussion

5.1 – Introduction

This section covers relevant discussion of the results and how they compare to the results previously discussed in Chapter 2. Only the tests that resulted in breakout were considered.

5.2 – Concrete Breakout of the Corner Tests

The results from the research conducted by Fuchs et al. (1995), as discussed in Chapter 2, were normalized to better compare the tests due to varying parameters. Due to this, normalized results are only compared here. The corner testing conducted at MSOE yielded an average $V_{u,tested}/V_{u,predicted}$ of 0.940 and a coefficient of variation 12.75%; this is compared to ~1.20 and 26% for the ACI 349 method and ~0.96 and 17% for the CCD method. Table 18 compares the summary of values. Table 18 provides a summary of the comparison of the percent difference of the test data between ACI 349, CCD and the testing performed at MSOE for the corner tests.

Table 18 – Summary Comparison of Testing Data Between Fuchs *et al.* (1995) and MSOE Capstone Testing for Corner Tests

	ACI 349	CCD	MSOE	Percent Different from ACI 349 & MSOE [%]	Percent Different from CCD & MSOE [%]
Average of $V_{u,tested}/V_{n,predicted}$	1.10	0.96	0.94	17.02	2.13
Coefficient of Variation [%]	26	17	12.75	103.92	33.33

The values represented from ACI 349 and the CCD method were approximated from Figure 9; the authors did not specify what exactly the values were. Figure 9 represents the test results from Europe and were used as comparison instead of the U.S. results because the testing setup is more similar to what was used in the testing at MSOE. There were no prestressing forces present in the testing done at MSOE.

The results from the testing performed at MSOE yielded a percent difference of 2.13% and 33.33% for the average of $V_{u,tested}/V_{u,predicted}$ and coefficient of variation, respectively, with

respect to the results found by Fuchs et al. (1995) for the CCD method and supports that this method better predicts the concrete breakout strength of thick members when subjected to a shear load toward an edge.

5.3 – Concrete Breakout of the Non-Corner Tests

The results from the research conducted by Fuchs et al. (1995), as discussed in Chapter 2, were normalized to better compare the tests due to varying parameters. Due to this, normalized results only are compared here. The corner testing conducted at MSOE yielded an average $V_{u,tested}/V_{u,predicted}$ of 0.96 and a coefficient of variation 13%; this is compared to ~1.20 and 26% for the ACI 349 method and ~0.96 and 17% for the CCD method. Table 19 provides a summary of the comparison of the percent difference of the test data between ACI 349, CCD and the testing performed at MSOE for the non-corner tests.

Table 19 – Summary Comparison of Testing Data Between Fuchs *et al.* (1995) and MSOE Capstone Testing for Non-Corner Tests

	ACI 349	CCD	MSOE	Percent Different from ACI 349 & MSOE [%]	Percent Different from CCD & MSOE [%]
Average of $V_{u,tested}/V_{n,predicted}$	1.10	0.96	0.96	14.58	0.00
Coefficient of Variation [%]	26	17	13	100.00	30.77

The values represented from ACI 349 and the CCD method where approximated from Figure 9; the authors did not specify what exactly the values were. Figure 9 represents the test results from Europe and were used as comparison instead of the U.S. results because the testing setup is more similar to what was used in the testing at MSOE. There were no prestressing forces present in the testing done at MSOE.

The results from the testing performed at MSOE yielded a percent difference of 0% and 30.77% for the average of $V_{u,tested}/V_{u,predicted}$ and coefficient of variation, respectively, with respect to the

results found by Fuchs et al. (1995) for the CCD method, which supports that this method better predicts the concrete breakout strength of thick members when subjected to a lateral load toward an edge.

5.4 - IBC Railing Strength Requirement

For the testing conducted at MSOE, all tests for the given parameters consistently met the live load strength requirement of 200 lb. required by IBC. The dimensions of the parameter were chosen to mimic common embedded railing posts in concrete used in practice.

5.5 – Uncoupling the Moment into Shear

When calculating the capacity for concrete breakout when subjected to the lateral load, the moment was uncoupled and the shear from the uncoupled moment was transferred into the concrete. The code does not specifically cover this situation. Since the results of the tests conducted at MSOE match the results found by Fuchs et al. (1995), this finding supports the assumption that uncoupling the moment and transferring the shear into the concrete is sufficient in the design for the specific application used in the testing described earlier in the paper.

5.6 – Deflection

The overall deflection at the point of the load could be mainly found from three different sources:

1. Elastic deformation,
2. Plastic deformation,
3. Rotation of the concrete specimen in the wooden frame.

Deflection from elastic deformation can be found from basic mechanics of material calculations. The elastic deformation is represented in the deflection graphs as a linear line. The plastic deformation can be observed in the deflection graphs as well. The plastic deformation started to

occur around 450 lb. which is consistent with Table 20. The elastic and plastic deformation can easily be calculated from standard mechanics of material equations.

Table 20 – Range of Elastic and Plastic Deformation.

Elastic Range	0-450	lb
Plastic Range	450-636	lb

The deflection caused by the rotation of the concrete specimen in the wooden frame can easily be observed in the deflection graphs previously presented in the paper. The deflection caused by the rotation was mainly between 0 lb. and 200 lb. During this period between 0 lb. and 200 lb., the concrete specimen was fixing itself in the wooden test frame. After fixing itself in the frame, the concrete specimen generally did not move. Before testing each concrete specimen, wedges were inserted to help fix the concrete specimen as well as possible to mitigate rotation. The rotation of the concrete specimen in the wooden frame can easily be observed in the deflection graphs. Figure 61 provides an example of the deflection that is mainly attributed to the rotation of the concrete specimen in the wooden frame. The ovals represent deflection caused by the rotation of the concrete specimen during loading. It is also important to reiterate that the maximum rotation of any one concrete specimen in the testing frame was 2.203 degrees, as stated in Table 16.

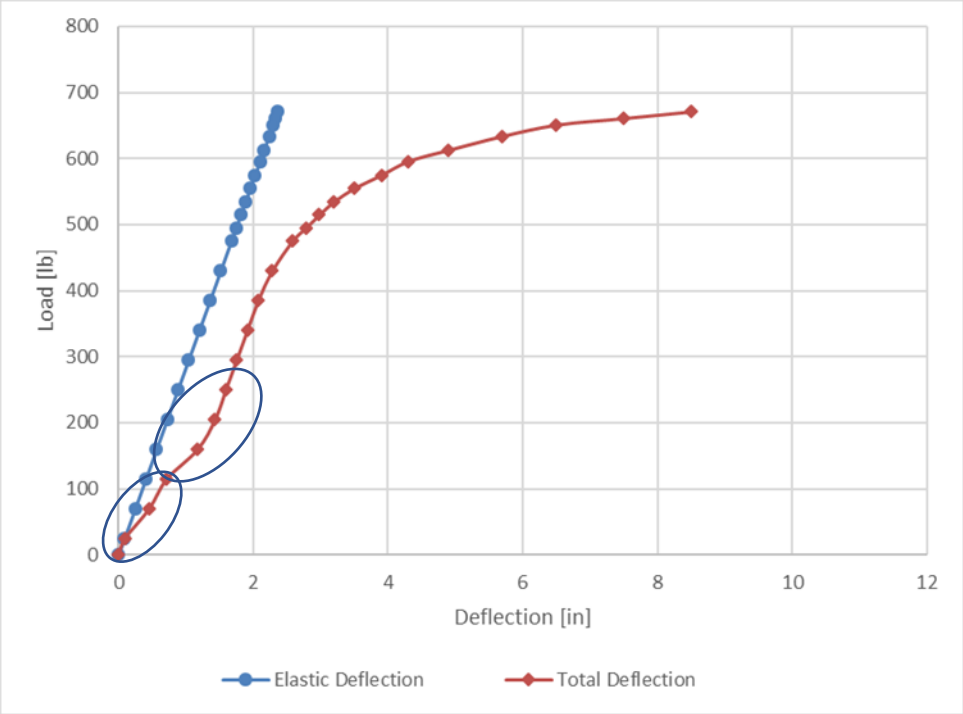

Figure 61 – Example of Where Rotation is Represented in the Deflection Graphs.

There are different loads that caused the basket of weights to bottom out. This is due to the fact that the straps were shortened to allow the pipe to deflect farther in order to achieve a better possible chance of breakout after previous tests bottomed out.

5.7 – Recommendation for Future Work

A recommendation for future work would be to strengthen the testing frame for whatever material it is made out of. The testing for this project utilized wood for the construction of the main testing frame. This caused the concrete specimen to rotate a small amount in the test frame partially because of the soft nature of wood.

A second recommendation for future work is to utilize two sets of 2X4's to hold the pipes during the concrete pour and embedment of the pipes, one set at the top of the pipe and another set at the bottom of the pipe, to hold the pipes straighter while the pipes are being cast in place.

The third recommendation for future work is to order the concrete from a ready mix plant to provide a more consistent mix and to reduce the workload on the student, along with the use of a vibrator to compact the concrete instead of a rod.

The fourth recommendation for future work would be to allow more than three inches of clear space between the influence cones to allow for a breakout cone that has an angle less than 35 degrees to have less of a chance to interfere with adjacent tests. The spacing used in the testing performed at MSOE utilized a three inch clear space between the influence breakout cones so that the breakouts would not influence one another; some cones were larger than what the code predicts with the CCD model and possibly reduced the capacity of the test

The last recommendation for future research is to actually embed a full railing set with multiple connected posts to see how additional posts potentially add to the capacity of the embedded post connection.

5.8 - Summary

The test results from this experiment agree more favorably with the CCD method as compared to the provisions in ACI349-85. The results from the experiment support the conclusion by Fuchs *et al.* (1995) that the CCD method is a more accurate and user friendly model to predict the concrete failure loads for a single fastener in uncracked concrete when subjected to a lateral load toward an edge. All tests for the given parameters, which mimic dimensions used in standard practice, consistently met the live load strength requirement of 200 lb. required by IBC. Lastly, since the results agree with what Fuchs et al. (1995) found, the assumption that the moment can be uncoupled and accounted for by just shear is supported.

References

ACI Committee 318, “Building Code Requirements for Structural Concrete (ACI 318-14),” American Concrete Institute, Detroit, 2014

ACI Committee 349, “Code Requirements for Nuclear Safety Related Concrete Structures (ACI 349-85),” American Concrete Institute, Detroit, 1985

Fuchs, W., Eligehausen, R., and Breen, J. E. (1995). Concrete Capacity Design (CCD) Approach for Fastening to Concrete. *ACI Structural Journal, 92*(1), 73-94. https://doi.org/10.14359/1533

Fuchs, W., “Entwicklung eines Vorschlags für die Bemessung von Befestigungen (Development of a Proposal for the Design of Fastenings to Concrete),” Report to the Deutsche Forschungsgemeinschaft, Feb. 1991. (in German).

International Building Code. (2015). Country Club Hills, IL: International Code Council.

Appendix A - Pictures of Tests

Test 1, 6-in. Slab Thickness, Corner Test, 3-in. Setback, 4-in. Embed

Figure A-1 – Test 1 Specimen.

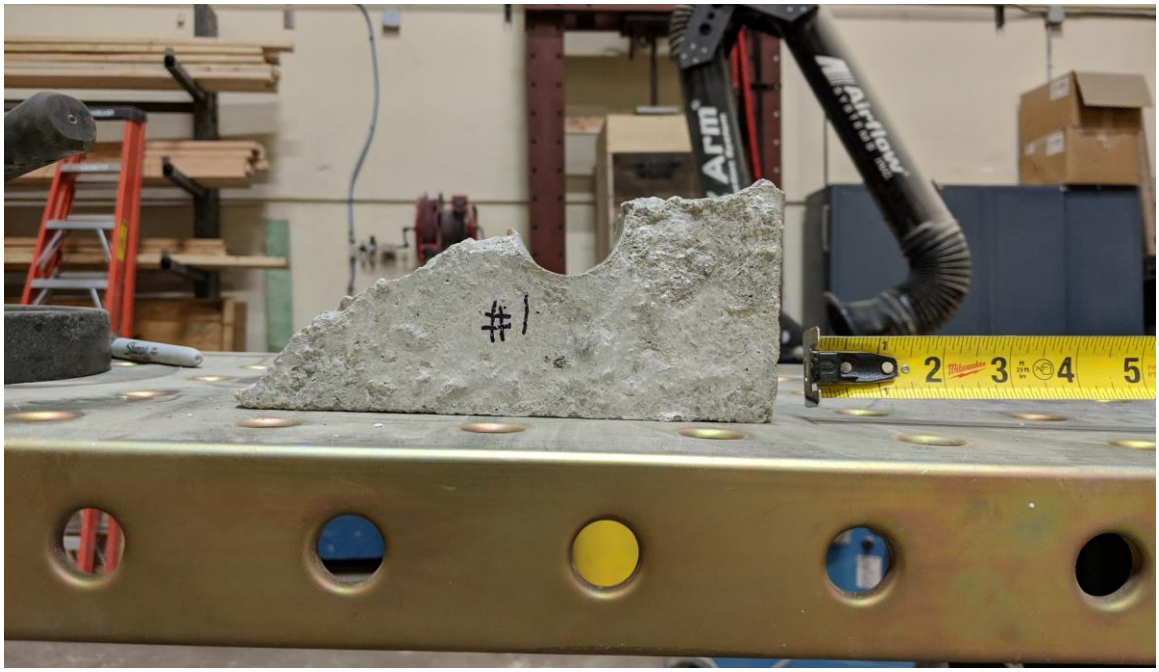

Figure A-2 – Front View of Test 1 Breakout Piece.

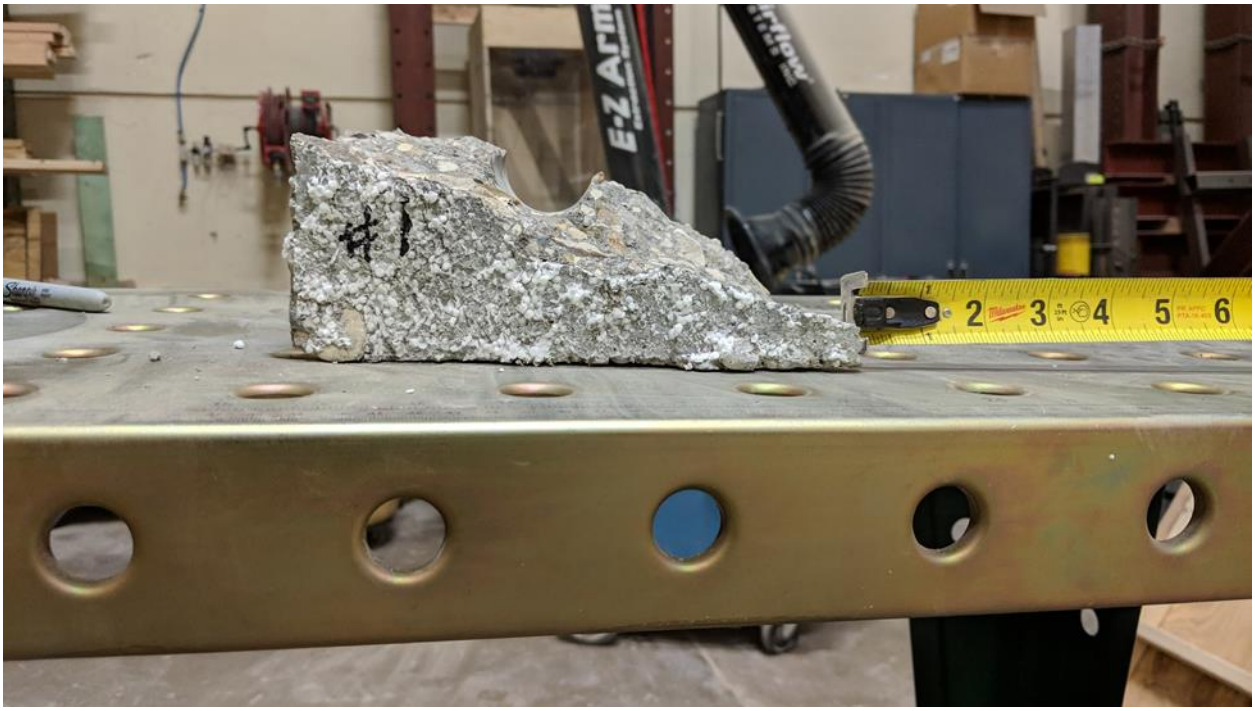

Figure A-3 – Back View of Test 1 Breakout Piece.

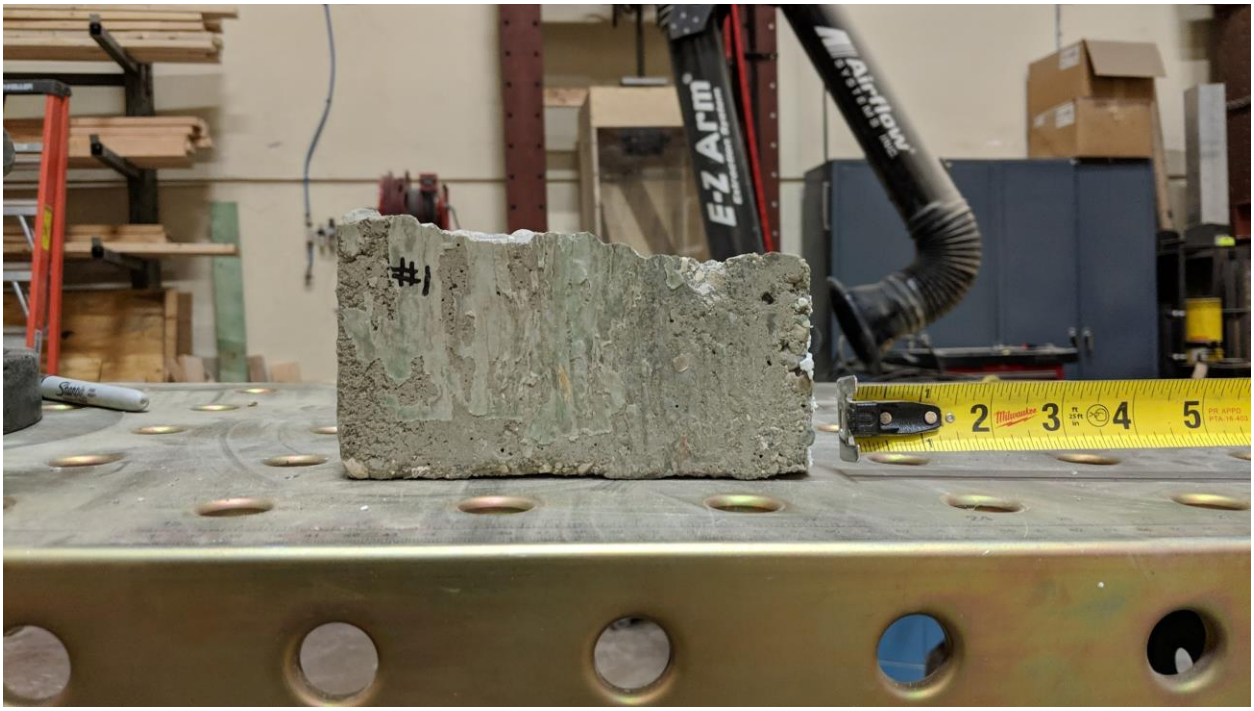

Figure A-4 – Side View 1 of Test 1 Breakout Piece.

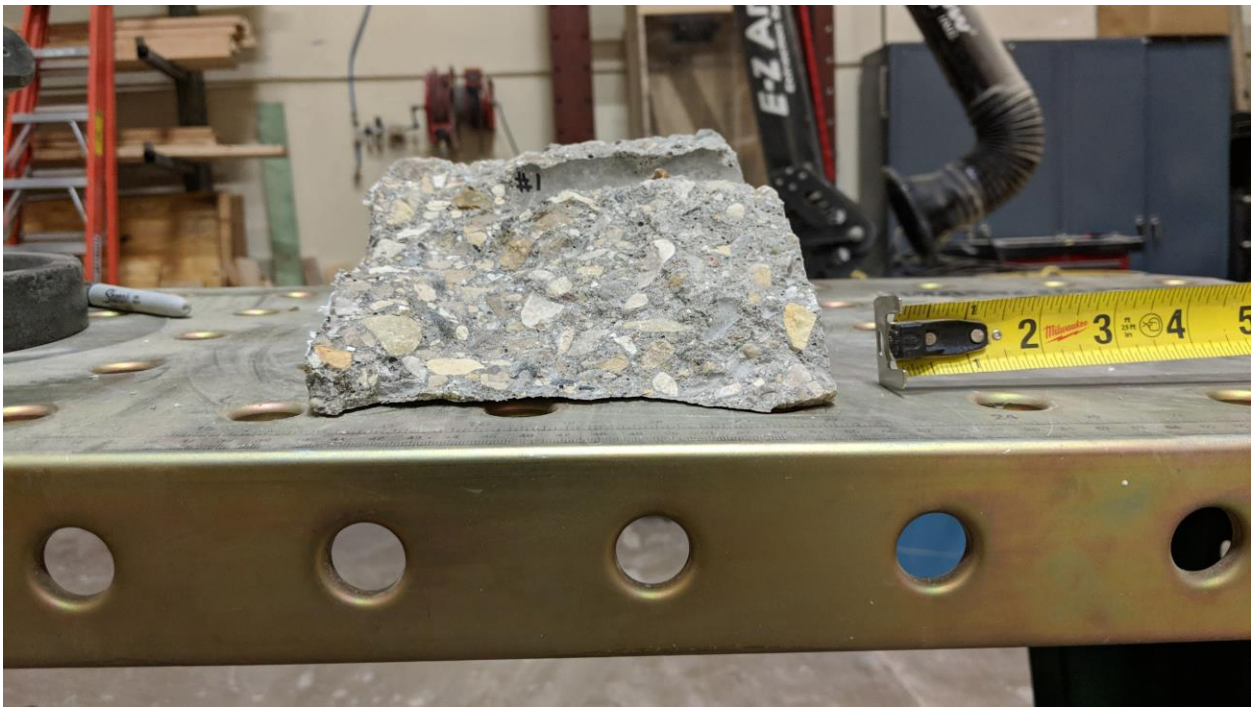

Figure A-5 – Side View 2 of Test 1 Breakout Piece.

Figure A-6 – Top View of Test 1 Breakout Piece.

Test 2, 6-in. Slab Thickness, Non-Corner Test, 3-in. Setback, 4-in. Embed

Figure A-7 – Test 2 Specimen.

Test 3, 6-in. Slab Thickness, Non-Corner, 3-in. Setback, 4-in. Embed

Figure A-8 – Test 3 Specimen.

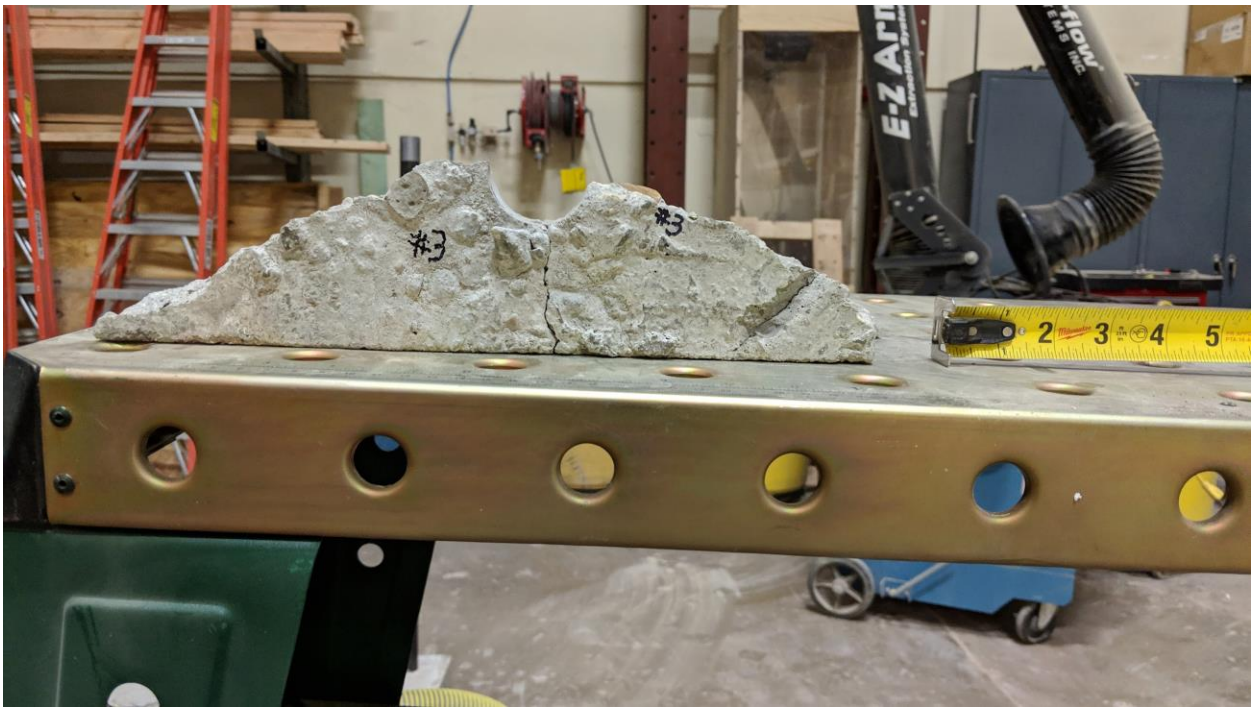

Figure A-9 – Front View of Test 3 Breakout Piece.

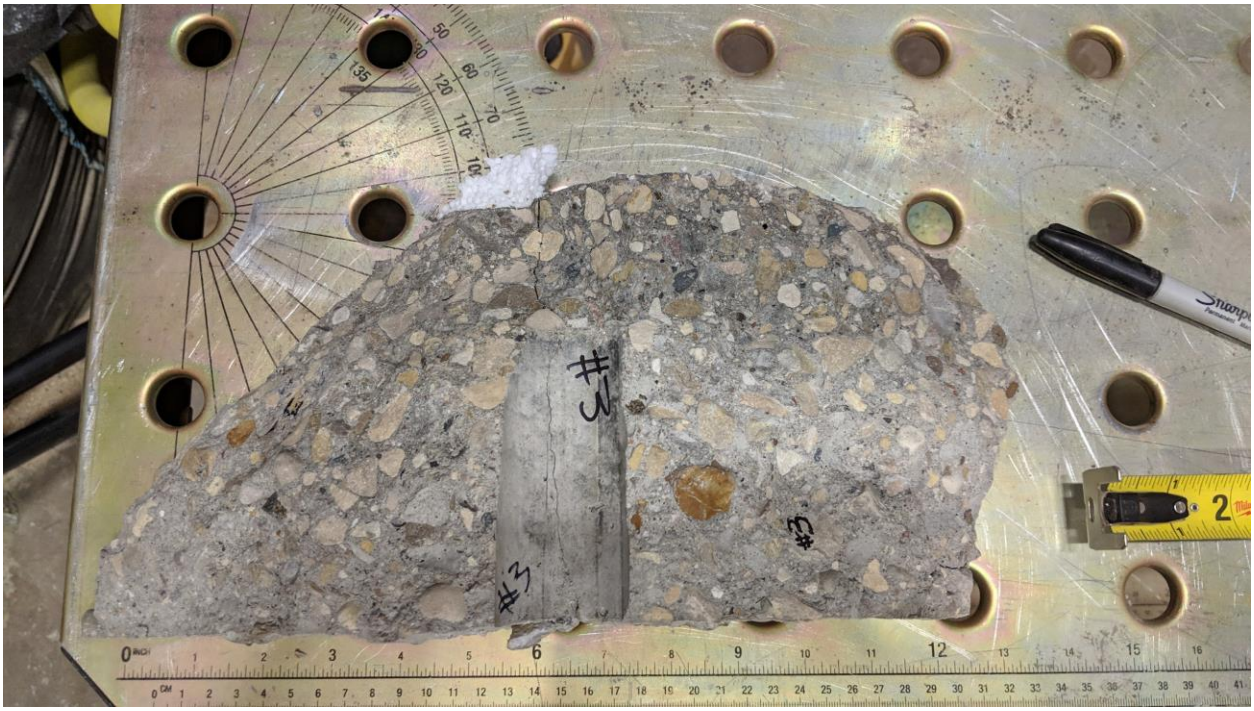

Figure A-10 – Top View of Test 3 Breakout Piece.

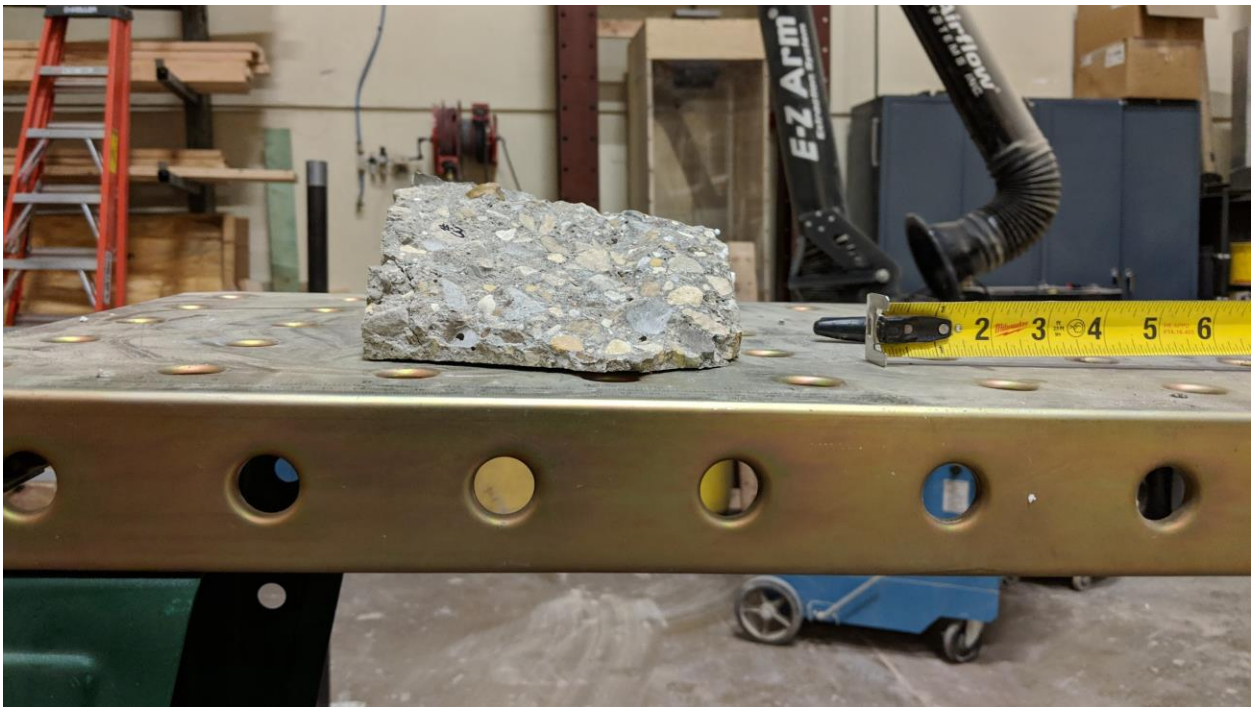

Figure A-11 – Side View 1 of Test 3 Breakout Piece.

Figure A-12 – Back View of Test 3 Breakout Piece.

Figure A-13 – Side View 2 of Test 3 Breakout Piece.

Test 4, 6-in. Slab Thickness, Non-Corner, 3-in. Setback, 4-in.Embed

Figure A-14 – Test 4 Specimen.

Test 5, 6-in. Slab Thickness, Corner, 3-in. Setback, 4-in. Embed

Figure A-15 – Test 5 Specimen.

Test 6, 6-in. Slab Thickness, Corner, 3-in. Setback, 3-in. Embed

Figure A-16 – Test 6 Specimen.

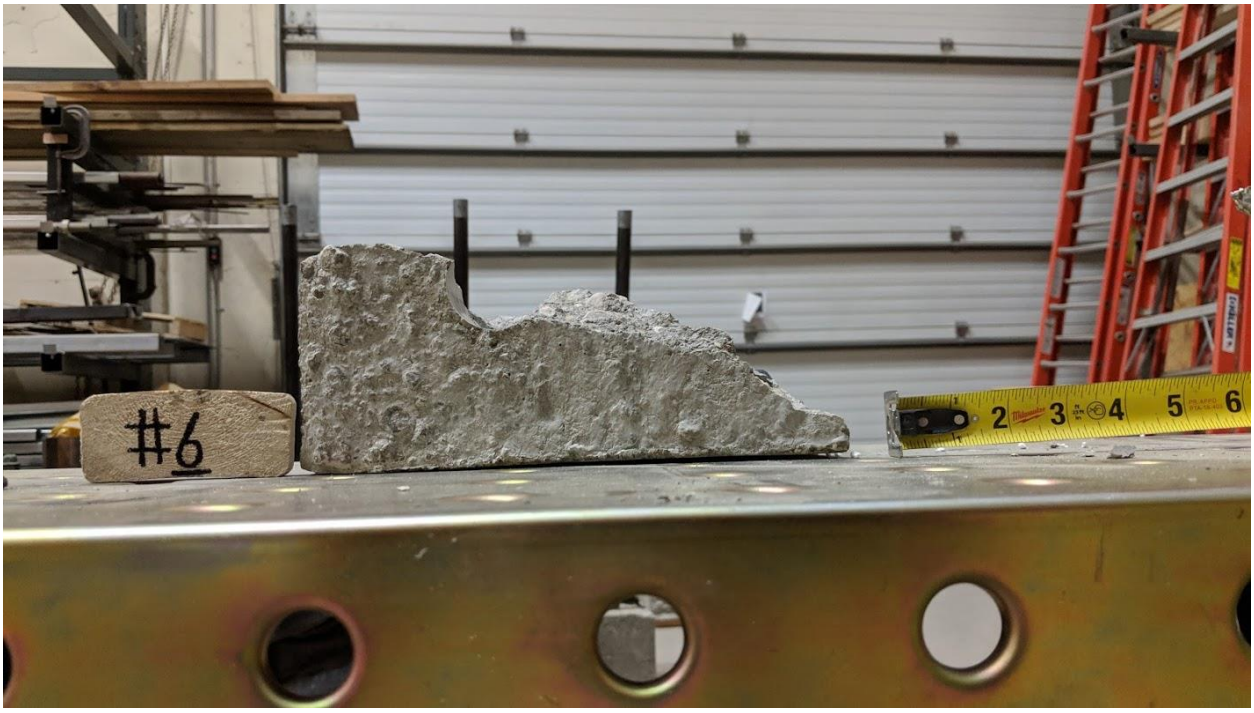

Figure A-17 – Front View of Test 6 Breakout Piece.

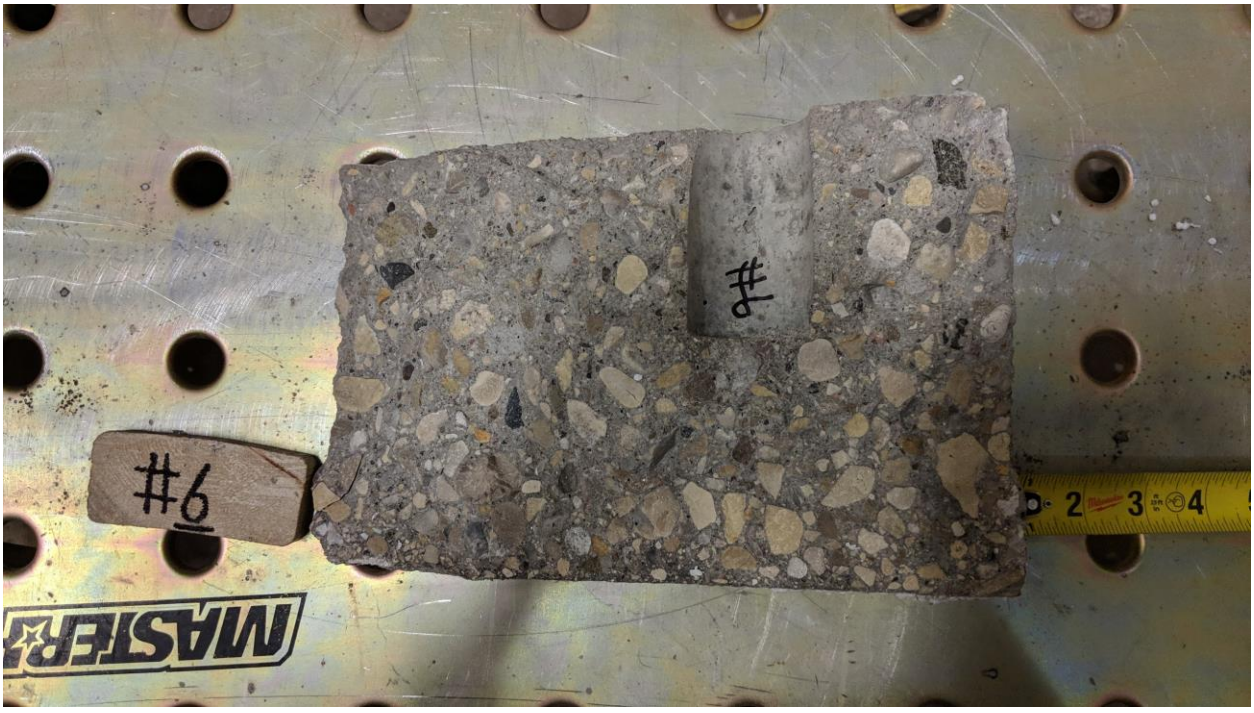

Figure A-18 – Top View of Test 6 Breakout Piece.

Figure A-19 – Back View of Test 6 Breakout Piece.

Figure A-20 – Side View of Test 6 Breakout Piece.

Test 7, 6-in. Slab Thickness, Non-Corner, 3-in. Setback, 3-in. Embed

Figure A-21 – Test 7 Specimen.

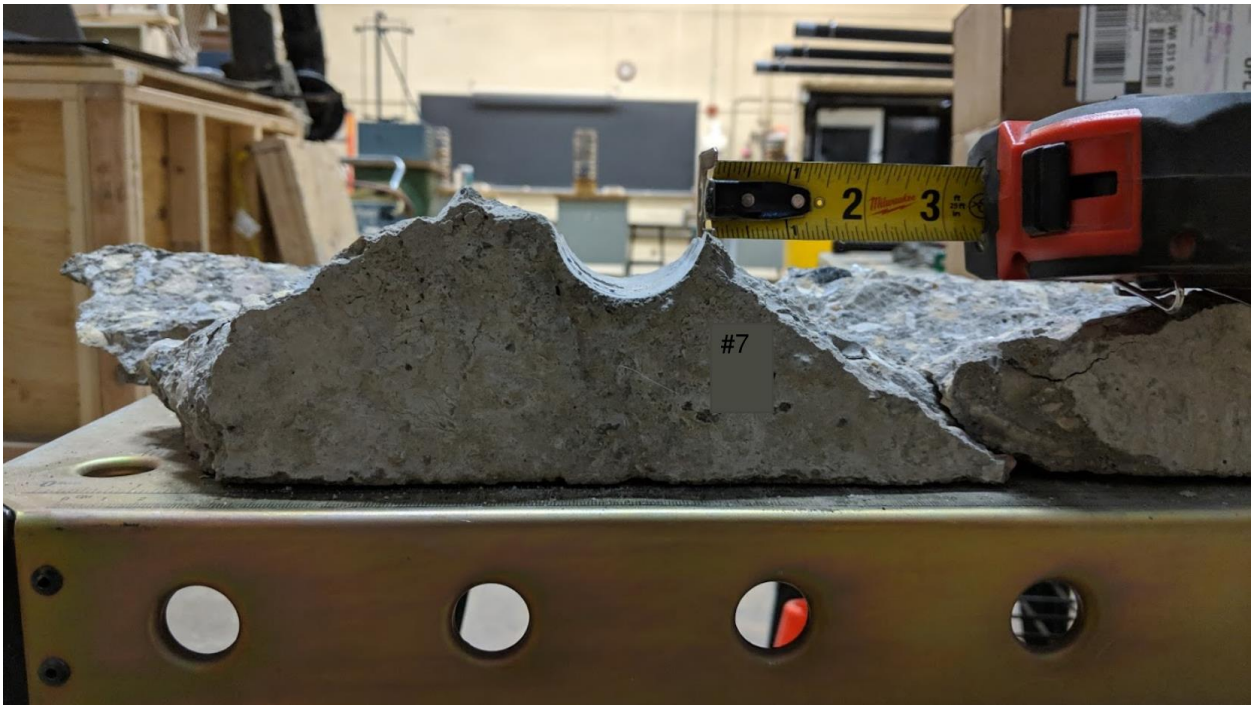

Figure A-22 – Front View of Test 7 Breakout Piece.

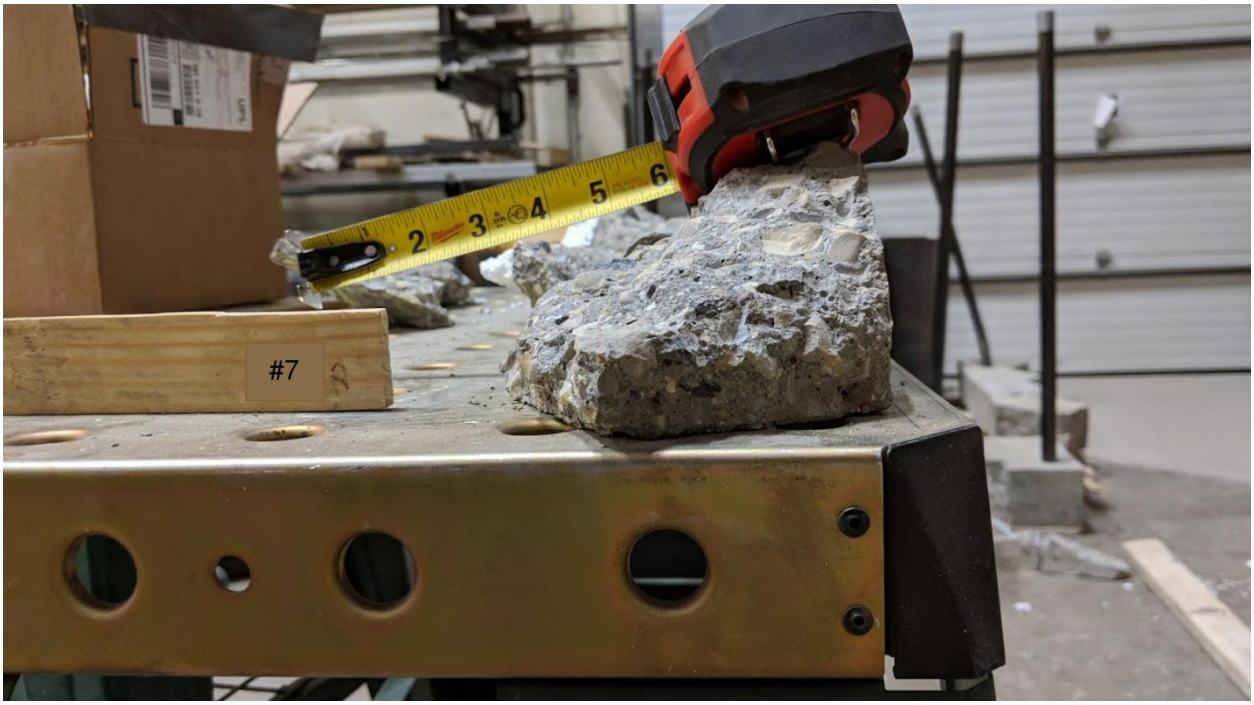

Figure A-23 – Side View 1 of Test 7 Breakout Piece.

Figure A-24 – Top View of Test 7 Breakout Piece.

Figure A-25 – Side View 2 of Test 7 Breakout Piece.

Test 8, 6-in. Slab Thickness, Non-Corner, 3-in. Setback, 3-in. Embed

Figure A-26 – Test 8 Specimen.

Figure A-27 – Front View 1 of Test 8 Breakout Piece.

Figure A-28 – Front View 2 of Test 8 Breakout Piece.

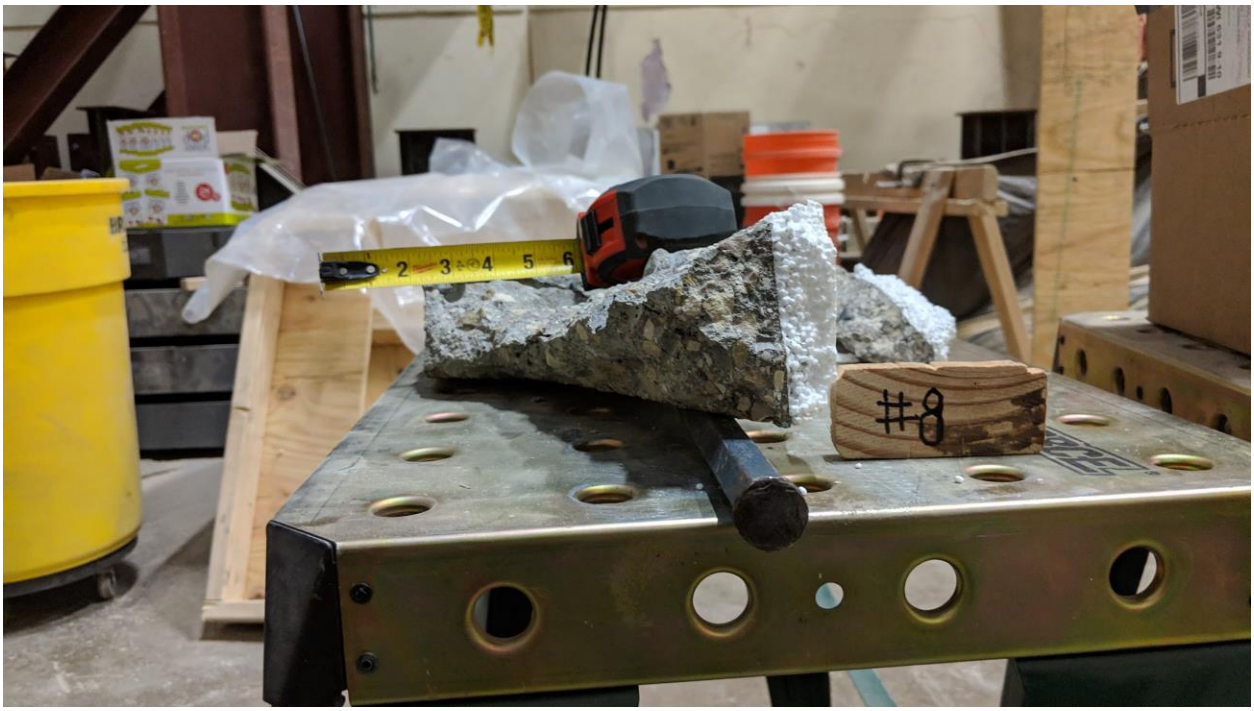

Figure A-29 – Side View of Test 8 Breakout Piece.

Figure A-30 – Top View of Test 8 Breakout Piece.

Test 9, 6-in. Slab Thickness, Non-Corner, 3-in. Setback, 3-in. Embed

Figure A-31 – Test 9 Specimen.

Figure A-32 – Front View of Test 9 Breakout Piece.

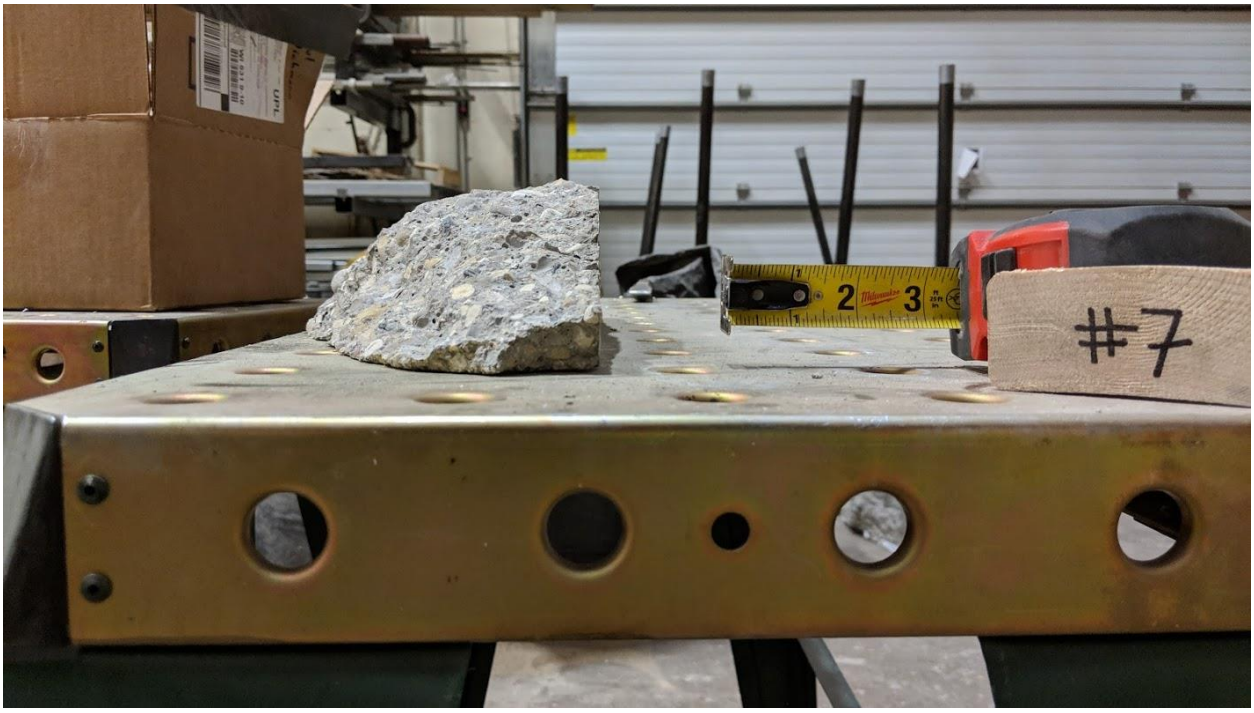

Figure A-33 – Side View 1 of Test 9 Breakout Piece.

Figure A-34 – Side View 2 of Test 9 Breakout Piece.

Figure A-35 – Top View of Test 9 Breakout Piece.

Test 10, 6-in. Slab Thickness, Corner, 3-in. Setback, 3-in. Embed

Figure A-36 – Test 10 Specimen.

Figure A-37 – Front View of Test 10 Breakout Piece.

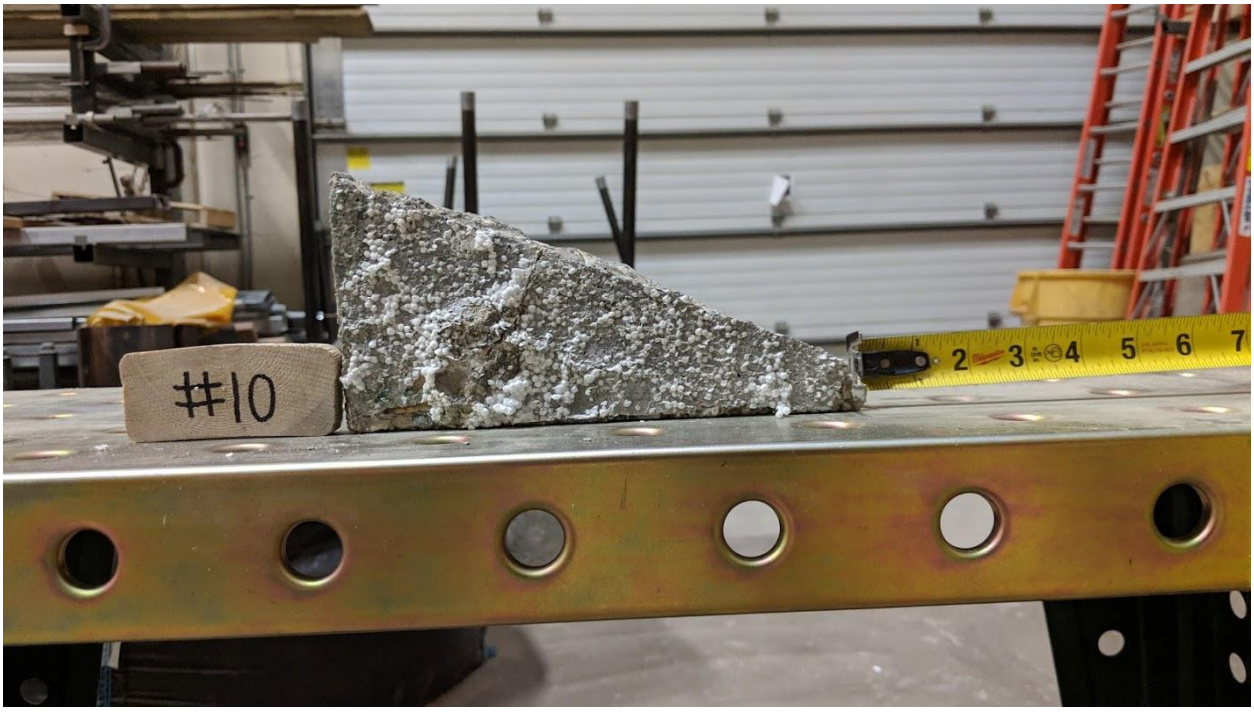

Figure A-38 – Back View of Test 10 Breakout Piece.

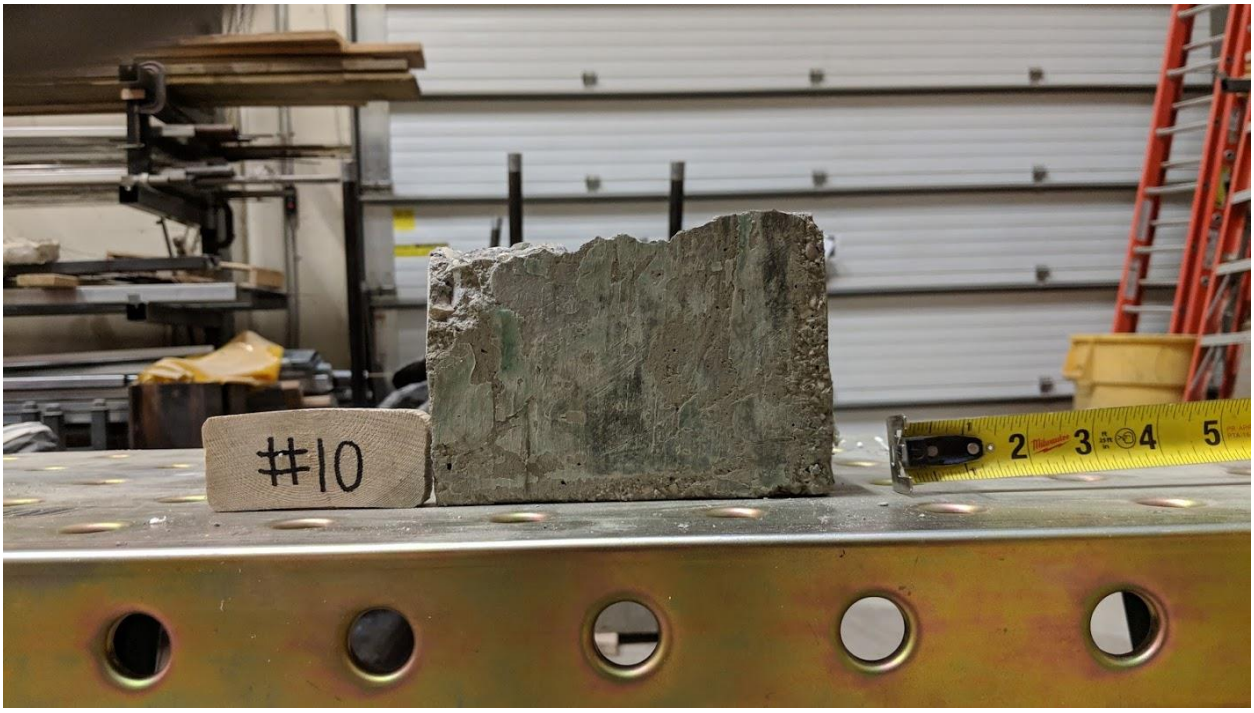

Figure A-39 – Side View 1 of Test 10 Breakout Piece.

Figure A-40 – Side View 2 of Test 10 Breakout Piece.

Figure A-41 – Top View of Test 10 Breakout Piece.

Test 11, 6-in. Slab Thickness, Corner, 4-in. Setback, 3-in. Embed

Figure A-42 – Test 11 Specimen.

Figure A-43 – Front View of Test 11 Breakout Piece.

Figure A-44 – Back View of Test 11 Breakout Piece.

Figure A-45 – Top View of Test 11 Breakout Piece.

Figure A-46 – Side View of Test 11 Breakout Piece.

Test 12, 6-in. Slab Thickness, Non-Corner, 4-in. Setback, 3-in. Embed

Figure A-47 – Test 12 Specimen.

Figure A-48 – Front View of Test 12 Breakout Piece.

Figure A-49 – Top View of Test 12 Breakout Piece.

Figure A-50 – Side View 1 of Test 12 Breakout Piece.

Figure A-51 – Back View of Test 12 Breakout Piece.

Figure A-52 – Side View 2 of Test 12 Breakout Piece.

Test 13, 6-in. Slab Thickness, Non-Corner, 4-in. Setback, 3-in. Embed

Figure A-53 – Test 13 Specimen.

Test 14, 6-in. Slab Thickness, Non-Corner, 4-in. Setback, 3-in. Embed

Figure A-54 – Test 14 Specimen.

Test 15, 6-in. Slab Thickness, Corner, 4-in. Setback, 3-in. Embed

Figure A-55 – Test 15 Specimen.

Figure A-56 – Front View of Test 15 Breakout Piece.

Figure A-57 – Back View of Test 15 Breakout Piece.

Figure A-58 – Top View of Test 15 Breakout Piece.

Figure A-59 – Side View 1 of Test 15 Breakout Piece.

Figure A-60 – Side View 2 of Test 15 Breakout Piece.

Test 16, 6-in. Slab Thickness, Corner, 4-in. Setback, 4-in. Embed

Figure A-61 – Test 16 Specimen.

Figure A-62 – Front View of Test 16 Breakout Piece.

Figure A-63 – Back View of Test 16 Breakout Piece.

Figure A-64 – Top View of Test 16 Breakout Piece.

Figure A-65 – Side View 1 of Test 16 Breakout Piece.

Figure A-66 – Side View 2 of Test 16 Breakout Piece.

Test 17, 6-in. Slab Thickness, Non-Corner, 4-in. Setback, 4-in. Embed

Figure A-67 – Test 17 Specimen.

Test 18, 6-in. Slab Thickness, Non-Corner, 4-in. Setback, 4-in. Embed

Figure A-68 – Test 18 Specimen.

Test 19, 6-in. Slab Thickness, Non-Corner, 4-in. Setback, 4-in. Embed

Figure A-69 – Test 19 Specimen.

Test 20, 6-in. Slab Thickness, Corner, 4-in. Setback, 4-in. Embed

Figure A-70 – Test 20 Specimen.

Figure A-71 – Front View of Test 20 Breakout Piece.

Figure A-72 – Back View of Test 20 Breakout Piece.

Figure A-73 – Side View of Test 20 Breakout Piece.

Figure A-74 – Top View of Test 20 Breakout Piece.

Test 21, 8-in. Slab Thickness, Corner, 3-in. Setback, 4-in. Embed

Figure A-75 – Test 21 Specimen.

Test 22, 8-in. Slab Thickness, Non-Corner, 3-in. Setback, 4-in. Embed

Figure A-76 – Test 22 Specimen.

Figure A-77 – Front View 1 of Test 22 Breakout Piece.

Figure A-78 – Front View 2 of Test 22 Breakout Piece.

Figure A-79 – Top View of Test 22 Breakout Piece.

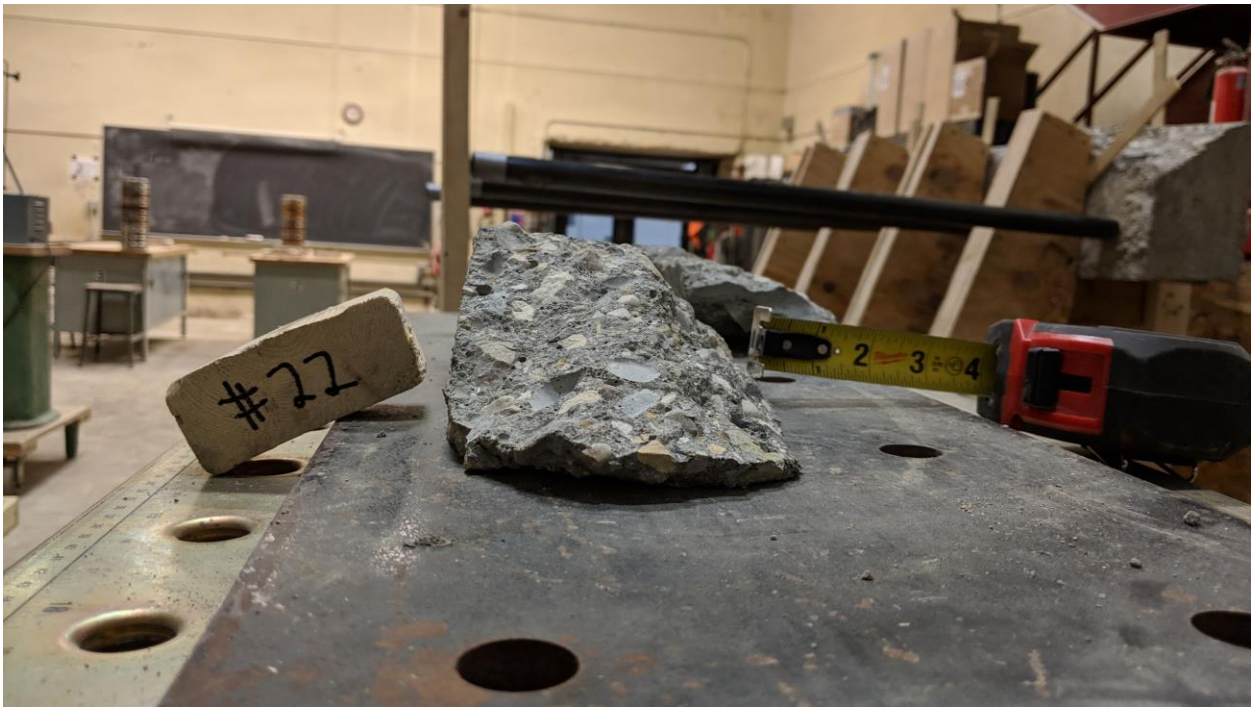

Figure A-80 – Side View 1 of Test 22 Breakout Piece.

Test 23, 8-in. Slab Thickness, Non-Corner, 3-in. Setback, 4-in. Embed

Figure A-81 – Test 23 Specimen.

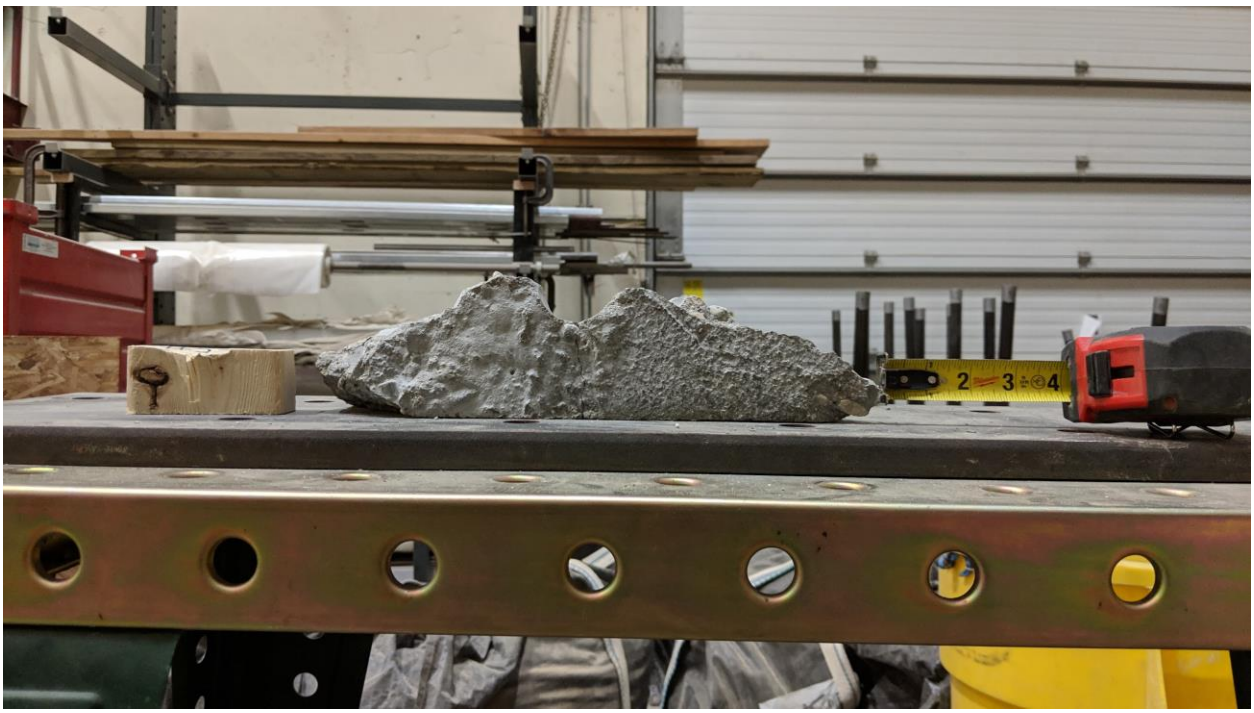

Figure A-82 – Front View of Test 23 Breakout Piece.

Figure A-83 – Top View of Test 23 Breakout Piece.

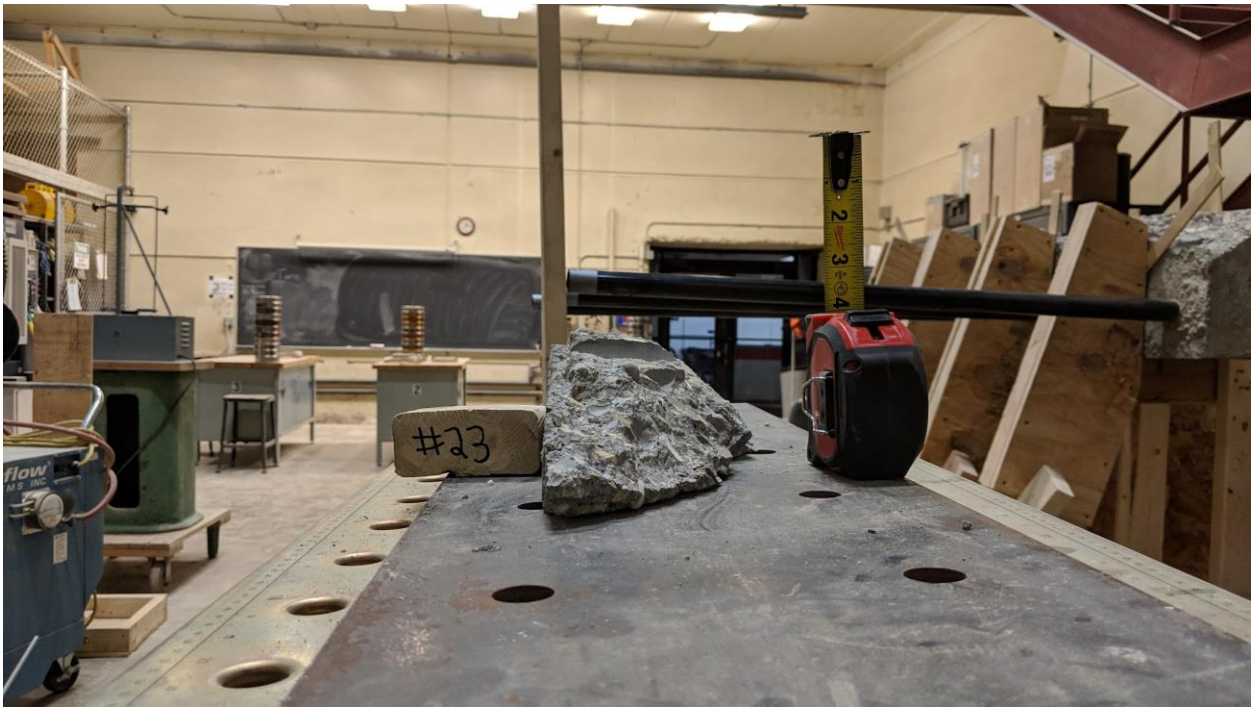

Figure A-84 – Side View 1 of Test 23 Breakout Piece.

Figure A-85 – Side View 2 of Test 23 Breakout Piece.

Test 24, 8-in. Slab Thickness, Non-Corner, 3-in. Setback, 4-in. Embed

Figure A-86 – Test 24 Specimen.

Figure A-87 – Front View of Test 24 Breakout Piece.

Figure A-88 – Top View of Test 24 Breakout Piece.

Figure A-89 – Side View 1 of Test 24 Breakout Piece.

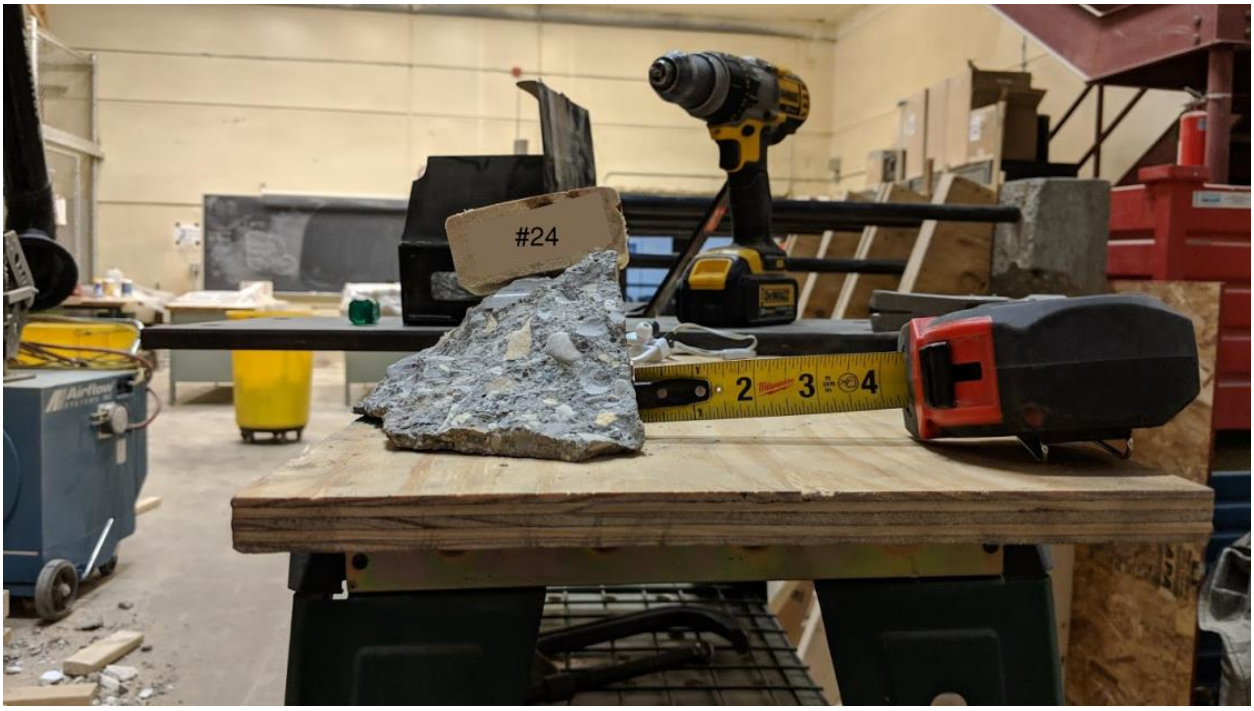

Figure A-90 – Side View 2 of Test 24 Breakout Piece.

Test 25, 8-in. Slab Thickness, Corner, 3-in. Setback, 4-in. Embed

Figure A-91 – Test 25 Specimen.

Figure A-92 – Front View of Test 25 Breakout Piece.

Figure A-93 – Top View of Test 25 Breakout Piece.

Figure A-94 – Side View of Test 25 Breakout Piece.

Test 26, 8-in. Slab Thickness, Corner, 3-in. Setback, 3-in. Embed

Figure A-95 – Test 26 Specimen.

Figure A-96 – Front View of Test 26 Breakout Piece.

Figure A-97 – Side View of Test 26 Specimen.

Figure A-98 – Top View of Test 26 Breakout Piece.

Figure A-99 – Side View 1 of Test 26 Breakout Piece.

Figure A-100 – Side View 2 of Test 26 Breakout Piece.

Test 27, 8-in. Slab Thickness, Non-Corner, 3-in. Setback, 3-in. Embed

Figure A-101 – Test 27 Specimen.

Figure A-102 – Front View of Test 27 Breakout Piece.

Figure A-103 – Back View of Test 27 Breakout Piece.

Figure A-104 – Side View 1 of Test 27 Breakout Piece.

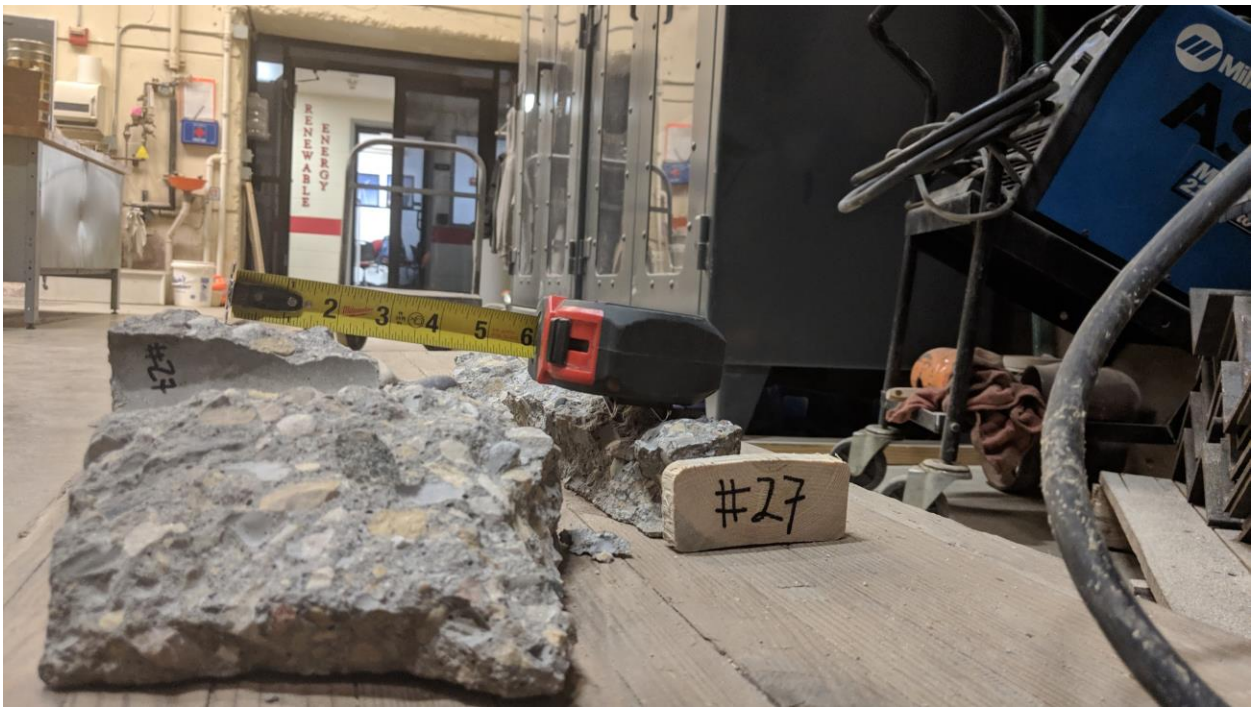

Figure A-105 – Side View 2 of Test 27 Breakout Piece.

Figure A-106 – Top View of Test 27 Breakout Piece.

Test 28, 8-in. Slab Thickness, Non-Corner, 3-in. Setback, 3-in. Embed

Figure A-107 – Test 28 Specimen.

Test 29, 8-in. Slab Thickness, Non-Corner, 3-in. Setback, 3-in. Embed

Figure A-108 – Test 29 Specimen.

Test 30, 8-in. Slab Thickness, Corner, 3-in. Setback, 3-in. Embed

Figure A-109 – Test 30 Specimen.

Figure A-110 – Front View of Test 30 Breakout Piece.

Figure A-111 – Side View 1 of Test 30 Breakout Piece.

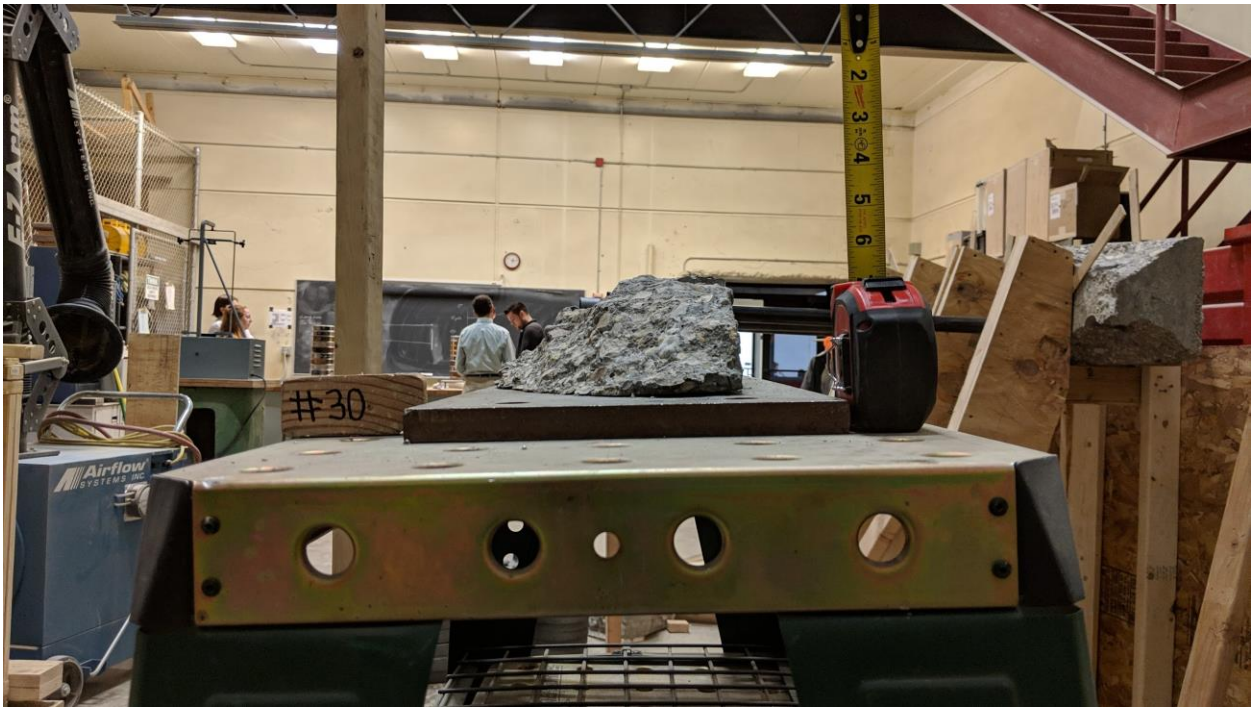

Figure A-112 – Side View 2 of Test 30 Breakout Piece.

Figure A-113 – Top View of Test 30 Breakout Piece.

Test 31, 8-in. Slab Thickness, Corner, 4-in. Setback, 3-in. Embed

Figure A-114 – Test 31 Specimen.

Test 32, 8-in. Slab Thickness, Non-Corner, 4-in. Setback, 3-in. Embed

Figure A-115 – Test 32 Specimen.

Test 33, 8-in. Slab Thickness, Corner, 4-in. Setback, 3-in. Embed

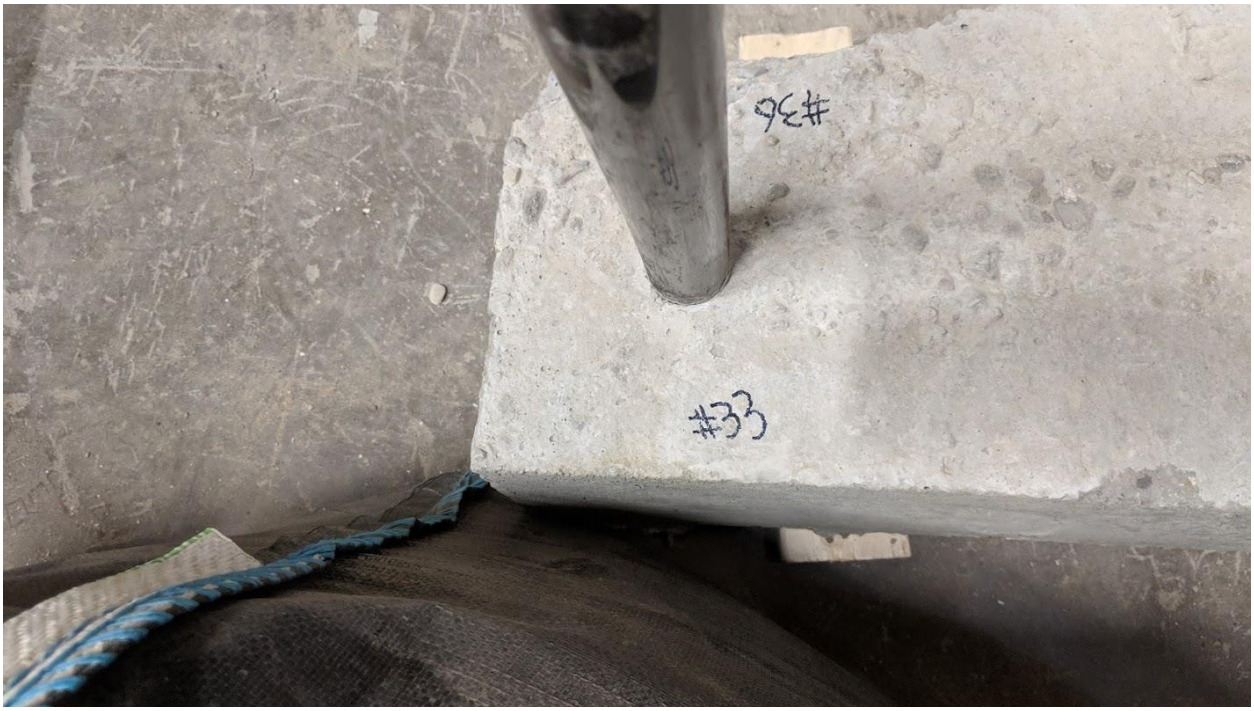

Figure A-116 – Test 33 Specimen.

Test 34, 8-in. Slab Thickness, Corner, 4-in. Setback, 4-in. Embed

Figure A-117 – Test 34 Specimen.

Figure A-118 – Front View of Test 34 Breakout Piece.

Figure A-119 – Top View of Test 34 Breakout Piece.

Figure A-120 – Side View 1 of Test 34 Breakout Piece.

Figure A-121 – Back View of Test 34 Breakout Piece.

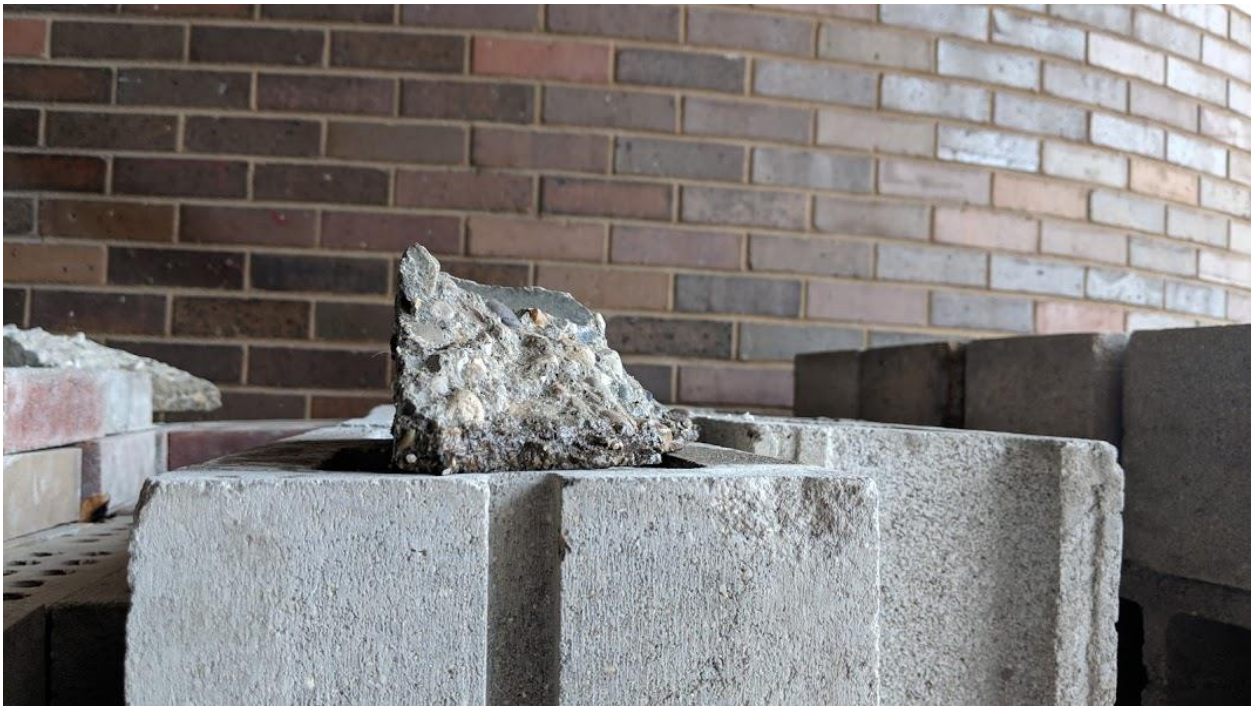

Figure A-122 – Side View 2 of Test 34 Breakout Piece.

Test 35, 8-in. Slab Thickness, Non-Corner, 4-in. Setback, 4-in. Embed

Figure A-123 – Test 35 Specimen.

Figure A-124 – Front View of Test 35 Breakout Piece.

Figure A-125 – Top View of Test 35 Breakout Piece.

Figure A-126 – Side View 1 of Test 35 Breakout Piece.

Figure A-127 – Back View of Test 35 Breakout Piece.

Figure A-128 – Side View 2 of Test 35 Breakout Piece.

Test 36, 8-in. Slab Thickness, Corner, 4-in. Setback, 4-in. Embed

Figure A-129 – Test 36 Specimen.

Figure A-130 – Front View of Test 36 Breakout Piece.

Figure A-131 – Back View of Test 36 Breakout Piece.

Figure A-132 – Side View 1 of Test 36 Breakout Piece.

Figure A-133 – Side View 2 of Test 36 Breakout Piece.

Figure A-134 – Top View of Test 36 Breakout Piece.

Appendix B - Pictures of Concrete Compression Tests

Figure B-1 – View 1 of Day 7 Cylinder Break for Tests 11-20 and 31-36.

Figure B-2 - View 2 of Day 7 Cylinder Break for Tests 11-20 and 31-36.

Figure B-3 - View 3 of Day 7 Cylinder Break for Tests 11-20 and 31-36.

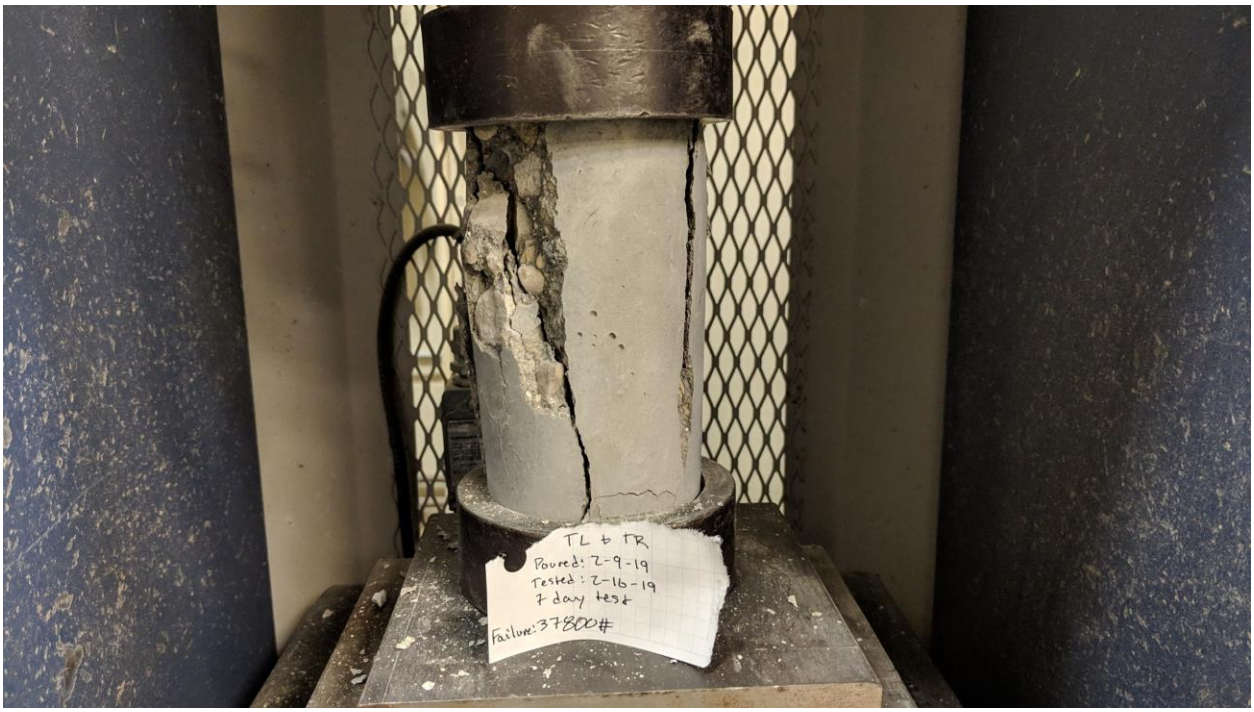

Figure B-4 - View 1 of Day 7 Cylinder Break for Tests 1-10 and 21-30.

Figure B-5 - View 2 of Day 7 Cylinder Break for Tests 1-10 and 21-30.

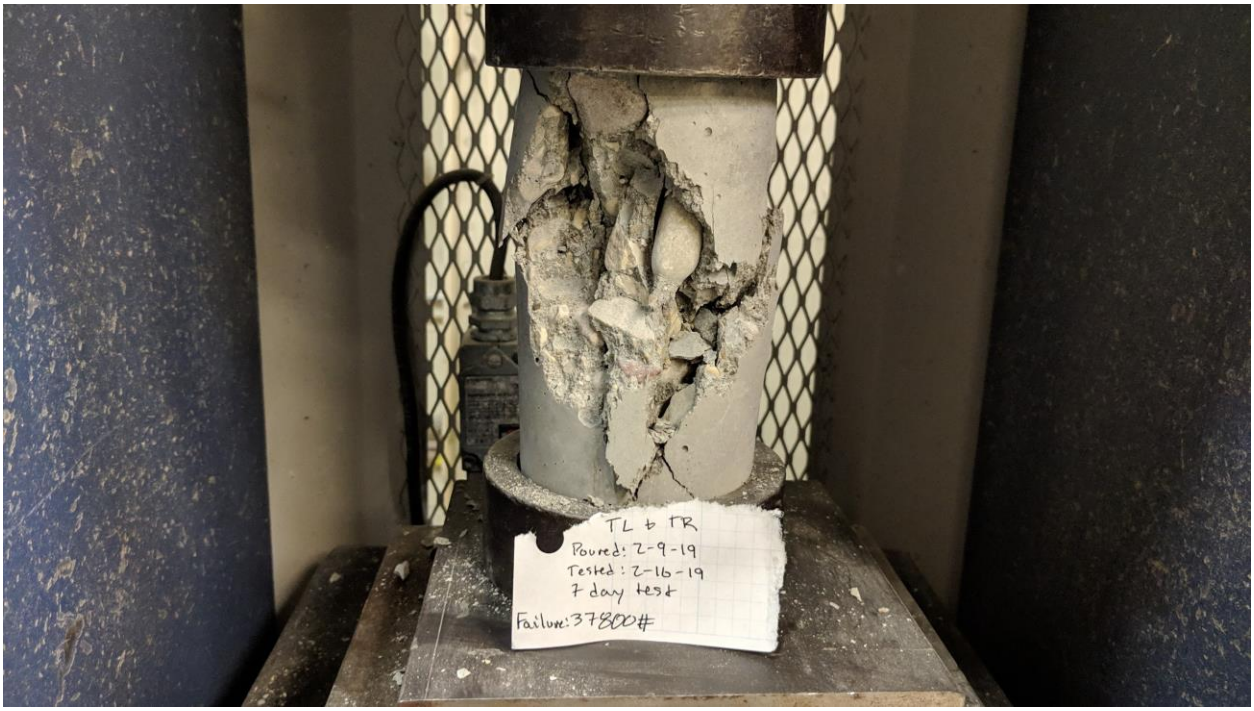

Figure B-6 - View 2 of 7 Day Cylinder Break for Tests 1-10 and 21-30.

Figure B-7 - View 3 of Day 7 Cylinder Break for Tests 1-10 and 21-30.

Figure B-8 – View 1 of Cylinder 1 of Cylinder Break for Tests 11-20 and 31-36.

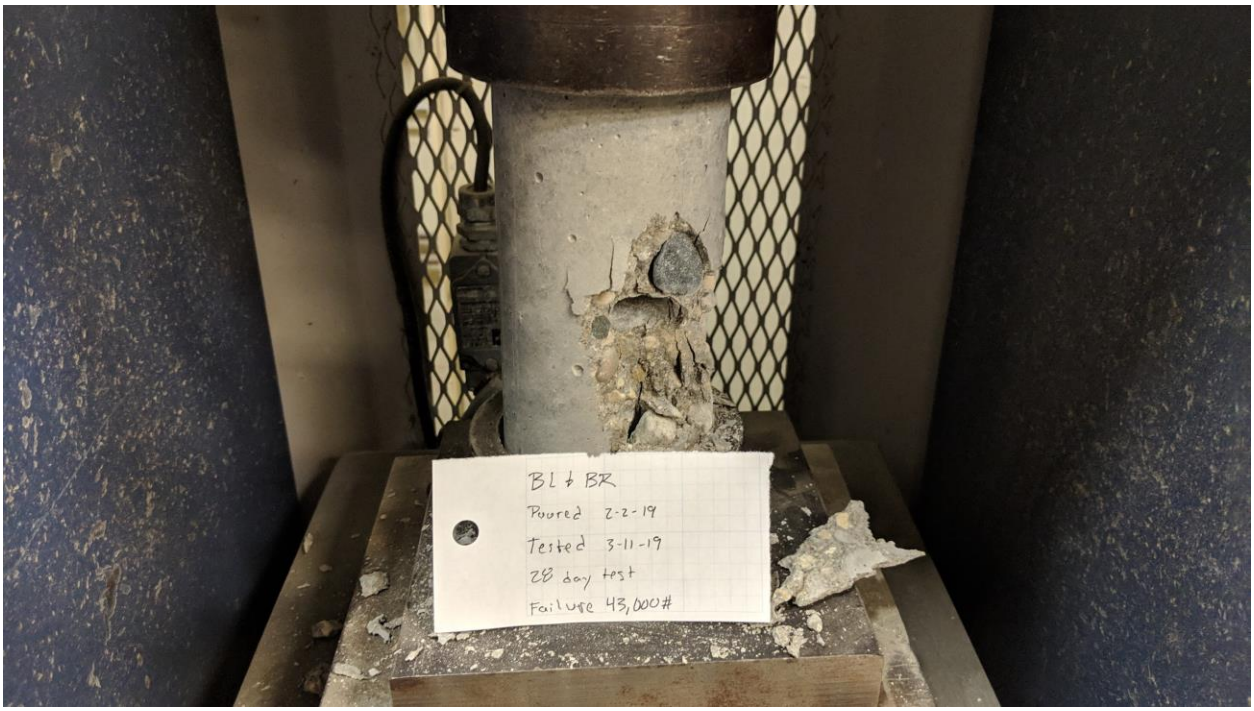

Figure B-9 - View 2 of Cylinder 1 of Cylinder Break for Tests 11-20 and 31-36.

Figure B-10 - View 3 of Cylinder 1 of 37 Day Cylinder Break for Tests 11-20 and 31-36.

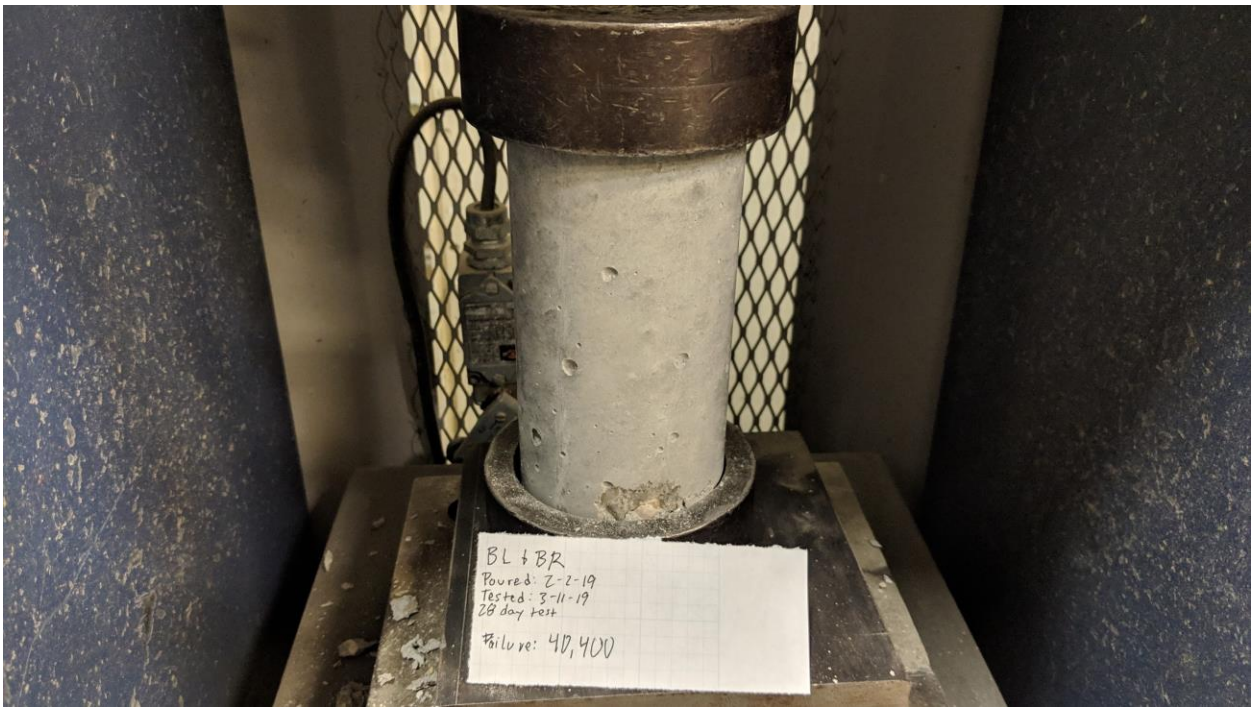

Figure B-11 - View 1 of Cylinder 2 of 37 Day Cylinder Break for Tests 11-20 and 31-36.

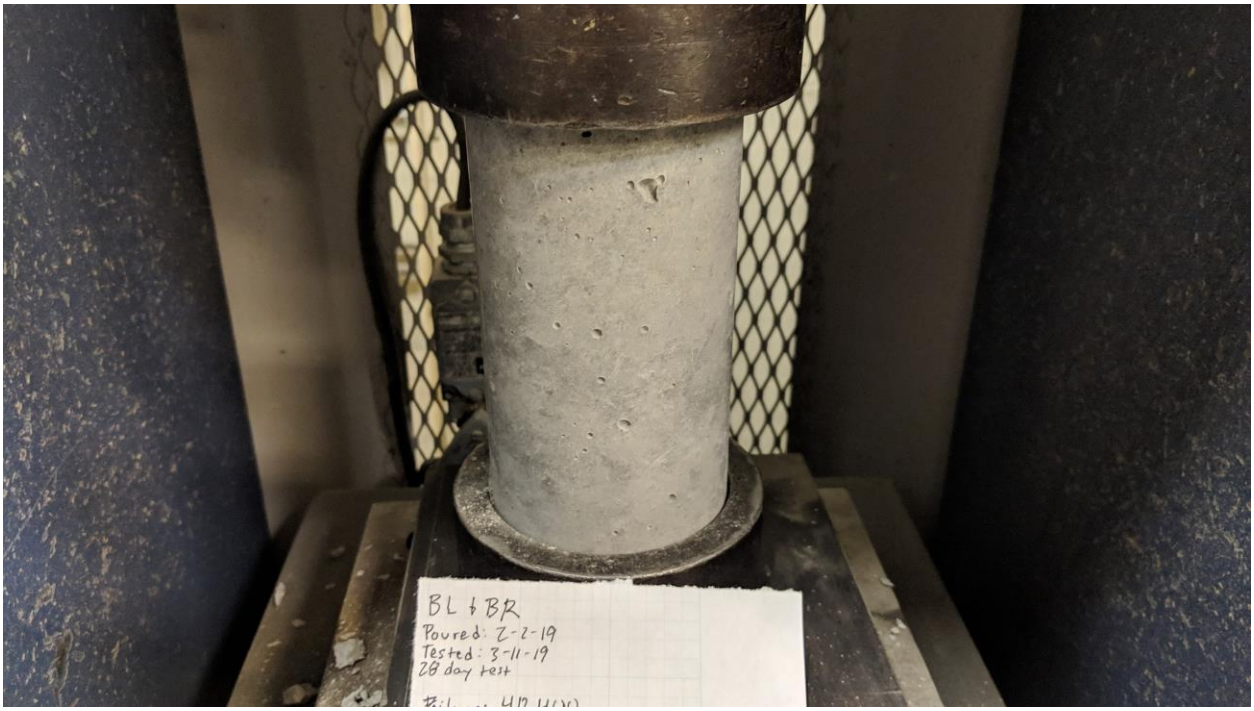

Figure B-12 - View 2 of Cylinder 2 of 37 Day Cylinder Break for Tests 11-20 and 31-36.

Figure B-13 - View 3 of Cylinder 2 of 37 Day Cylinder Break for Tests 11-20 and 31-36.

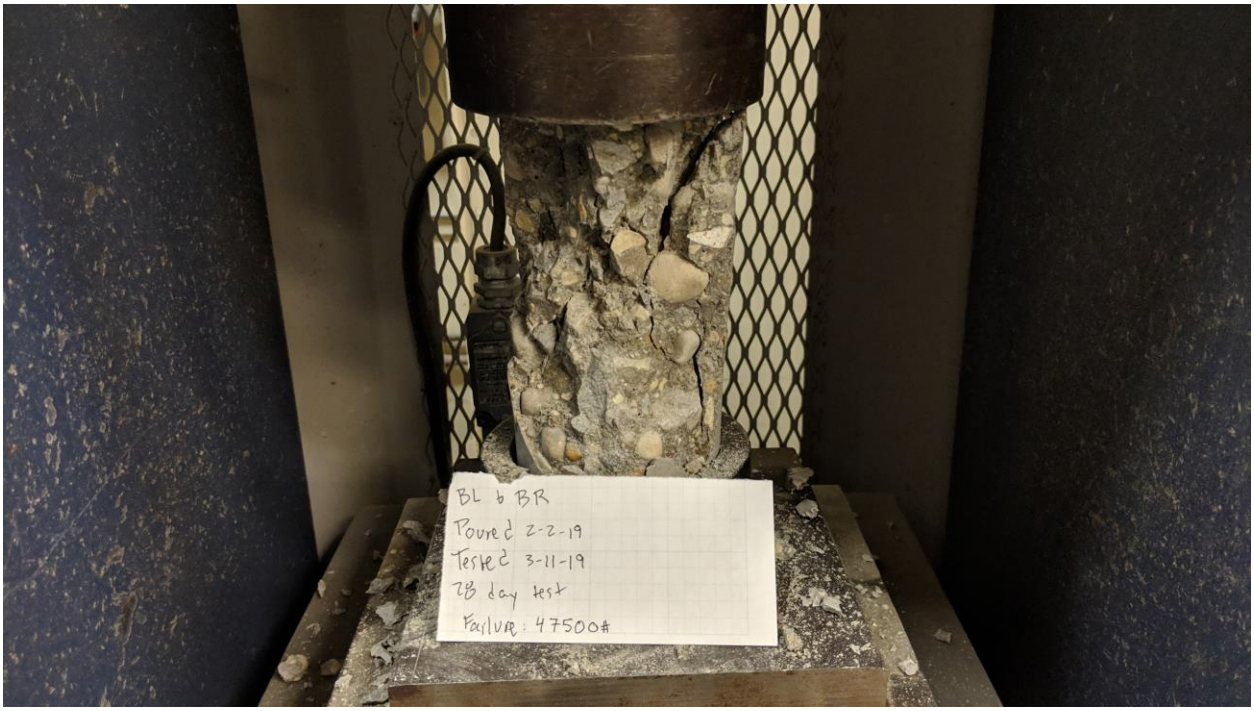

Figure B-14 - View 1 of Cylinder 3 of 37 Day Cylinder Break for Tests 11-20 and 31-36.

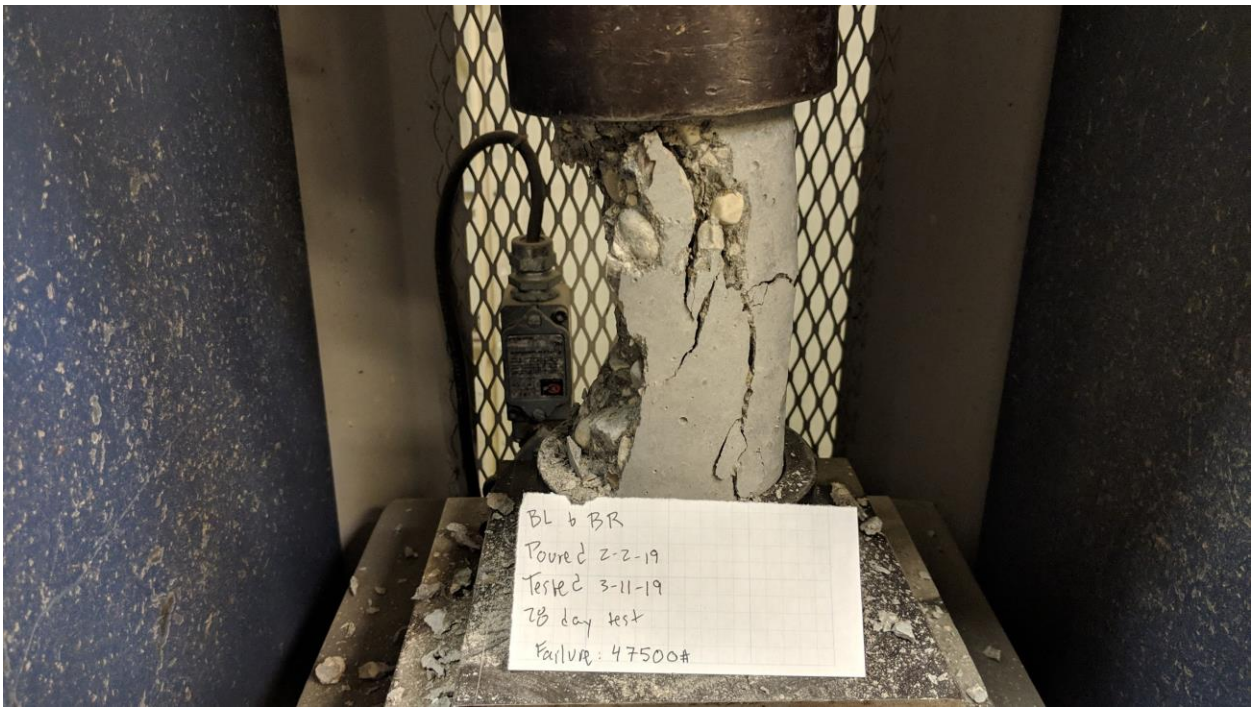

Figure B-15 - View 2 of Cylinder 3 of 37 Day Cylinder Break for Tests 11-20 and 31-36.

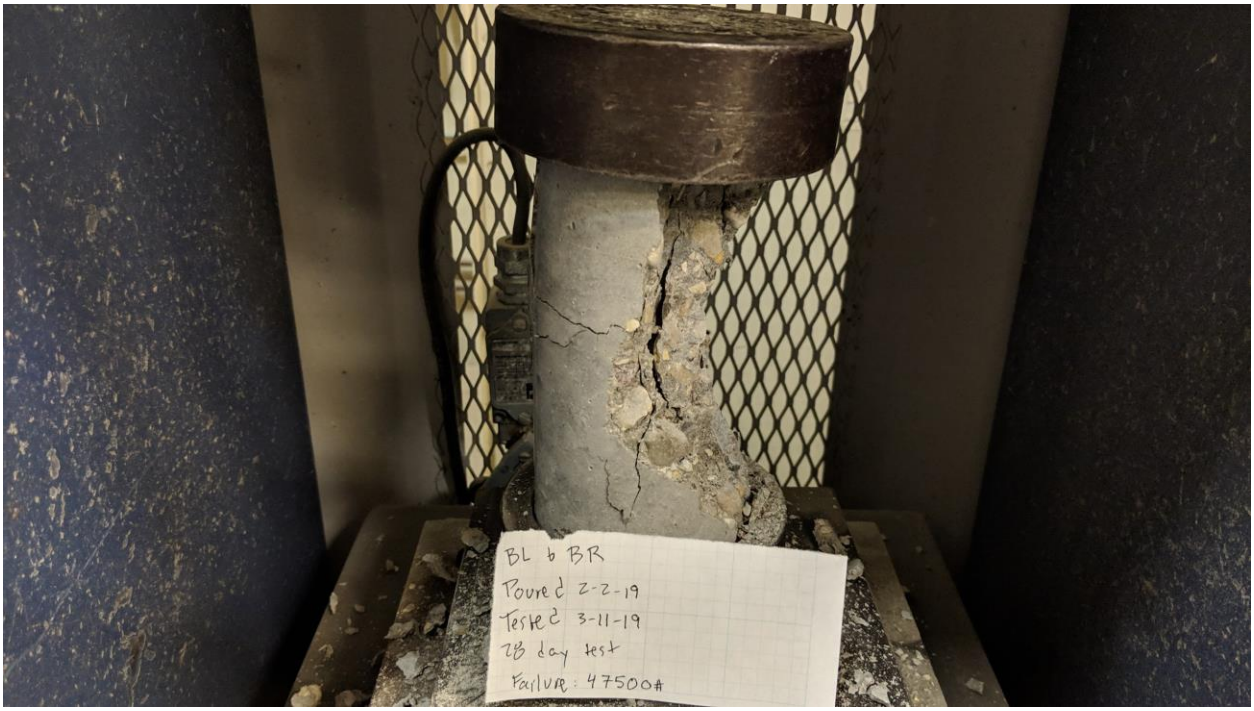

Figure B-16 - View 3 of Cylinder 3 of 37 Day Cylinder Break for Tests 11-20 and 31-36.

Figure B-17 - View 4 of Cylinder 3 of 37 Day Cylinder Break for Tests 11-20 and 31-36.

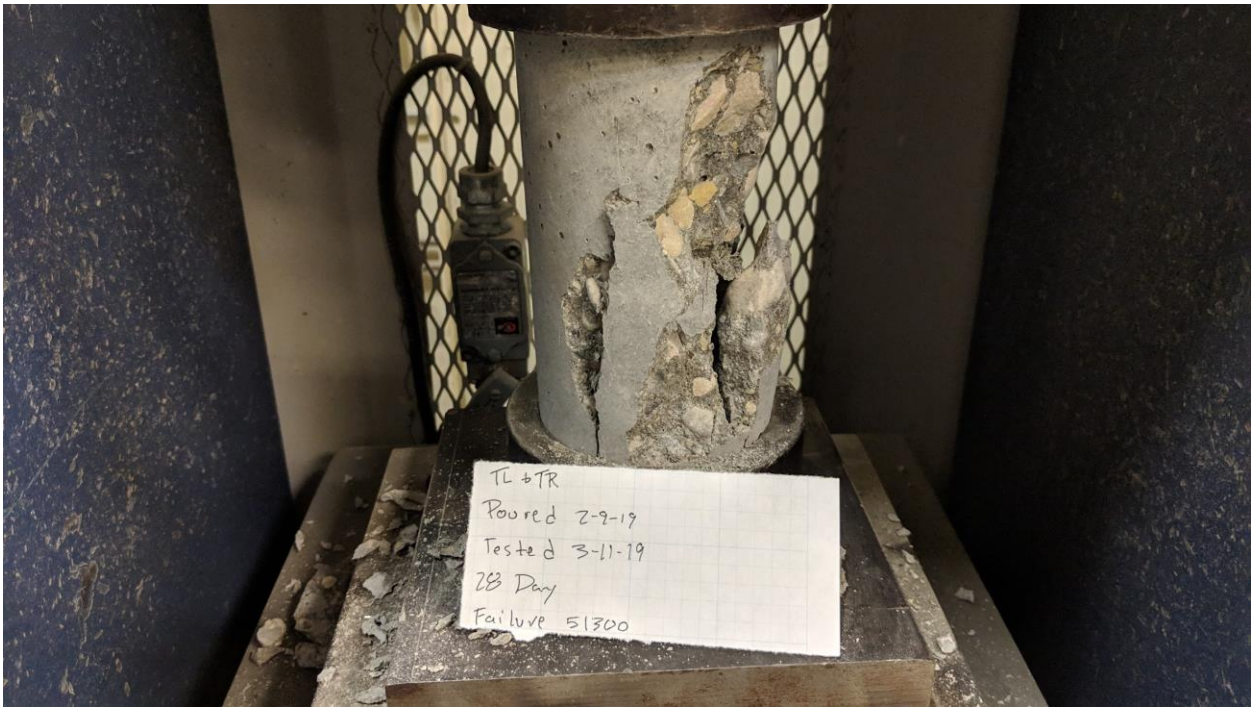

Figure B-18 - View 1 of Cylinder 1 of 30 Day Cylinder Break for Tests 1-10 and 21-30.

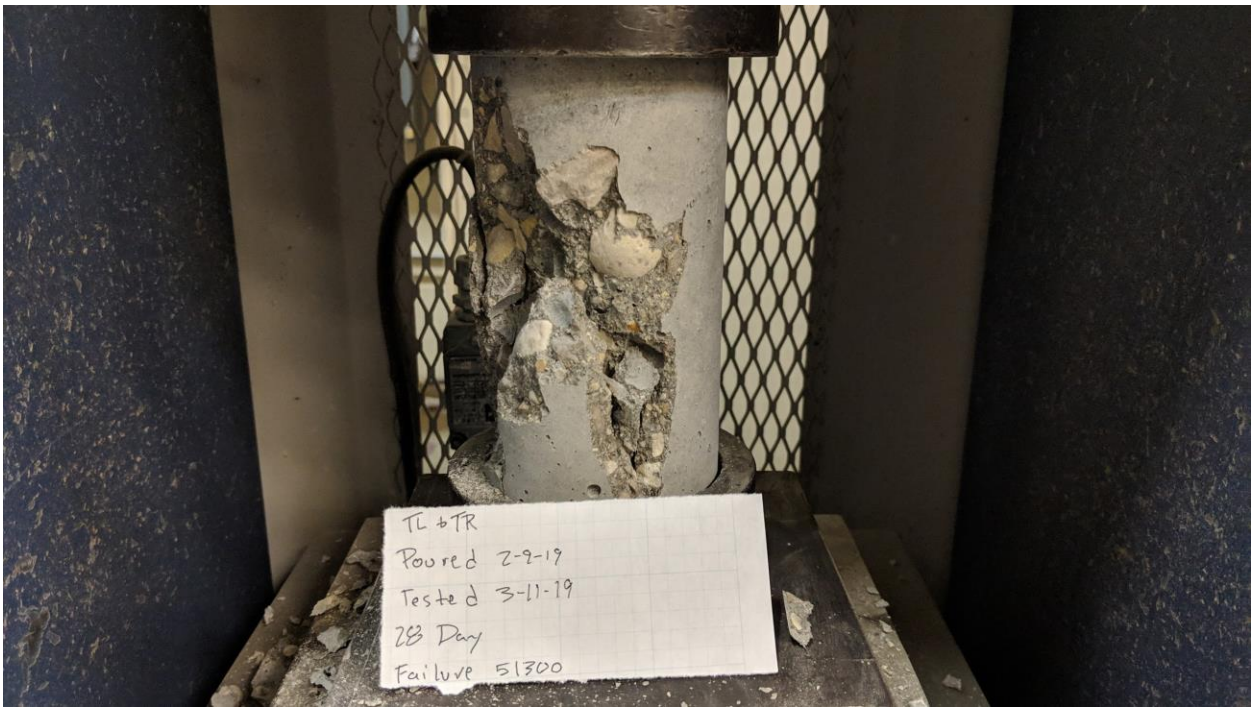

Figure B-19 - View 2 of Cylinder 1 of 30 Day Cylinder Break for Tests 1-10 and 21-30.

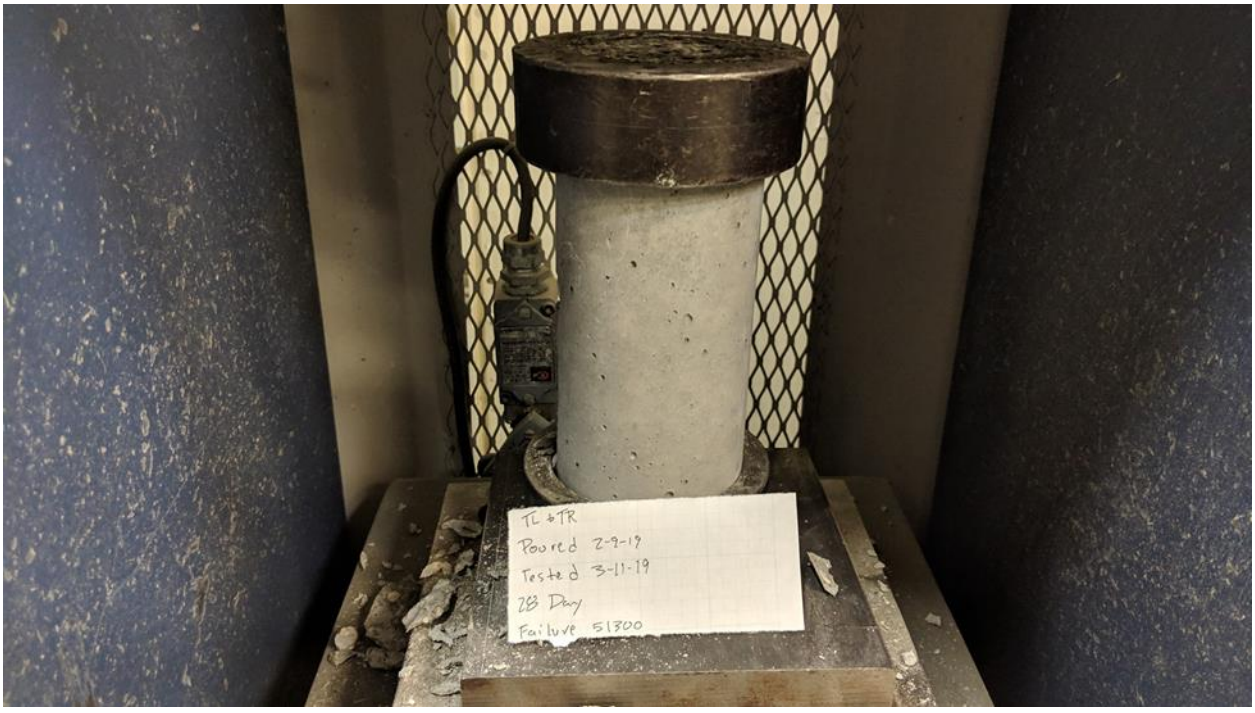

Figure B-20 - View 3 of Cylinder 1 of 30 Day Cylinder Break for Tests 1-10 and 21-30.

Figure B-21 - View 4 of Cylinder 1 of 30 Day Cylinder Break for Tests 1-10 and 21-30.

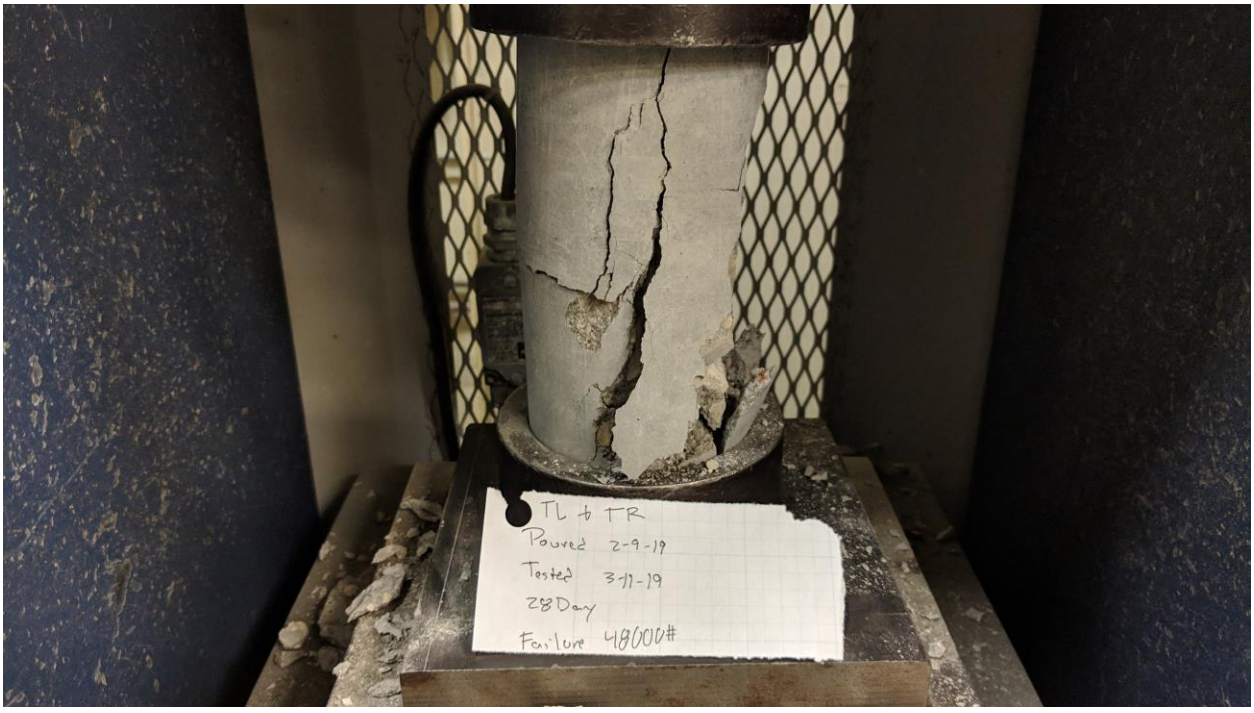

Figure B-22 - View 1 of Cylinder 2 of 30 Day Cylinder Break for Tests 1-10 and 21-30.

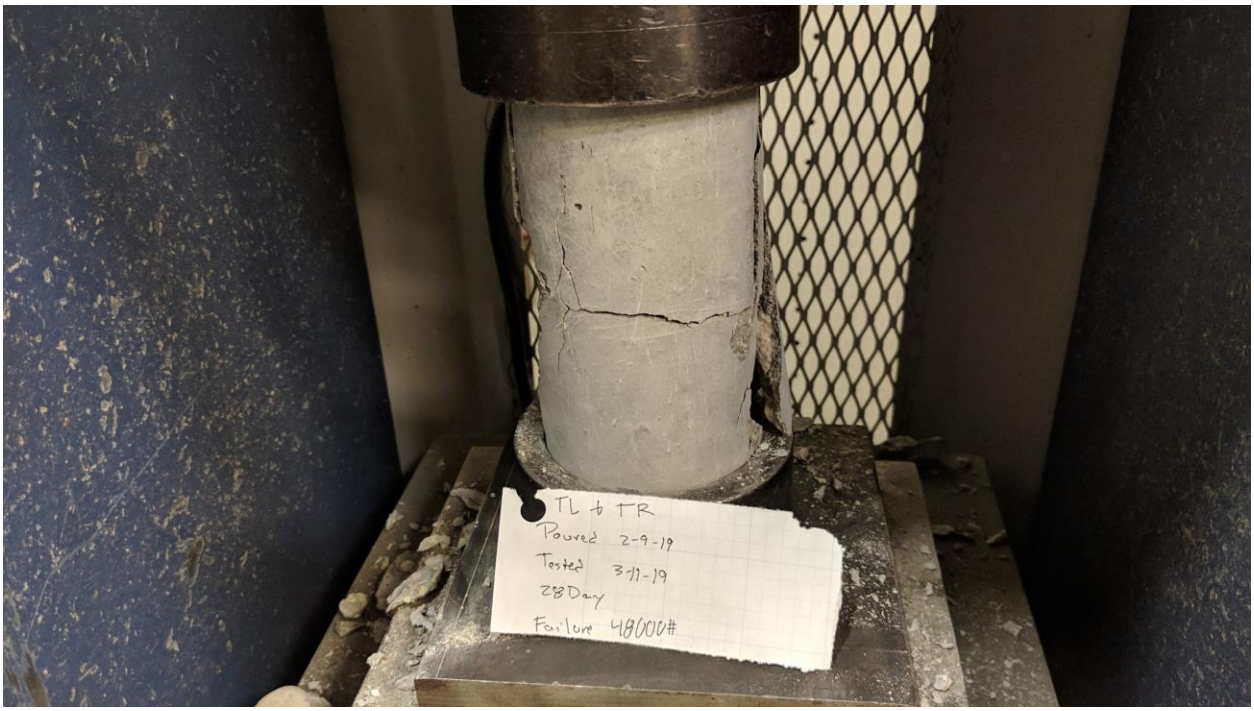

Figure B-23 - View 2 of Cylinder 2 of 30 Day Cylinder Break for Tests 1-10 and 21-30.

Figure B-24 - View 3 of Cylinder 2 of 30 Day Cylinder Break for Tests 1-10 and 21-30.

Figure B-25 - View 4 of Cylinder 2 of 30 Day Cylinder Break for Tests 1-10 and 21-30.

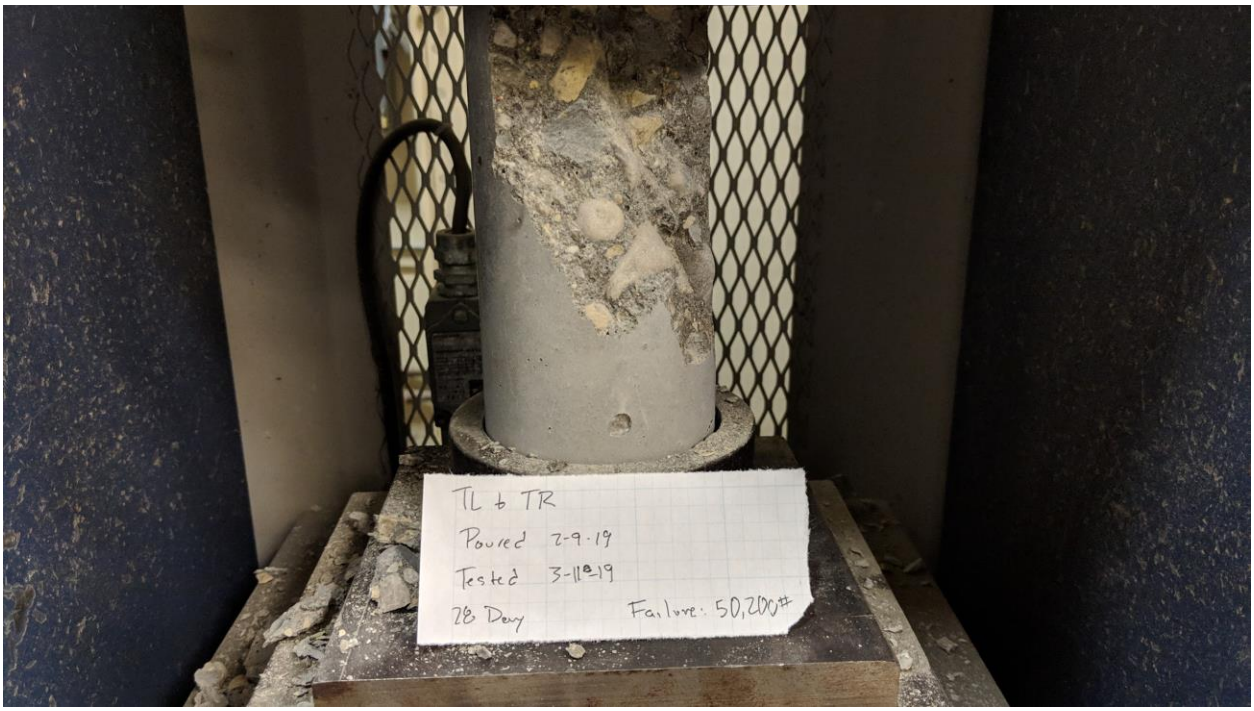

Figure B-26 - View 1 of Cylinder 3 of 30 Day Cylinder Break for Tests 1-10 and 21-30.

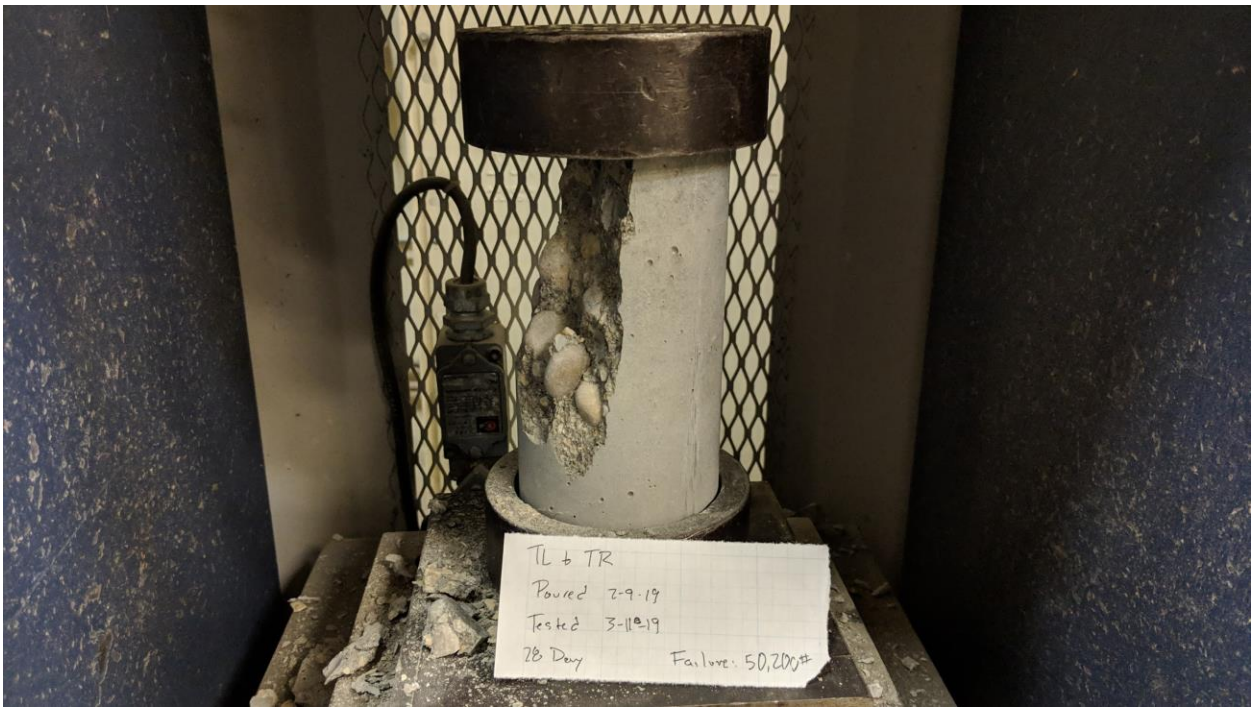

Figure B-27 - View 2 of Cylinder 3 of 30 Day Cylinder Break for Tests 1-10 and 21-30.

Figure B-28 - View 3 of Cylinder 3 of 30 Day Cylinder Break for Tests 1-10 and 21-30.

Figure B-29 - View 1 of All 37 Day Cylinder Breaks for Tests 11-20 and 31-3.

Figure B-30 - View 2 of All 37 Day Cylinder Breaks for Tests 11-20 and 31-36.

Figure B-31 - View 1 of All 30 Day Cylinder Breaks for Tests 1-10 and 21-30.

Figure B-32 - View 2 of All 30 Day Cylinder Breaks for Tests 1-10 and 21-30.

Appendix C - Pipe Certification

Customer Name	Customer PO#	Invoice No	Shipper No	Heat Number
BADGER RAILING	27221	1419139	1390451	B803789

HANNA

MATERIAL TEST REPORT 10/12/18 Page 1

Submitted By: Hanna Steel Corporation
Tuscaloosa Division
1701 Boone Blvd
P O Box 428
Northport AL 35476

Load Tally: 5-93543

Date Shipped: 10/12/2018

Send To: Infra-Metals
Marseilles
POB 409828
Atlanta GA 30384

Ship To: Infra-Metals
1601 Broadway St.
Marseilles IL 61341

Material: 1.660 SCH80 PIPE 21.000FT
Round Hot Rolled Carbon Steel Tubing

Sales Order: 068946-01 PO#: CE-562424
P/N: 1 1/4" SCH 80

Heat#: B803789 ASTM A500 2018 Grade B/C Type -

C	Mn	P	S	Si	Al	Cb	Cr	Cu	Mo	Ni	V	N	Nb	Ti	B
.060	.360	.007	.003	.020	.028	.000	.040	.090	.010	.030	.000	.0067	.0020	.0010	

Yield(psi)	Tensile(psi)	%E	Rock	CEV
68,000	70,000	23.0	B87	.138

Melted and manufactured in the USA

Flattening Test on Heat # B803789: Passed

LEED Information
Year 2016 Recycled Content 76.0% Scrap 95.0% Post consumer 5.0% Pre consumer
Exact scrap% per heat is unknown; LEED data is an average for that mill/production year.

Bundle#	Heat#	Pieces	Feet	Weight
4583906	B803789	61	1,281	3,838
4583907	B803789	61	1,281	3,838

Figure C-1 – Page 1 of the Pipe Certification.

Customer Name	Customer PO#	Invoice No	Shipper No	Heat Number
BADGER RAILING	27221	1419139	1390451	C86843

Independence Tube
a Nucor Company

6226 W 74th St
Chicago, IL 60638
708-496-0380
Fax 708-563-1950

https //www nucortubular com
https //www ntpportal com
Certificate Number MAR 907301

Sold By:
INDEPENDENCE TUBE CORPORATION
6226 W 74th St
Chicago, IL 60638
Tel 708-496-0380
Fax 708-563-1950

Purchase Order No CE-563552STOCK BUY
Sales Order No MAR 360549 - 1
Bill of Lading No MAR 210883 - 2
Invoice No
Shipped 11/5/2018
Invoiced

Sold To:
943 - INFRA METALS-MARSEILLES
1601 BROADWAY
MARSEILLES, IL 61341

Ship To:
1 - INFRA-METALS
1601 BROADWAY
*** HOLD FOR RELEASE ***
MARSEILLES, IL 61341

CERTIFICATE of ANALYSIS and TESTS

Customer Part No:

ROUND A500 GRADE B(C)
1.660"OD(1.25"NPS)X SCH40 X 21'

Certificate No: MAR 907301
Test Date: 11/2/2018

Total Pieces 854 — Total Weight 40.712

Bundle Tag	Mill	Heat	Specs	Y/T Ratio	Pieces	Weight
248591	13N	C86843	YLD=68970/TEN=72560/ELG=24 9	0 9505	61	2.908
248592	13N	C86843	YLD=68970/TEN=72560/ELG=24 9	0 9505	61	2.908
248593	13N	C86843	YLD=68970/TEN=72560/ELG=24 9	0 9505	61	2.908
248605	13N	C86843	YLD=68970/TEN=72560/ELG=24 9	0 9505	61	2.908
248606	13N	C86843	YLD=68970/TEN=72560/ELG=24 9	0 9505	61	2.908
248717	13N	A88979	YLD=66920/TEN=70180/ELG=24	0 9535	61	2.908
248718	13N	A88979	YLD=66920/TEN=70180/ELG=24	0 9535	61	2.908
248719	13N	A88979	YLD=66920/TEN=70180/ELG=24	0 9535	61	2.908
248720	13N	A88979	YLD=66920/TEN=70180/ELG=24	0 9535	61	2.908
248721	13N	A88979	YLD=66920/TEN=70180/ELG=24	0 9535	61	2.908
248722	13N	A88979	YLD=66920/TEN=70180/ELG=24	0 9535	61	2.908
248725	13N	A88979	YLD=66920/TEN=70180/ELG=24	0 9535	61	2.908
248726	13N	A88979	YLD=66920/TEN=70180/ELG=24	0 9535	61	2.908
248735	13N	A88979	YLD=66920/TEN=70180/ELG=24	0 9535	61	2.908

Mill # 13N Heat # A88979 Carbon Eq 0 1735 Heat Src Origin MELTED AND MANUFACTURED IN THE USA

C	Mn	P	S	Si	Al	Cu	Cr	Mo	V	Ni	Nb	Sn
0 0600	0 5400	0 0080	0 0010	0 0300	0 0320	0 1000	0 0500	0 0200	0 0010	0 0400	0 0010	0 0050

N	B	Ti	Ca
0 0068	0 0001	0 0020	0 0017

LEED Information (based on the most recent LEED information from the producing mill)

Method	Location	Recycled Content	Post Consumer	Post Industrial
EAF	Ghent, KY	66 9%	28 2%	38 8%

Mill # 13N Heat # C86843 Carbon Eq 0 1705 Heat Src Origin MELTED AND MANUFACTURED IN THE USA

C	Mn	P	S	Si	Al	Cu	Cr	Mo	V	Ni	Nb	Sn
0 0600	0 5300	0 0070	0 0030	0 0200	0 0260	0 1000	0 0400	0 0200	0 0010	0 0500	0 0000	0 0040

N	B	Ti	Ca
0 0080	0 0001	0 0010	0 0016

LEED Information (based on the most recent LEED information from the producing mill)

Method	Location	Recycled Content	Post Consumer	Post Industrial
EAF	Ghent, KY	66 9%	28 2%	38 8%

Figure C-2 – Page 2 of the Pipe Certification.

Customer Name	Customer PO#	Invoice No	Shipper No	Heat Number
BADGER RAILING	27221	1419139	1390451	C86843

Independence Tube
a Nucor Company

6226 W 74th St
Chicago, IL 60638
708-496-0380
Fax 708-563-1950

https //www nucortubular com
https //www ntpportal com
Certificate Number MAR 907301

Certification

I certify that the above results are a true and correct copy of records prepared and maintained by Independence Tube Corporation Sworn this day, 11/2/2018

WE PROUDLY MANUFACTURE ALL OUR PRODUCT IN THE USA
INDEPENDENCE TUBE PRODUCT IS MANUFACTURED, TESTED,
AND INSPECTED IN ACCORDANCE WITH ASTM STANDARDS
MATERIAL IDENTIFIED AS A500 GRADE B(C) MEETS BOTH
ASTM A500 GRADE B AND A500 GRADE C SPECIFICATIONS

CURRENT STANDARDS
A252-10
A500/A500M-18
A513/A513M-15
ASTM A53/A53M-12 | ASME SA-53/SA-53M-13
A847/A847M-14
A1085/A1085M-15

Chris Allen

Chris Allen, ASQ CMQ/OE
Quality Systems Supervisor

Figure C-3 – Page 3 of the Pipe Certification.